Asphalt Binders Characterization and Modeling

X-Ray Diffraction

by

Hekma Mohamed Seddig

A Thesis submitted to school of Graduate Studies in partial fulfillment of the requirements for the degree of

Master of Engineering

Faculty of Engineering and Applied Since

Memorial University of Newfoundland

Memorial University of Newfoundland

May 2018

ST. JOHN'S **NEWFOUNDLAND**

Contents

Abstract

Cracking is a common occurrence in asphalt pavements in colder climates, while pavements in hotter climates experience rutting; both of which are considered on-going problems from an industry standpoint. Asphalt presents in crude oil was studied to know their structure with the help of X-ray diffraction (XRD). Six samples of Asphalt binder were taken from Canada and USA then converted into thin films of 1mm to get XRD pattern. In addition, Cu-K-a monochromatic radiations were used at 40kV using a Rigaku DMax 2200V-PC at 40 mA with scan ranges from $2\theta = 5^{o}$ to 35^{o} and 60^{o} to 110^{o}. Mathematical functions such as Pearson VII and Pseudo-Voigt are used to profile fit the data obtained by the XRD. After profile fitting, they are modeled using GFF i.e. Generalized Fermi Function in Mathematica™. The analysis showed a correlation among the three mathematical functions.

The outcomes discussed here substitute to the accuracy of profile fitting whereas the exponents of Pearson VII and pseudo- Voigt Lorentzian differ. The Lorentzian values of Pseudo- Voigt are 0.3, 0.5, and 0.7 whereas the Exponent values of Pearson VII are 0.5, 1.0, and 1.5, and 3 backgrounds (linear, 3rd order polynomial, and parabolic) were applied in profile fitting. Further, profile fittings' accuracy made crystallite parameters to produce approximate results when calculated.

Acknowledgements

I wish to acknowledge the assistance of some individuals who have contributed to the success of this work. First and foremost, my appreciation goes to my supervisors Dr.John Shirokoff and Dr.John Lewis whose advice and helpful suggestion and support have directed the progress of this programme especially this project work from its inception to the conclusion. Their contributions, criticisms, and instructions improved this work greatly in quality and scope. Aside from the mentorship, encouragement, friendship, and support they gave me during the course of my studies in Memorial University, their guidance provided me with the experience needed in achieving my career objectives.

Their encouragement did not only develop me to be an experimentalist but it helped me to be a great independent thinker. My appreciation goes to Dr. John Shirokoff, Dr. John Lewis, and the Faculty of Engineering and Applied Since faculty and staff for all the friendly and professional support that they gave me through their discussion and whenever I need guidance. Moreover, I thank the Memorial University of Newfoundland and the Canadian Foundation for Innovation (CFI) for providing computing software, laboratory, and facilities to perform the research in this work. I will ever remain grateful to my beloved husband Abdulhamid Alkhalgi, who is Allah's gift to me, and my daughter Lareen.

I appreciate my father Mohamed Seddig, and my mother Khadega Naji for their prayers support, encouragement, and unwavering love was undeniably the bedrock upon which my life has been built. Also, my siblings, Amera, Hoor, Kader, and Mahmoud for their prayers.Also, the big thanks and gratitude to my home country Libya, for giving me a scholarship towards my Master's degree.

List of Tables

List of Figures

Abbreviations

AASHTO	American Association of State Highway and Transportation
ASTM	American Society for Testing and Materials
BBR	Bending Beam Rheometer
BisA	Bisphenol A
BMB	Bio-modified Binder
C	Carbon
Ca	Calcium
CA	Cyclic Aromatic
CCU	Catalytic Crude Upgrading
CGSB	Canadian General Standards Board
CPJ	Conversion Pierre Jorgensen
C5Pe	Polyaromatic Compound
DSR	Dynamic Shear Rheometer
DTT	Direct Tension Test
EDIEMAC	Edie Oil Inc. Process

ENI	Energetico Nacionale Italiano
FCC	Fluid Catalytic Cracking
FWHM	Full Width at Half Maximum of Profile
GFF	Generalized Fermi Function
GHU	Genoil Hydroconversion Upgrader
H	Hydrogen
HCAT	Hydrocracking Technology
HDT	Hydrotreating
HOUP	Heavy Oil Upgrade Project
HRH	Heavy Residue Hydroconversion
HTIG	Headwaters Technology
HTL	Heavy to Light
IFT	Interfacial Tension
IMP	Instituto Mexicano del Petróleo (of Petroleum)
IMP-HDT	The IMP Process Based Upon Catalytic Hydrotreatment and Hydrocracking of Heavy Oil
IXS	Inelastic X-ray Scattering

IYQ	Increased Yields and Qualities
LC	Chevron Lummus (LC-Fining Process)
NMR	Nuclear Magnetic Resonance
P	Pearson VII
PA	Polycyclic Aromatic
PAP	Permeable Asphalt Pavements
PAV	Pressure Aging Vessel
PAH	Polycyclic Aromatic Hydrocarbon
PG	Performance Grade
PPA	Polyphosphoric Acid
SARA	Saturates, Aromatics, Resins and Asphaltene
SHRP	Strategic Highway Research Program
SMA	Specially Modified Asphalt
TFOT	Thin Film Oven Test
TP	Total Phosphorus
TRU	TRU Process
V	Pseudo-Voigt

V(r) Central Potential

WRITE Western Research Institute Thermal Enhancement

XPS X-ray Photoelectric Spectroscopy

XRD X-ray Diffraction

Specimen ID	XRD Filename
T1	655-lagelW
T2	655- 2agelW
T4	655 - 4agelW
T7	655 - 7agelW
L2	RR21agelW
L5	RR51agelW

Symbols

(002) $_{graphene}$	*(002)* $_{graphene}$ band (peak) on XRD pattern
(10)	(100) band (peak) on XRD pattern
(11)	(110) band (peak) on XRD pattern
γ	Gamma band (peak) on XRD patter
θ	Theta
λ	Lambda
I	Intensity
S	Scattering Vector
d	Diameter
F	The Form Factor
R	Radius

Chapter 1

Introduction

1.1 Asphalt and Asphaltene

Asphalt mixture is made up of aggregates, filler, and binder, basically utilized in the construction and maintenance of different kinds of parking spaces, airports, roads, etc. A typical mixture of asphalt is made up of aggregates of sand, gravel and grounded rock. A binder is used to hold the aggregates together to make them a strong cohesive mixture. A typical binder which is used for binding aggregates is bitumen. Asphalt pavement is made up of the road structure above the subgrade that includes mixed and unmixed bituminous materials making it possible for pavement to distribute the traffic loads before breaching at the subgrade or level of formation [1].

Also, asphalt is a very viscous liquid, which is found mostly in crude petroleum, and some natural deposits like natural asphalt found in the lake of Trinidad. Asphalt, because of its outstanding application for pavement has been the main choice in the construction of roads and pavement. The key factor that results in the aging or deterioration of pavement is asphalt because it is too sensitive and oxidizes easily. Hence, it becomes needful to know asphalt pavement performance at the minute level, like its properties, structure to enhance improved durability [1].

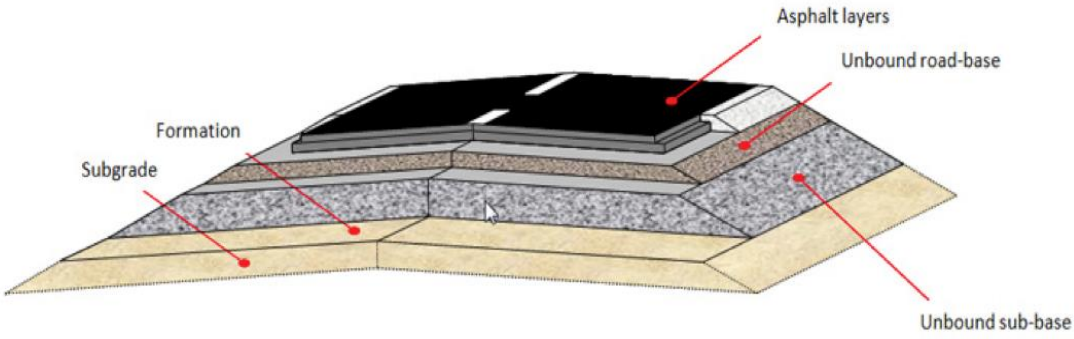

Figure 1.1: Schematic layers of pavements [1].

Asphaltene is brown to black solids with a high molar mass and consist of heavy complex mixture constituents of crude. They are soluble in aromatic solvents such as toluene, benzene and they are not soluble in paraffinic solvents such as n-heptane, n-pentane [1].

The deposits of asphaltene can be extracted in the process of production, transportation and the upgrading of petroleum as a result of the alteration in pressure, composition, and temperature. Several scholars proposed the methods that could be applied to the investigation, conducting an experiment, and for the analysis of the aging of an organic compound. Specifically, the most mysterious part of bitumen constituent, asphaltene, with the use of nuclear magnetic resonance (NMR), X-ray diffraction (XRD) analysis, etc. (Yen et al., 1961) did a major pioneered study in asphaltene; they used X-ray analysis of Asphaltene to know the structure [2].

1.1.1 Properties of Asphaltene

Asphaltene is commonly classified, as molecular compounds, and it comprises some huge number of chemical species that share the same solubility behavior but to some extent are different in

chemical structures, sizes, and shapes. A high percentage of the scientific researchers carried on Asphaltene show that the Asphaltene chemical species have the feature of being polynuclear aromatics that also contain n-alkane chains, cyclic alkanes, and heteroatoms such as sulfur, nitrogen, and oxygen. Also; some metallic chemical elements such as nickel, vanadium, and iron (Speight, 1999) were implemented through an investigation study to predict the elemental composition of Asphaltene [3]. In this study, different Asphaltene was investigated through using some crude oil specimens that were picked up from around the world as shown in the table (1.1). The hydrogen to carbon (H/C) atomic ratios of C5-Asphaltene was of great interest to some other researcher like (Moschopedis et al., 1976) who concluded that these ratios are in the range of 1.15 ±0.5% [4]. As a composition, the normal asphaltene molecule may involve sulfur in forms of thiophenes, thiols, sulfides, disulfides and oxidized forms. Nitrogen can also exist as pyrroles and pyridines structures. In addition to these elements, the experiments had identified oxygen in forms of carboxylic, phenolic and ketonic locations, while metals (nickel and vanadium) are usually present as porphyrins. In general, Asphaltene was considered as the “highly polar” fraction of the crude oil due to reasons like Asphaltene are insoluble in n-heptane and a non-polar 16 solvent. However, Asphaltene may be considered as soluble in nonpolar solvents like benzene, toluene, and dichloromethane whilst they are not in polar solvents like water, glycerine, and methanol. Therefore, and based on the facts mentioned above, Asphaltene is non-polar chemically and relatively more polar when compared to other components of crude oil.

Table 1.1: Elemental composition of Asphaltene from world sources [3].

	Canada	Iran	Kuwait	Venezuela
Carbon (wt%)	79.0-88.7	83.7	81.6-82.4	81.1-84.7
Hydrogen (wt%)	6.9-11.1	7.8	7.8-8.1	7.8-8.3
Nitrogen (wt%)	0.7-2.8	1.7	0.6-1.7	0.2-2.0
Sulphur (wt%)	0.3-8.1	5.8	7.4-8.0	2.7-6.9
Oxygen (wt%)	0.4-3.9	1.0	0.6-1.8	1.0-4.2
H/C Ratio	0.98-1.56	1.19	1.14-1.19	1.13-1.19
N/C Ratio	0.007-0.029	0.017	0.008-0.017	0.002-0.02
S/C Ratio	0.001-0.038	0.026	0.034-0.039	0.012-0.032
O/C Ratio	0.004-0.037	0.009	0.005-0.017	0.013-0.039

Factors such as the method of extraction and solvents used for separation are highly affected physical properties of this Asphaltene, and this is because; the amount and exact chemical composition of extracted Asphaltene will vary according to the different procedures used in the process of extraction. To clarify more, Asphaltene precipitated using n-heptane are more aromatic in comparison to Asphaltene precipitated using n-pentane [5]. In fact, the H/C atomic ratio plays a major role in the process of precipitation. It is lower when the Asphaltene precipitated using n-heptane than when the Asphaltene precipitated using n-pentane. Therefore, the grading of Asphaltene is usually carried out operationally and not chemically. Different methods were adopted in the process of Asphaltene characterization; for example (Kharrat, 2009) used the method of addition of various diluents [6]. (Dettman et al., 2005) implemented the method of gel permeation chromatography [7]. [8; 9; 10] performed the characterization using the addition of the

same solvent at different dilution ratios. To explain in detail, (Yang et al., 2004) partitioned Athabasca Asphaltene into six subfractions based on the dilution ratio of n-heptane to bitumen [11]. (Zhao et al., 2007) used kNano-filters to split bitumen and heavy oil into several fractions to predict the composition and size distribution of asphaltene enriched nanostructures. In conclusion, the asphaltene composition is found to be varied continuously, but to some extent, there is no spectacular change in the composition of the fraction to fraction [12].

1.1.2 Molecular Structure of Asphaltene

Petroleum is one of the most salient of the mixtures found in molecules as molecules are said to occur in mixtures naturally. It is also one of the most complicated or rather complex materials with more than 100,000 chemical components. Asphaltene stands out to be the basic unresolved component of crude oil [13]. Having the knowledge of the structure of Asphaltene is of great economic significance and requirement in the establishment of the function-structure relation in petroleomics although the structure of their molecules has been for a long time being subjected to a debate. Identification of the molecular structure of Asphaltene provides a basis for the understanding of all concepts of the science of petroleum ranging from petroleum thermodynamics to interfacial interactions and structure, enhancing the first-principles approach to optimize utilization of resources.

Studies over time have shown different results in that while some studies suggest that Asphaltenes molecules contain several PAHs (polycyclic aromatic hydrocarbon), others suggest that Asphaltenes molecules have a single PAH.Asphaltenes are usually associated with major economic problems. Some of the problems include unwanted phases of Asphaltenes which hinder

the refining, production, and transportation of petroleum, its interfacial activities with rocks impacts wettability thus preventing recovery of oil and causes reservoir uncertainty. The chemical complexity of Asphaltene has caused challenges in the analysis of its structure. In the past, STM (scanning tunneling microscopy) has been used in the characterization of Asphaltene although atomic-resolution was not achieved on the molecules of Asphaltene [13].

Current advancement in AFM (Atomic Force Microscopy) has enabled the visualization of the of the structure of the atoms of single molecules. The strategy was also used to discover chemical synthesis products and on-surface reactions, identification of the molecular structure of graphene nanoribbons and natural compounds and analyzation of the order of the bonds. One can also track molecular orbitals through the use of STM and a substrate such as ultrathin insulating films. Combining the STM and AFM investigations can be utilized as a very potent methodology for screening mixtures of theoretical molecules for molecular electronics as well as application in photovoltaic gadgets and organic light emitting diodes [13].

Orbital imaging is used to provide information regarding the electron delocalization in the frontier molecular orbitals. In instances where AFM is unable to scan the structure of molecules directly, orbital imaging makes the structural information accessible. Generally, orbital imaging stands out as a useful complement to the atomic-resolution images of AFM. It is regarded as a self-reliant cross-check for hypothesis testing of a structure obtained from the AFM. It is also a source of content about the delocalization of electrons in the frontier molecular orbitals. Asphaltene molecules and peripheral alkane chains contain a basic aromatic core. In some instances, the core is divided into different PAHs attached by an individual bond meaning that archipelago-type

molecule is present. The dominant Asphaltene molecular structure is a monoaromatic core containing peripheral alkanes, and it helps in proving the basic concept by the Yen Mullins model.

The diverse PAH architecture of PAs and CAs is similar even with their notable differences in their post-processing and formation. PA is seen to contain more substituted rings and have longer side groups as compared to CA. Previous studies have shown that both CA and PA have shorter molecules which have been proven wrong by the current study. In the study of PAHs, CA molecules are suitable for use and they can also be used for constant-height AFM imaging since they have a few side-chains and they are typically planar. From an economic point of view, PAS is more crucial although they are said to have longer and more side-chains that are connected to the PAH core complicating both analysis and measurement. When scanned in AFM or STM mode, the side-chains at times tend to go through tip-induced conformational shifts [13].

Imaging orbitals are significant for PA since the peripheral alkanes make it difficult for PA interpretation of AFM images. Even if a mixture is diverse and the molecule is rare, the presence of a certain molecule in a convoluted mixture can still be stipulated. AFM is rendered a valuable complimentary prick for the molecular mixtures characterization of conventional strategies for structure elucidation such as X-ray diffraction, magnetic resonance, and mass spectrometry. STM and AFM can be used in the analyzation of complex polydisperse molecule mixtures when put on a mono-molecule basis with atomic-resolution. STM and AFM elucidation of mixtures through the process of scanning probe microscopy involves an epitome change for the establishment of newfound molecules such as molecular electronics and light emitting diodes. Various distinct molecules in a mixture can undergo the process of screening with the use of a high-resolution

scanning probe microscopy in a mono formulation with the lack of a long purification, chemical synthesis and description for each one of them. AFM is used to assign molecular structures for individual molecules while the STM is used to investigate the shape, level of electron affinity, molecular frontier orbitals extent and the ionization potential [13].

Despite that, higher asphaltene content of the crude oils makes the refining process difficult, which in turn is caused by the high molecular weight, structure, and aromaticity of the asphaltene. At the standard temperature and pressure, asphaltene exists as a colloidal structure that is comprised of some asphaltene molecules. Scientists have developed a number of different ways to determine the molecular structure of Asphaltene. The basic purpose of this study was to compute the hypothetical structure of asphaltene sample, which was drawn from different locations across Turkey. Of all the components of crude oil, Asphaltene is deemed as the most understudied and the least understood fractions [14].

For this experiment, four samples of crude oil were obtained from different locations of Turkey that include Yenikoy oil field, Batiraman oil field, Besikli oil field, and Garzan oil field. The asphaltene residue from the four samples of Turkish crude oil was obtained through the distillation process. The molecular structure of these samples was determined through the application of various techniques that include elemental analysis, nuclear magnetic resonance, X-ray diffraction technique; chromatography, nuclear magnetic resonance, and last but not the least is Fourier transform infrared spectroscopy. The major reason behind the application of a large number of methods is to calculate the molecular structure of Turkish asphaltene with great precision and accuracy [14].

The analysis of data obtained with the help of these techniques demonstrates that all the four samples of Turkish Asphaltene have similar distance between the layers of aromatic sheets of Asphaltene, and also the distance between aliphatic chains is quite similar. In all the four samples of Turkish Asphaltene, the first point of difference arose in the diameter of cluster values which came out to be different. The result of this research study was inconsistent with that of previous studies, according to which the basic structure of Asphaltene is comprised of polyaromatic and hydroaromatic elements, and these units are connected through aliphatic chains and atoms of oxygen, nitrogen, and sulfur [14].

Fourier transform infrared spectroscopy of these samples indicated that there exists double bond between two atoms of carbon, and also between two atoms of carbon and oxygen in the molecular structure of asphaltene. It also revealed that asphaltene also contains methyl (CH_2) and alkyl (CH_3) functional groups in its molecular structure. The samples were drawn from Yenikoy and Batiraman oil fields which contain more aromatic sheets than the samples obtained from Besikli and Garzan oil fields [14].

Research has indicated that Asphaltene is one of the most complicated compounds which are found in crude oil. A typical asphaltene molecule is comprised of abridged polyaromatic elements that contain aliphatic and alicyclic groups with the heteroatom molecules containing sulfur, oxygen, and nitrogen that constitute the aromatic structure. The complex structure of asphaltene hinders the usual processing of the feedstock as it diminishes the hydrodesulfurization reactions, blocks the porous surface of the catalysts that are used to increase the reaction process, and cause the hydrotreatment catalyst to become neutralize during the whole process. The underlying reasons

behind these problems can be better understood by thoroughly examining the chemical structure and composition of the Asphaltene. So, nuclear magnetic resonance spectroscopy and X-ray diffraction techniques have been found to be quite effective when it comes to the assessment of the structural factors of the hydrocarbons [15].

For the experiment, atmospheric residue (AR) was obtained through hydrotreatment of the Kuwaiti crude, in which AR and 5% light cycle oil were blended in an autoclave. The optimum pressure of the autoclave was 8 Mpa, and optimum temperature was kept at 350∘C. From this atmospheric residue, Asphaltene was obtained through precipitation, which resulted in three samples, which were named as AR-F-ASP, AR-P-ASP, and ARLCO-P-ASP of which AR-P-ASP and ARLCO-P-AS were hydrotreated samples [15].

In order to determine the concentration of nitrogen, oxygen, sulfur, and hydrogen, the element analysis was performed with the help of X-ray fluorescence analyzer. Moreover,"Matrix-assisted Laser Desorption Ionisation mass spectrometer" was used for the molecular analysis of the sample, and X-diffraction of the said samples was performed using X-ray diffractometer that has the power calibration of 12 kW. NMR spectroscopy of samples was done with the help of JNM-ECA 600 (JEOL) NMR spectrometer, the frequency of which was kept at 400 and 600 MHz for the sake of experimental convenience [15].

The analysis of data that was obtained as a result of the aforementioned experiments and procedures indicates that hydrotreatment changes the structure of Asphaltene in such a way that its aromatic cores become small and squashed. Moreover, hydrotreatment also reduces the length as well as the number of alkyl branches in Asphaltene. Adding light cycle oil to the atmospheric

residue of Kuwaiti crude oil also resulted in enhanced aromatic substitution, improved carbon-hydrogen content per molecule and better-quality microstructure of the asphaltene [15].

Crude oil has always been considered a source of social and economic value for a country owing to its profound impact on the community. For this very reason, scientists are keen to conduct experiments so that they could determine the chemical composition of crude oil. Several experiments have shown that crude oil is comprised of different proportions of organic and inorganic compounds. The most important components of crude oil are alkanes, aromatic hydrocarbons, mastics, and Asphaltene [16].

The color of Asphaltene ranges from dark brown to black, and their polarity is also very high. In order to determine the aging patterns of crude oil, it is important to analyze the small and large structures of Asphaltene, and the X-ray diffraction is very helpful in this regard. According to the most updated definition of Asphaltene, these compounds have high molecular weight, and their solubility is higher in aromatic solvents such as toluene [16].

The structure of Asphaltene is very complex, and that is why sophisticated techniques like X-ray diffraction are used for analysis. When X-ray diffraction is coupled with Raman spectroscopy, it becomes a twin technique to determine the aromatic content of hydrocarbon materials. Both techniques are quite useful in that X-ray diffraction determines structural aspects of the aromatic and aliphatic components of Asphaltene, whereas Raman spectroscopy tends to analyze the molecular interfaces of aromatic and aliphatic constituents of Asphaltene [16].

In order to determine the chemical aspects of Asphaltene that are present in Egyptian crude oil, four samples were collected from different oil fields across the country. In order to remove the mixed water, all the four samples were subjected to centrifuge at 50^0C temperature. Asphaltene samples were prepared by heating the crude oil and using the n-heptane and toluene to transfer the residual material on filter paper. After that, crystals were powdered for the sake of measurement. The X-ray diffraction pattern of extracted Asphaltene was documented with the help of PANalytical instrument that has scan rate calibrations of 0.01 2θ per second. For Raman spectroscopy, a different sample of Asphaltene was used and the name of the instrument was Dispersive Raman spectrometer [16].

The structure of the molecules is very important in their study and also its complexity hinders the detailed inspection of the molecular design. In this thesis we have studied four pairs of heavy oils, i.e., A1- crude oil asphaltene and A2- asphaltene from deposit from A1 oil field, B1- vacuum resid asphaltene from a heavy oil and B2- asphaltene from hydro converted product from B1 oil, C1- asphaltene from steam cracker tar and C2- vacuum residue after asphaltene removal and D1- shale oil bitumen asphaltene (Green River) and D2- shale oil bitumen asphaltene (Eagle Ford). All these samples have been taken from a wide range of crude sources, chemical compositions, aromatic contents and petroleum processes to investigate the structural differences between the samples and to gain individual molecular structures for every sample, specifically in between each pair of samples [17].

The measured molecules from each sample were selected at random, about 50 to 150 molecules per sample. First, STM topography images were taken and then determined for the STM footprints

of each molecule. By comparing both the crude oil A1 and the deposit A2, it was found that their area of distribution is very similar and the distribution of the hydrotreated sample B2 was expanded towards the larger sizes as compared to the feedstock material B1. Moreover, for C1/C2 and D1/D2 the latter in the sets were larger than the former on average. When the average molecular weight was gained by MS, similar results were found. In this case, the number of molecules measured has chiefly determined the quality of sampling. About 50 to 100 molecules were a lower limit to represent the spread of molecules in these samples [17].

Significantly the good qualitative agreement between the area of distributions observed with STM and the mass distribution measured by MS has corroborated that a consistent set of molecules was measured in these experiments. The characterization of each sample is based on the complete set of AFM images. All the structures cannot be assigned based on their respective AFM image because they contain significant information on compactness, size, and planarity of each molecule and size and content of polycyclic aromatic hydrocarbons (PAHs), methyl side groups and aliphatic side chains [17].

In samples A the comparable largest variety of different structure is found, for example, molecules with an extended aromatic core, isolated aliphatic chains, and more three-dimensional (bulky) molecules with approximately identical proportionality and where other samples were normally dominated by one or two out of these three types of molecule structures. On the basis of the structure assignments inferred from AFM measurements, the double-bond equivalent (DBE; where DBE=C – H/2+1) is also evaluated as a function of the carbon number of samples A and compared to atmospheric pressure photoionization Fourier transform ion cyclotron resonance MS

(APPIFT-ICRMS) data. Different mass spectrometry techniques can give some different asphaltene mass distribution but MS technique is better than all [17].

We have observed a wide variety of different heavy oil hydrocarbon mixtures by high-resolution scanning probe microscopy and resolved individual molecular structures. We have identified the repeating and distinguishing structural motifs by AFM. Furthermore, statistical analysis of molecular footprints obtained by STM and comparison of AFM data with MS indicates the statistical importance of the sampling. The measurements showed here have opened the prospects to analyze complex geological formation processes and chemical reactions on the single-molecule level [17].

The results indicated that the yields of Asphaltene that were obtained with the help of n-heptane are lower in content but their tendency of crystallization is higher than that of Asphaltene yields that were obtained with the help of toluene. For all the four samples, the horizontal facet of the sheets containing Asphaltene molecules was 11–13A and these values were same for X-ray diffraction and Raman spectroscopy [16].

The results also indicated that there exists a difference in the diameter and crystal size of Asphaltene of crude oil of Western and Eastern deserts. The samples for this research were collected from four oil fields namely Petrobras-15, Petrobras-24 and West Bakr and El-Wahat, of which first three samples were collected from Eastern desert and the last one i.e. El-Wahat was obtained from the Western sample. The results indicated that of all the four samples studied, El-Wahat was less in age if compared with other three samples [16].

1.2 Physical Characteristics of Petroleum-Derived Asphalt.

Softening point: This is similar to the melting point and indicates the temperature at which the asphalt softens suitable for use for specific purposes. This is determined using ASTM test D-36.

Penetration: This is sink time of a weighted needle in asphalt for a set period of time under specific temperatures [19].

This is determined using ASTM test D-5. Units 15 analyzed 0.1 mm are used to measure penetration results.

Viscosity: The flow of liquid asphalt at varying temperatures is determined by viscosity and is tested using ASTM test D-88 and D-2170.

Flashpoint: This indicates the temperature at which when heated the asphalt will ignite. This is given by ASTM test D-92.

Softening point and viscosity are closely related in such a way that, as softening increases, viscosity also increases and conversely penetration drops leading to a rise in flashpoint [19].

1.3 Uses of Crude Oil Derived Asphalts.

Asphalt produced from crude oil is mostly employed in road paving and a large proportion of the use is accounted for asphalt in North America. The purpose of the asphalt is to serve as a binder

that holds the composite aggregates together. In road construction, asphalt may be mixed in several ways and in varying proportions such as:

Cutback asphalt: This contains solvents mentioned previously and is referred to as cutbacks.

Mastic asphalt: It is composed of approximately 93% aggregate and 7% petroleum asphalt.

Rolled asphalt concrete: It is made up of 5% petroleum asphalt and 95% aggregate.

Asphalt emulsions: It contains a greater amount of asphalt at the rate of 70% versus 30% water and chemical additives [19].

1.3.1 Application of Roofing Shingles

Oxidized asphalts are mostly used in the production of roofing shingles and account for a smaller proportion of asphalt consumption in North America. According to (Pujadó et al., 2006) there are major grades of asphalt for roofing purposes [18]. These are:

Type 1: Penetration at 25 °C = 25 – 50 dmm and a softening point of 60 – 66 °C.

Type 2: Penetration at 25 °C = 20 – 30 dmm and a softening point of 74 – 79 °C.

Type 3: Penetration at 25 °C = 15 – 25 dmm and a softening point of 88 – 96 °C.

In the United States alone, asphalt shingles account for over 60% shingles used for roofing based on their economic nature. As discussed in a previous section on shingles, asphalt shingles may either be organic or fiberglass depending on their based building blocks. The fiberglass shingles

are made from mineral fillers and it becomes waterproof as a result of the addition of asphalt obtained from petroleum distillation. Organic shingles contain about 40% more asphalt than the fiberglass making them heavier and resistant to adverse environmental conditions after being embedded with ceramic granules [20]. The embedded granules are a useful tool when determining reflectance. Reflectance is important especially in warmer environments to determine and evaluate the performance of the shingles [21].

Other applications of petroleum asphalt include:

- Widespread application of cattle sprays, battery casings, and floor tiles.
- Used in the waterproofing of fabrics, fence posts, and wooden objects to avoid moisture penetration.
- The lining of canals, reservoirs, and dams.
- Pavements of landing strips, parking lots, and take off runways for aircraft.

1.3.2 Asphalt Shingles for Roofing Material

Asphalt shingles were first used in the United States in 1901. Made from organic materials called felt, shingles are composed of two types of based materials; fiberglass and felt. In both types of asphalt shingles, asphalt-saturated based are used and covered with any of the following: quartz, ceramics, sand, talc, mica, schist, slate, etc. [22].

The shingles are mostly UV resistant, and the top coated granules provide the characteristic color associated with shingles. Polymer modified bitumen in some cases are used to increase resistance

to high winds In the United States, ASTM D7158 is the code employed for this purpose. Conversely, copper may be added to the asphalt shingles to discourage the growth of algae.

Thermal cracking in asphalt is prevented through the use of styrene-butadiene-styrene (SBS), an additive typically used to reduce the impact of damage from hail. Additionally, scrim, which is made from fabrics, is infused into shingles to reduce impact from hail, wind, and heat [23].

1.3.3 Organic Made Asphalt Shingles

Organic type asphalt shingles are procured from a base made of waste paper, cellulose or even wood, which was saturated with asphalt to render it waterproof and subsequently embedded with ceramic granules and adhesive asphalt. Organic shingles are more resistant to breakage and less resistant to fires when compared with fiberglass shingles. However, shingles made from aged woods and pulps are sturdier and more resistant to tears. Earlier versions of organic shingles were suggested to contain asbestos [22].

1.3.4 Fiberglass Shingles

This type of shingle is made from fiberglass base and laid out randomly on a mat reinforced with a resin made of urea formaldehyde. This is then coated with asphalt making it water resistant and has a class A fire resistant rating. Fiberglass shingles evolved from the use of asbestos making a suitable replacement with sizes ranging between 1.8 – 2.3 pounds per square foot. When compared with its organic counterpart, the fiberglass shingles is considered sturdier and is gradually replacing the former as it has a 1700g tear value. Sections 1507.2.1 – 1507.2.2 of the international

building code of 2003, requires that asphalt shingles be employed on roof slopes of at least 17% of two vertical units [24].

1.3.5 Designs

3-Tab and Architectural shingles are the two basic designs options available in asphalt shingles. 3-Tab designs are characterized by a uniform shape and size and therefore utilize less material. In this regard, they are considered cost-effective and lighter in weight. This, in turn, is impacted by its thinner built and less durability status [25]. For this reason, they are mostly employed in low-value buildings. The architectural shingle, on the other hand, is considered more expensive, thicker and durable with a lifespan of up to 30 years. This being because architectural shingles offer more protection against the elements with the most minimal leaks [23].

1.3.6 Quality Criteria

The durability of asphalt shingles is highly dependent on quality. Though, variables depending on the shape and texture of asphalt shingles offer design fixtures that affect water resistance and at the same time increase aesthetic appeal. The reflective surface of solar shingles is a better conservator of energy by reducing air conditioning costs, especially when applied in warm temperature zones.

Wind and hail damage to asphalt shingles is drastically reduced through high fastener pull and is most effectively accomplished through the use of a durable underlayment such as ASTM D3161

and UL 997 class 1 for bond strength and wind resistance respectively [24]. Whereas, UL 2218 offer the best impact resistance even though susceptibility to damage may arise due to age.

Fiberglass asphalt shingles have better resistance to fires and are classified as A, whereas, the organic version is classed at C due to lower flame resistance. Algae are not believed to possess any risk to asphalt shingles, but it affects the quality of the shingles in terms of aesthetic appeal due to discoloration. Copper is embedded in shingles to discourage the growth of algae and maintain its appeal.

The durability of asphalt shingles depends on the factors mentioned above and in some cases, manufacturers offer lifetime warranties based on prorated repair costs as well as the cost of materials [25]. Consistent weather conditions encourage durability in shingles. This may be consistent warm or cold weather. The inconsistent of weather that makes the temperatures to fluctuate between warm and cold causes a thermal shock and may lead to damages occurring in the shingles. Thermal loading causes oxidization of the asphalt in the long run leading to aging and brittleness [23].

In this regard, the way a roof is orientated and ventilated will aid its durability by bringing down the temperature on the asphalt shingles. The application or installation of shingles is discouraged at temperatures of below 10°C as this will prevent a monolithic structure from being formed and further reduce the chance of exposed asphalt being directly hit and softened by sunlight and subsequent heat which is essential for the adherence of the asphalt [26].

For asphalt shingle to offer adequate protection, the long chain hydrocarbons must impregnate the underlying paper. When sunlight consistently hits the hydrocarbons, it is softened and adheres more firmly. However, with age and rain, the hydrocarbons are likely to be washed off as water runs in between the eaves and complex rooflines. This may result in shrinkage of the fibers due to loss of oils in those areas [23].

Thus, nails become exposed to the shingle flaps and breakage occurs in the surface coating of sand in the surface area. This results in wear and tear of the paper. Exposure to this nature causes water to seep in through the shingle nail areas with a subsequent rotting of materials, and further damage is encouraged.

1.4 X-ray Diffraction Measurements

X-ray diffraction (XRD) is employed in the characterization and identification of crystalline materials through a process of rapid analytical techniques. The fundamental principles follow after that discovered by [28].

XRD may provide vital information pertaining to the phase, atomic spacing, crystal structures and orientation, crystallinity, and crystal defects as well as grain size. Cathode ray tubes are used in the production of X-rays when monochromatic beams cause a constructive inference at specific angles as it is directed at a sample. The constructive interference at play results from Bragg's Law ($n\lambda=2d \sin \theta$). The arrangement of lattice atoms is a determining factor of peak intensities to be obtained. The detected diffracted X-rays are processed and counted through the process of 2θ angles range scanning [29].

X-ray diffraction systems allow powders, coatings, slurries and epitaxial films to be analyzed. Basic components of a diffractometer are X-ray detector, sample holder, and the X-ray tube. The X-ray tube is in charge of producing electrons and accelerating them towards their target. X-ray detector processes signal produced from the X-ray which is recorded on the monitor. According to [29], "The geometry of an X-ray diffractometer is such that the sample rotates in the path of the collimated X-ray beam at an angle θ while the X-ray detector is mounted on the arm to collect the diffracted X-rays and rotates at an angle of 2θ." This is depicted in Figure (1.4).

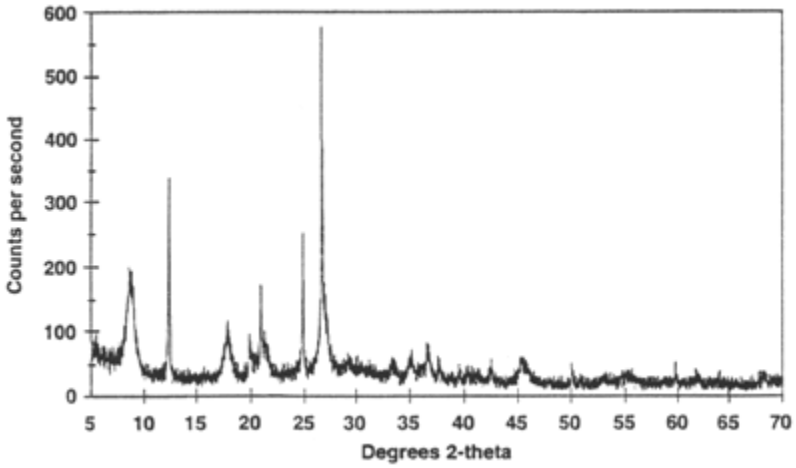

Figure 1.2: X-ray powder diffractogram. Peak positions occur where the X-ray beam has been diffracted by the crystal lattice [29].

Measurement of an unknown sample requires an instrument to grinding up the sample into a sample holder. Pure samples are used and ground to fine powder, smeared on a glass slide and placed in a sample holder. Rotation of the sample and detector in different angles produce varying intensities which are constantly recorded. Once a peak in intensity occurs, the diffraction is measured. Typically, there are 2 combined peaks reflecting $K\alpha_1$ and $K\alpha_2$ which overlaps leading

to a separation at a value higher than θ. It is customary to treat the combined peaks as one. Results appear as an x-y plot and in some cases in a table format where Intensity (I) = peak height intensity and relative intensity = I/I_1 x 100 [29].

For the unknown sample, d-spacing of obtained peaks are measured using Bragg equation mentioned earlier. The unknown d_s obtained are matched with known materials based on the unique nature of the d-spacings of each mineral. Matching is obtained by comparing with d-spacings data of inorganic compounds found at the International Centre for Diffraction Data [30].

1.5 X-ray Scattering Theory

X-ray scattering theory is based on a set of techniques used to analyze the crystalline structure, chemical composition as well as physical nature of materials [31]. The scattered intensity of the beam of X-ray as it hits a sample is related to the angle of scattering, wavelength, and polarization. X-ray diffraction is an offshoot of X-ray scattering as both are considered elastic and the material being scattered is crystalline. Generated patterns from scattering are analyzed using X-ray crystallography.

There are two basic types of scattering techniques; elastic and inelastic scattering (IXS). X-ray diffraction falls under the category of elastic scattering. During elastic scattering, the scattered wave generated from the process has equal amounts of wavelength and energy. This as a result of the dipole nature of the waves as it sends out spherical oscillating motions at the electron base. Basically, scattering starts at the electrons in the atomic shell. In this regard, it may be comparable

to a set of oscillating waves traveling transversely while it generates both magnetic and electric waves in a self-propelling manner [32].

Small-angle X-ray scattering, X-ray reflectivity, and wide angle X-ray scattering are other forms of elastic scattering. In inelastic scattering, the energy and angle of inelasticity are measured [32]. Because of intermediate phases in inelastic scattering (IXS), they are not applied in X-ray crystallography. The classical theory of X-ray scattering is based on a central potential (V(r)) having a scattering angle that predicted by parameter b (θ). For every particle scattered per unit time occurring at θ and θ + dθ, there are incident particles per unit time of b and b + db [33].

In general, in scattering theory, the scattering vector is obtained which is equivalent to $2\pi/\lambda$ (S-S_o) and relies heavily on the wavelength, and unit vector directions of the scattered (S) and incident X-rays (S_o) [34], "The Use of Monte-Carlo Simulations to Calculate Small-Angle Scattering Patterns" [35].

It follows that $S + S_o = 2\theta$, causing the scattering vector to be 4psinq/l of magnitude. It may be seen that most equations resulting from the scattering theory are directly based on the scattering vector.

Incoherent Scattering: incoherent scattering also known as Compton scattering is impossible to achieve at small angles. In this sense, Compton scattering occurs when waves change wavelength and phase [36].

Coherent scattering: This, on the other hand, it refers to as the opposite of incoherent scattering as is represented by [33] as;

$$\frac{I(q)}{I_e(q)} = \sum_k^n \sum_j^n f_k f_j cos[\![q(r_j - r_k)]\!] \quad (1.1)$$

Here, a single fixed particle is responsible for the scattering of X-rays. The equation above forms the standard scattering equation, where I_e represents electron scattering intensity [32], which is used in this case only for a single electron and measurements taken under similar conditions as was obtained in I(q).

Figure (1.5) below depicts the scattering ability of jth and kth atoms which are represented by f_j and f_k. In relation to the equation above, vectors r_j and r_k are randomly selected to form the center the atoms jth and kth.

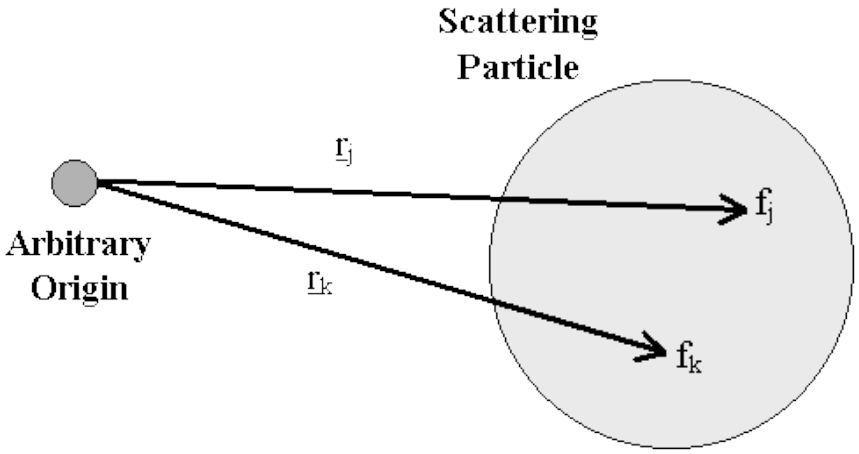

Figure 1.3: Scattering of jth and kth [33].

Form factor (F_k) is represented by the square root of equation 1.1. In general form factors are as a result of facile geometrics [33]. This is depicted in equation 1.2 below:

$$\frac{I(q)}{I_e(q)} = [F_k(q.\mathrm{Rs})]^2 = \left[3\frac{sin(qR_s)-(qR_s)cos(qR_s)}{(qR_s)^3}\right]^2 \quad (1.2)$$

In the equation above, the form factor is for the radius R_s and represented as F(qR) in some instances when applied in scattering expressions of composite nature. Systematic expressions employed in form factors include but are not limited to the following: cylinders, spheroids, parallelepipedon, spherical shells, thin rods, concentric spherical shells, and infinitely flat circular disks [33].

With the increase in particle density, interference in the individual locations of the particles becomes a factor. Where particle density = $\frac{Particle\ volume}{Total\ volume}$

Inter-particle interference becomes a dominating factor in the scattering curve if the density of the particles heightens. This assumption is supported by Debye equation which is equivalent to equation 1.1 mentioned in the previous paragraph. In Debye equation, scattering is effectively done from several particle systems which include inter-particle interference. Debye equation is given below:

$$\frac{I(\underline{q})}{I_e(\underline{q})} = \sum_k^N \sum_j^N F_k\left(\underline{q}\right) F_j\,(\underline{q}) cos\left[\underline{q}(\underline{R_k - R_j}\right] \quad (1.3)$$

Where there are different representatives (N particles) of the form factor as well as R_k-R_j being vectored in standing in the middle of jth and kth scattering particles [37]. This is aptly depicted in Figure (1.6) below:

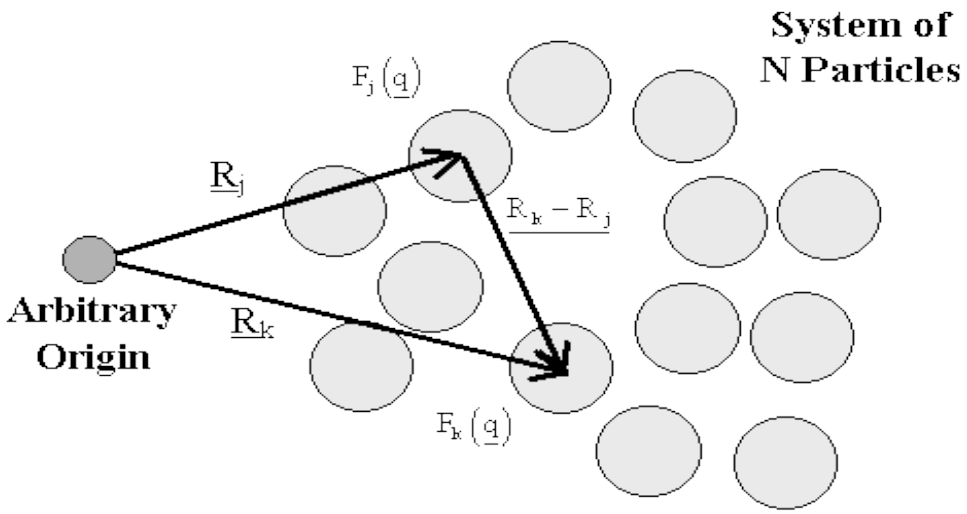

Figure 1.4: Illustration of the Debye equation [33].

Difference between equation 1.1 and 1.2 is that while the former is based on scattering points, the latter is based on scattering particles. There is a definite volume to scattering particles which is lacking in scattering points. This means that it is possible to randomly choose scattering points during scattering modeling, whereas, this cannot be done with scattering particles. This is based on the principle that two particles cannot make use of the same space.

1.6 Objectives of the Research

This research aims to investigate XRD analysis on the structure and performance of asphalt. Furthermore, it is intended to develop the deterioration of pavement model for asphalt pavement with a focus on the molecular level of the asphalt binders. Different samples of asphalt bitumen of a total of twenty-three are gotten from several parts of Canada and tested for aging in the laboratory to investigate their aggregates composition at a microscope level.

The aging asphalt specimens are simulated with the use of three of the main mathematical functions (Pseudo-Voigt, Pearson VII, and Generalized Femi Function). This simulation relies on real aging asphalts from the specimen, the profile of the XRD performed and the analyzed results. It is shown from the XRD data that there are possibilities for different asphalts of different classifications and standards through peak parameters and centroid like crystallite and aromaticity are put into consideration.

Chapter 2

2. Literature Review

2.1 Modelling Asphalt as a Cubic Material (Yen Model).

The modeling of asphalt concrete is an active area of study to make an effective overall performance of pavements. Continuing improvements and developments on issues in computational power and test procedures enable asphalt materials and pavements and microstructure figure (2.1).

(Narve et al., 1975) have exhibited the discovery of bubble points and asphaltene aggregation onset pressures by near-infrared spectroscopy (NIR) for both a live crude oil and model systems. The aggregation onset pressure is viewed as a standard elevation of the NIR spectra resulting from light scattering [57].

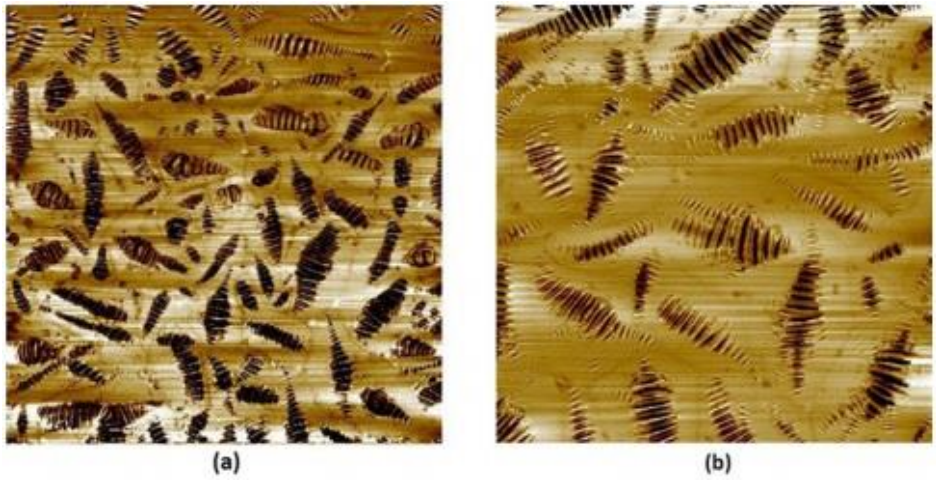

Figure 2.1: Microstructural Features of Asphalt Binders a and b [81].

The asphaltene aggregation from a live crude oil has been demonstrated to be entirely reversible, although 72h of equilibration was required to dissolve the asphaltene aggregates. The outcomes acquired by (Narve et al., 2002) proved that non-precipitate of asphaltene aggregates formed by pressure reduction of model asphaltene system was only partly reversible [57]. Acquiring a good model of asphaltene at the minute level has a tremendous effect on the macroscopic model concrete pavement. Asphalt concrete pavement is a complex system that contains several layers of various materials, different combinations of irregular traffic loading, and diverse environmental conditions. Hence, a practical idea of the high usability of asphalt pavements is one of the most demanding tasks for pavement engineers [59]. The performance of asphalt concrete pavements is closely related to the efficiency of asphalt concrete. It is performance models of asphalt concrete that present the links between several procedures required in asphalt mixture design, pavement design, construction, and rehabilitation.

Some of the factors that influence the deformation behavior and performance of asphalt concrete are maturation, humidity, temperature, and model of loading. (Kim, 2008) explained that many asphaltene models had been designed to capture the consequences of these factors on asphalt concrete performance [59].

The majority of these models, created prior to the Strategic Highway Research Program (SHRP), are scientific in nature. The significance of mechanistic models for material specifications, mixture design and pavement design and created a number of research products depending on the principles of mechanics. The development of using empirical to mechanics during the SHRP made a considerable influence on the function of models in asphalt pavement engineering [59].

Asphaltene is the fraction of petroleum that is insoluble in n-alkanes such as; pentane and heptane but soluble in toluene. According to the given definition, Asphaltene stands out to be made up of molecules polydisperse in the functions, structure, and weight of the molecules and not a homogeneous fraction. They are held responsible for the various issues in the oil industry as it affects the processing as well as production and transportation of crude oil [60]. The Asphaltene is said to comprise of polyfunctional molecules, and their unknown and complex structure of molecules makes it difficult to understand their properties. Since crude oils are a continuum of thousands of distinct molecules of hydrocarbon, the characterization of crude oil through the determination of its composition based on its molecules is not possible. The type of analysis that is often used is the hydrocarbon group type such as; SARA-separation. Another controversy in determining properties of Asphaltene is found in the determination of its molecular weight [60].

Several experiments have been conducted to determine the molecular weight of Asphaltene, but they all have different solutions, and this is due to the fact that the products self-associate regardless of the quality of the solvent. Over the past more than ten years, scholars have projected various Asphaltene model molecules and conducted studies on them so as to realize how well they can mimic Asphaltene' components and the mechanics accompanying the components of Asphaltene[60]. There are two models that have been projected, and they depict Asphaltene' structure. The models are the continental and archipelago models.

The first model has it that asphaltene is made up of a mono polyaromatic ring with naphthenic and aliphatic chains. The second model has it that Asphaltene comprises of small polyaromatic sections that consist of naphthenic and aliphatic moieties. The size of the polyaromatic rings is usually

assessed by studying the UV-visible spectra and the direct imaging of molecules with high-resolution transmission electron microscopy accompanied by molecular orbital calculations [60].

The polyaromatic sections of the Asphaltene are made up of seven amalgamated aromatic rings. The component is known to concentrate the common section of the metallic elements and heteroatoms in crude oil. The Asphaltene have both the basic and acidic functionalities as they have both the acid and the base numbers. The derivatives of pyridines and the benzolog are said to form the basic components of Asphaltene while the acidic nature is known to be formed by the phenolic and carboxylic acids [60]. The self-association of characteristics of Asphaltene have been studied and experimented by taking the measurements of the molecular weight of contents in solution. To vindicate the self-association of Asphaltene as observed, several models have been postulated by different scholars. The models include the fractal model and the peptization model.

According to Gray, Kilpatrick and Yarranton 2005-2008, the main factors that rule the self-association property of Asphaltene are yet to be identified [60]. This means that the self-association models are to be ruled out as there is no evidence of their effectiveness. The three researchers discovered this as they tried to characterize and design series of model molecules so as to mimic the Asphaltene' solution components. The pyrene derivatives used by the scholars lacked basic characteristics to mimic the demeanor of Asphaltene in solution. Non-charged molecules are said not to assemble at the toluene-water interface, but the charged terminal groups have a distinguishable attraction for the toluene-water interface. In the study of the impact of side-chain on self-association components of molecules, the researchers discovered that the degree of

aggregation has nonmonotonic relation with the length of the side-chain in that short side-chains have a minimum interference with the mounding of the polyaromatic core [60].

To represent the properties of Asphaltene in the correct manner, the asphaltene model compounds that are perylene-based must give similar solubility characteristics the scholars conducting the experiment discovered that permeable asphalt pavements (PAP) and total phosphorus (TP) flexures are soluble in the existence of little or rather small quantities of a polar compound such as acetone. The interfacial characteristics of Asphaltene are tested through the measurement of the tension of the interface at the toluene-water interface with a PH of 9. The PH provides for ionization of the acid molecules that are in a carboxylate form. The results of the experiment have it that interfacial tension (IFT) goes down with the increase in PH of aqueous phase that is caused by the carboxylic acid groups' ionization. When charged, the perylene-based compounds become more active on the surface [60].

The force acting between two surfaces can be measured using the Surface Force Apparatus strategy. This method was used by some scholars in the determination of the interactions between mica surfaces that are ailed with the model compounds C5Pe (polyaromatic compound) in heptane and toluene (organic solvents) and an aqueous phase. The measured force showed that model compounds behave qualitatively similar with the extracted Asphaltene. Ca^{2+} induces the fabrication of large C5Pe aggregates on the surfaces of mica that end up in longer steric repulsion. Differences in the side chains' structure and the head groups' polarity lead to important variations dynamics of molecular nonsegregation, molecular association and structure of nano-aggregates in large. C5Pe and TP are said to form larger aggregates while PAP and Bisphenol A (BisA) are

known to form aggregates that are small and less structured [60]. Generally, the self-aggregation characteristics of Asphaltene are found to be stronger in heptane than it is in toluene. This is the case because of the hindered association of molecules caused by weakening pie-pie stack from the solvent made of aromatic. Asphaltene does not structure in water bulk phase although the segment between the oil-water interface and bulk organic phase depends on the polar head group of Asphaltene and the organic phase aromaticity. Both the PAP and C5Pe usually orient a lot of head-on at the interface made of oil-water regardless of the side-chain solvent property and substituents of the oil phase [60].

Asphaltene is held accountable for the stableness or rather the stability of the crude oil emulsions. Reduction in the interfacial causes the surfactants surrounding the water area to gain or to be discharged into the oil phase. This will lead to increase in the surfactant concentration thus the reason behind a locally, dynamically stabilized emulsion at the interface [60]. During the production of petroleum crude oil, H_2O is made available as water-in-oil emulsions. The composition, as well as the purpose of the root of crude oil, is concluded to cause variation in the stability of the emulsions. Asphaltene is among the properties that cause the stabilization of petroleum emulsions.

Asphaltene has been declared to be the most effective element in the stabilization of emulsions when closer to the precipitation point. The ability to stabilize water-in-oil emulsions [60]. Particles can act as stabilizers, and such emulsions are referred to as the Pickering emulsions after the name of the person who discovered this idea. Asphaltene is said to behave more like particles rather than molecular surfactants in the stabilization of emulsions, and it could also be the rational motive

behind the interface's elasticity. The Asphaltene models presented in this work helps in increasing the knowledge of the chemical functionalities of the various properties of Asphaltene. More researchers are being conducted to verify the effectiveness of the models presented [60].

XRD Asphaltene has four peaks. The first peak gamma is seen as the saturated packing distance structures, which are from the aliphatic X-ray scattered chains or saturated rings that are inconsistent. The second is the graphane peak or (002) peak which is from a diffraction of X-ray by the aromatic stack molecules [38].The third and the fourth peak is (100) and (110) in the X-ray diffraction which is of the plane structure of the aromatic that could be seen in figure (2.2). They both correspond to the first and the second nearest neighbors that are in the compound of the ring.

The broader the peaks that are in the pattern of the XRD, the shorter the order range and the less long-range order that are in existence in the type of the structure. In overall, the sharp arrow of the XRD pattern peaks is gotten from crystalline samples that have a high degree of order that are in long range. In the asphaltene case, there is a good range long order in a similar direction.

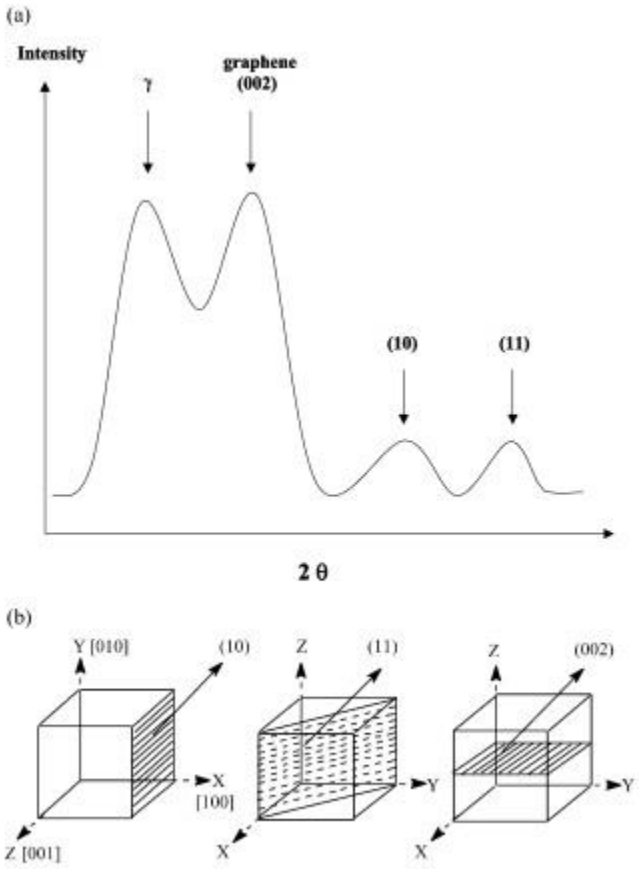

Figure 2.2: X-ray diffraction pattern peaks and corresponding planes [82].

In the crystal that is solid and a short-range order in the order, this is the reason they are in some peaks shape and a broad peak in the whole of the patterns of diffraction.

2.1.1 The modified Yen Model (Yen-Mullins Models)

The asphaltene research structure, the weight of the molecular and properties have all been revolutionized in recent times. (Mullins, 2010) investigated and showed that the uncertainties most especially the molecular weight of the asphaltene is dramatically improved. Many studies

have been conducted using different procedures to uncover or even improve the molecular uncertainties and the structure of the colloidal of Asphaltene for previous years [40]. However, it is clear that the more one moves deeper in the study of Asphaltene' structure and chemical properties, the more difficult is getting due to the complex structure of the Asphaltene as seen in figure (2.3).

The Yen model that has been modified gives us a method of handling, designing, and analyzing data that is enormous. The present research on asphaltene is active, and it is reaching beyond applications that are familiar in order to enhance new objectives in the area of resource utilization [40]. Due to this progress, making use of the Yen model, the asphaltene science can be approached based on a first principles basis in associated part with the bulk properties of asphaltene, thereby simplifying the analysis [40].

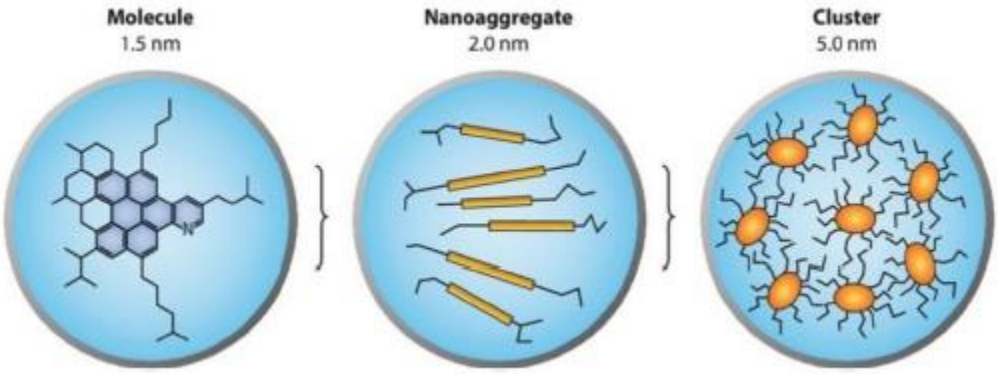

Figure 2.3: The modified Yen Model [41].

In the year 2012, Mullins investigated asphaltene nanoscience model and concluded that it correlates with the modified model of Yen. We believe that the finding discloses and finds a solution to

existing problems at the non-scale of the asphaltene where the majority of the compounds relative acted consistently which includes the structure, composition and the behavior phase of asphaltene in the below figure (2.4) [42].

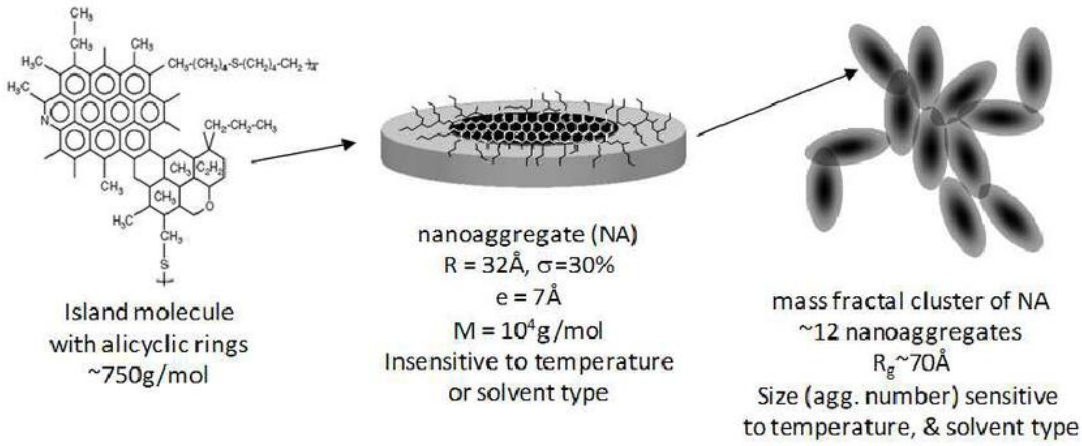

Figure 2.4: An altered figure of the asphaltene nanoscience showing the consistency of phase behavior of asphaltene from the modified Yen model [42].

However, for a better understanding of hydrocarbons, reservoir fluid technique is quite important. It is a matter of the fact that fluids extracted from reservoirs are not in the state of equilibrium, and it is mainly due to the gas discharges owing to the effective procedures. The gas discharge occurs at the later stages of extraction, and it has potential to affect the concentration of the fluid. This study takes into account the one-dimensional diffusive model of Zuo, for the sake of delineating gas discharge in oil reservoirs and the authors have used its simplified form along with the Maxwell-Stefan diffusivity and the thermodynamic non-ideality. To explain further, (Zuo et al., 2016) came up with a model that specifically resolved the issue of moving boundary delinquent that is confronted while gas charges into oil basins [41]. On the other hand, Maxwell-Stefan

diffusivity is a model that is used to explain and comprehend the process of diffusion in multicomponent systems [43].

The diffusive model is reformed by attenuation of the three components in the Flory-Huggins regular solution model with the help of Peng-Robinson equation of state. The reformed model, which is developed through the combination of three components in the Flory-Huggins, then contributes in triggering the gas from the oil reservoirs. Flory-Huggins regular solution model is actually a theory that is based on the mathematical aspects of thermodynamics of polymer solutions. The findings have been clarified to a large extent that the process of triggering the gas from oil reservoirs is subjected to the alteration in the volume of fluid owing to the impact of Asphaltene' dissemination and ejection that is manifested by the gas leakage that occurs at the later stages of the process [43]. The overturn of density causes the asphaltene to move from top to the bottom of oil, and it happens very quickly.

Other uses of the thermodynamic model include; generation of the vapor-liquid equilibrium, production of the liquid to liquid stability, and some boundaries that include the spinodal and bi-nodal phase. Followed by the calculations of Spinodal Curve and Binodal Curve, activity coefficient model was calculated that helped to derive the findings of experiments in an effective manner. For the sake of comparison, the differences in the concentration of the fluid, which are generated with the help of altered model are plotted against the phase boundaries [43]. The poor solvents are responsible for triggering instability in the asphaltene phase, for instance, gases. Moreover, the diagrams demonstrate that if the temperature is increased then instability of the asphaltene phase tends to decrease and vice versa.

The sensitive analysis of phase designates that the phase volatility of asphaltene upsurges with a reduction in the gas and solubility indicators of maltene, temperature, the molecular mass of maltene and augmenting the parameters that are related to the solubility of asphaltene, for example, the molecular weight of asphaltene [43].

2.2 Aging of Asphalt Binder

The asphalt aging is one of the main factors that are responsible for the deterioration of pavement of asphalt in the roads, and it decreases under traffic conditions that are heavy. The aging method of asphalt binder has been studied extensively by [44]. The majority of the procedure involves a temperature of about 100°C to 200°C. It found by the author that the correlation of the laboratory method relative to the aging field was almost created on the basis of the number that is limited factors that are left without consideration and this includes penetration, softening, etc.

It was observed and analyzed from the research that the use of (XRD and GFF analysis) the effects of the aging of asphalt binder caused by improper mix and weather changes in the petroleum asphalts of the Canadians that have been used to construct all of the transportation road networks. (Shirokoff et al., 2007) discovered that X-ray diffraction has shown that wax content contributes majorly to the reversible process of aging in figure (2.5) and (2.6). In addition, they reported that at a low-temperature conditioning, small and large clusters asphaltene sheet measurement are also reasons for the loss of grade during a low-temperature condition [45].

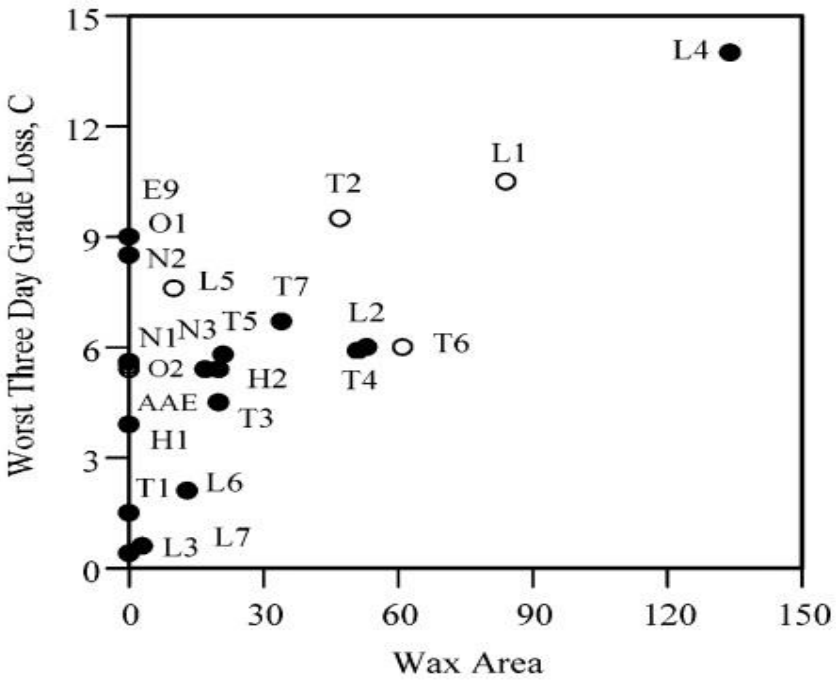

Figure 2.5: A modified wax area in the diffraction spectrum X-ray for a worst three days loss of grade [45].

(Dow, 1903) studied that all bitumen goes through a more or even less quick change with aging with two major causes responsible. (a) Surface hardening and this is as a result of aging and maybe possible as a result of the evaporation of few light oils. The process begins at the surface and slowly to penetrate into the bitumen and (b) Hardening of the entire mass, this occurs as a result of condensation of molecules the two changes happen in the bitumen [46].

In addition, (Brown, 1958) proposed that when asphalt oxidizes in the pavement, few of the resins and oil surge into the pavement subgrade while the major aging process is that of the oxidation. As the course of aging goes on, the non-polar oil will remain unchanged substantially as a result of a decrease in the resins and increase in Asphaltene [47].

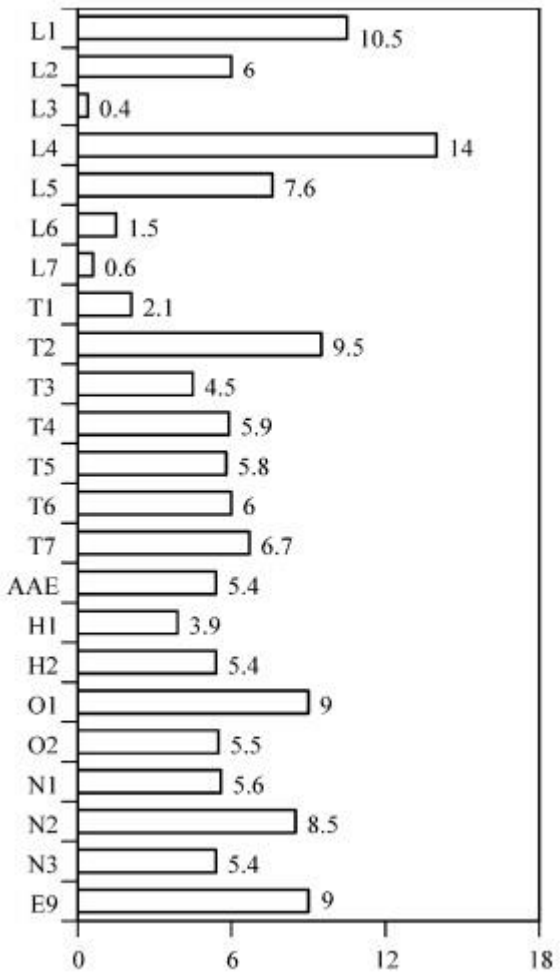

Figure 2.6: The Aging of Asphaltene in worst three-day grade loss [45].

This indicates how the smaller resin molecules are being converted to a larger aging of the asphaltene [47]. Then again, longtime aging is influenced when being exposed to high temperature and precipitation; also, relies on asphalt binder in various regional areas. Asphalt binders do change their physical and chemical characteristics as a result of maturation process on time [48]. A small period of aging occurs during the blending, clearing, compacting and long-haul maturing

amid transportation service when it comes to highways. The rolling thin film oven test (RTFOT) has been approved as an effective process especially in analyzing week old maturation.

The solidifying of petroleum asphalt used in the construction of the road as a result of a decrease in the movement of oxidation is one of the key reasons that restrict the life to become meaningful and differs based on the source of asphalt performance is very vital. Road asphalts in cold moderate environments such as Canada hardly get to a high temperature of more than 60^0C. In the lab, modeling of the age solidifying process is, however, usually performed at higher temperatures to acquire information within a given time [48].

The relationship among long-term maturation of asphalt in the field and high-temperature research laboratory aging have, specifically, an inclination towards higher average molecular weights and variations in the fractional composition such as a pattern to higher levels of the more polar fractions. [49] [50] have analyzed in detail the formation of oxygen that contains functional groups during oxidation of 15 part per million (ppm) films at 130^0C. This and other work associated with asphalt composition and resilience has been examined by [50]. Results for laboratory-aged (24 h, 130^0C, 15 ppm films) and the same field aged asphalt produced from eleven to thirteen-year-old asphaltic concrete cores were compared [50]. An understanding was enhanced considerably provided the probable difference in air void content of the mixes and the benefits of this factor in asphaltic concrete oxidation rates [50]. Nevertheless, the importance of 130^0C asphalt maturation is inquired by variations in the availability of reactive species when compared to standard temperatures. In the field, slow reversible molecular structuring may tend to obstruct available reaction sites serially [50].

As asphalt source and the propensity for steric hardening is associated, evaluation of oxidation rates at high temperatures may cause glitches and wrong conclusions. This would have an impact in reducing the rate of reaction in the field when compared to it when at a high temperature beyond that anticipated from the most basic Arrhenius temperature [51].

Also, asphalt aging has a propensity to go fragile and harden as a result of direct exposure to heat, oxygen and Ultra-violet light during storage, mixing, transport and setting up, and in-service life. These maturation processes lead to a decrease in asphalt properties as stated in introduction section such as high-temperature cutting and low-temperature cracking, and reduce the lifespan of pavement. The photochemical transformation of asphalts must be taken into consideration in the study of the performance of asphalt pavement, particularly in regional areas where high solar radiation intensity takes place, for example, Africa.

Several methods have been used since, to examine the procedure of asphalts maturation and where the greater part of the study applied standard rolling thin film oven (RTFO) test to replicate the short-term aging of bitumen. The aging of asphalt is simulated by applying two of the main mathematical functions (Pseudo-Voigt and Pearson VII). Make use of real aging asphalts from the specimen. Frequently, the XRD profiles were measured, and the results examined [51]. The XRD showed that it is possible to identify asphalts of various standards classification through peak centroid and other factors.

One of the significant factors for identifying the lifespan of constructions in which asphalt has been applied is the impact applied on the asphalt by the climatic conditions. The overall complex

changes in the properties of asphalt by environmental impacts, to the detriment of the construction concerned, is called aging or maturation. The aging phenomena of asphalt are broadly examined by [51].

Only empirical methods seek correlations between aging phenomena and properties of the asphalt. Several methods explained the purpose of acquiring direct data by short time tests on asphalt behavior after long exposure. Based on the literature, the action of oxygen is one of the major elements responsible for the occurrence of the aging/maturation process. When asphalt is subjected to atmospheric oxygen, the chemical nature of which relies upon a vast extent upon the temperature will experience change. (Shenoy, 2002) revealed that at temperatures above 100^0 C, dehydrogenation occurs, as is noticeable from the water produced and carbon dioxide produced. At lower temperatures such as 25^0 C or 50^0 C, the oxygen required for the oxidation is quantitatively bound in the bitumen, and no water or carbon dioxide is produced [52].

The rate of the oxidation may be put into practice using oxygen absorption measurements. The total rate oxygen absorption was discovered not only to be identified by the chemical nature of the asphalt but also by the physical transport of the oxygen from the encompassing atmosphere to the interior of the material. For that reason, it is also a physical problem, one of diffusion specifically.

Asphalt binders age primarily due to two major components:

(a) Volatilization of light oils found in the asphalt

(b) Oxidation by reacting with the oxygen in the environment

The mixing and anxiety in the hot blending facility and through placement ages the binder by both mechanisms simply because of the high temperature and airflow needed in the process. In this work, the rolling thin film oven (RTFO) process is used to induce this form of maturation. Immediately after the asphalt road is constructed, maturation precedes, but the oxidation mechanism rules mainly because of the comparatively average temperatures of the environment [53].

The bituminous binder is becoming expensive day by day owing to augmented prices of petroleum and crude oil products. It is expected that depletion of fossil fuels will lead to more high prices and scarcity of bituminous binder in the new future, and that is why construction companies are looking for the alternative of the bituminous binder. Experiment based researchers have shown there are great prospects that bituminous binder can be replaced with the bio-binder owing to its better rheological properties. This research is quite important in that it tends to explain the rheological and morphological characteristics of the bio-modified binder, which is obtained from swine manure [54]. Before proceeding, it is necessary to know the chemical characterization of bio-binder from swine manure.

The process of thermochemical liquefaction uses carbon dioxide, which can minimize the concentration of greenhouse gases in the environment. On the other hand, nutrients containing nitrogen, phosphorus, and potassium are left, that are used as fertilizers for crops. Bio-binder was produced from swine manure by using nitrogen gas, at 305°C temperature, 10.3 MPa pressure and 80 minutes run time of reactor. Residue material containing bio-binder was collected after the mixture was cooled down and separated from water [55].

Chemical characterization involved the assessment of the compatibility of bio-binder with that of asphalt binder. SARA analysis was carried out, in which the four major constituents, i.e., naphthenes, saturates, resins, and aromatics, of asphalt binder, were separated by chromatography [55]. The comparison depicted that the major components of bio-binder are resins and some polar aromatics. Chemical characterization and comparison between asphalt binder and bio-binder reveal that there is no compatibility between the two as both have nothing in common except resins and few saturates.

The assessment of rheological characteristics was performed by combining the bio-binder with PG 64-22, which acted as a base binder. Both the components were mixed meticulously at 120^{o}C for 30 minutes. Bio-modified specimens of bio-binder with base binder were prepared using 2%, 5% and 10% of bio-binder with respect to the base binder. The results depicted that more concentration of bio-binder reduces the viscosity, and 10% weight of bio-binder in base binder lowered its temperature up to 4.6^{o}C. Moreover, the evaluation of chemical characterization of bio-binder and asphalt binder revealed that bio-binder is comprised of olefins, unsaturated carbon bonding, and high concentration of oxygen and nitrogen [55].

The findings of these tests shed light on useful properties of bio-binder. Bio-binder was obtained from swine manure, and the conditions for experiments were 380^{o}C temperature and 400 atmospheric pressure. In order to convert the swine manure into bio-binder, thermochemical liquefaction process was used. For this experiment, the base binder was PG 64-22 which is an asphalt binder, and it was mixed with bio-binder 5% by weight of PG 64-22 [54]. The result was a homogenous mixture of bio-binder, and base binder and the mixing process was carried out with

the help of the mechanical shear device. In order to ascertain the rheological characteristics of bio-modified binder (BMB) and non-bio modified binder, chemical tests namely; rotational viscosity test, dynamic shear rheometer test, and bending beam rheometer test were performed, and these tests are also termed as Superpave characterization test. These results of these tests revealed several distinct features of bio-binder.

First, the addition of bio-binder reduced the viscosity of base binder to large extent, and the viscosity of bio-modified binder (BMB) was inversely proportional to the concentration of bio-binder [54]. Second, bio-modified binders (BMB) are very elastic owing to the lower phase angle attributed by the bio-binder obtained from swine manure. Third, the bio-modified binder (BMB) is capable of remaining stable at a higher temperature, which will be helpful to avoid low-temperature cracking of pavement with the change of temperature. The chemistry of PG 64-22 was not affected by the addition of bio-binder in any way, thus revealing that mixing does not disturb the traditional chemical properties of asphalt binder. In the context of aging, aged sample bio-modified binders (BMB) showed 62.9% decrease in viscosity, if compared with the base binder. Fourier transforms infrared spectroscopy of modified bio-binder showed that the bio-binder reduces the stiffness of base binder as weakens the bond between carbonyl and sulphoxide chains of base binder [54].

If bio-binder is used with the asphalt binder, then it will enhance its rheological properties. Moreover, use of bio-binder will help in the reduction of carbon dioxide and depletion of fossil fuels and that of pollution caused by animal muck. The use of bio-binder will also reduce the need for storage houses to dispose of animal waste [55].

Increase in oil prices equally affects the price of hot mix asphalt, which led to the discovery of alternative unstable petroleum products. Asphalt binder is an important component of hot mix asphalt, which is used for the construction of pavements of airports. In order to improve the quality of asphalt binder, different components like polyphosphoric acid (PPA) and crumb rubber are combined with it. The environment friendliness of fossil fuel is questionable, and moving to the environment-friendly material is the priority of modern scientists [56].

Bituminous-binder can be replaced with a bio-based binder which can be produced by swine manure through hydrothermal processing. The process involves the liquefaction of the swine waste in the high-pressure batch reactor. The optimum temperature for this experiment was 500^{o}C, and the optimum pressure was 34.4 MPa. In order to mix the swine manure in the reactor, the magnetic mixture was used [56]. The obtained liquefied oil was hydrogenated to obtain the gasoline, bio-binder and other useful components.

The obtained bio-binder is the residue of the process of thermal cracking. The chemistry of the bio-binder was ascertained with the help of an E 2400 II CHNS/O analyzer. Moreover, Karl Fischer titration was adopted to determine the amount of water in bio-binder and concentration of ash was found by using ASTM D482 specification. The assessment of different compositions of saturates, aromatics, resins and Asphaltene was carried out with the help of solvent separation process [56].

The comparison of bio-binders and asphalt binders reveal that bio-binders contain more composition of Asphaltene and resins and comparatively less composition of saturated and

aromatic composites. The bio-modified binder was added to the asphalt binder, and four tests were carried out to determine the important flowing characteristics of the asphalt binder, namely viscosity, dynamic shear rheometer, bending beam rheometer and the asphalt binder cracking device [56]. The findings reveal that adding the bio modified binder to the asphalt binder has significant benefits like reduction in viscosity, enhanced contact with the solid, increased toughness of the composition, and reduced mixing temperature.

The results of this research study present bio-binder as a viable chemical that can be added to the asphalt binder for improved properties. Moreover, the use of swine manure to produce bio-binder will significantly reduce the environmental degradation which is caused by the rampant use of fossil fuels. Despite the advantages of BMB, there is still a need of PPA, when the temperature is increased, and further research can help to find the replacement of PPA in the asphalt binder [56].

There are four main factors of physical degeneration of asphalt pavement.

a) Rutting (permanent deformation) as said before, caused by progressive movement of materials under recurring application of loads at high temperature.

b) Fatigue cracking caused by application of loading which is higher than the structural design requirements.

c) Low-temperature thermal cracking caused by the progression of thermal stress that exceeds the fracture strength at low temperatures.

d) Moisture damage (stripping) of asphalt pavements caused by the lack of an adhesive bond between the asphalt and aggregate as a result of the presence of moisture. Stripping is one of the factors that lead to rutting and fatigue cracking and it can lead to the disintegration of the pavement [70].

An asphalt concrete failure brought about by low-temperature cracking is a big task for suitable pavement performance and service life.

Early maintenance or replacement of the damaged road is the periodic task by the construction expertise and engineers. The effects on the economic aspect of this maintenance are a tremendous amount of money for the taxpayers also putting more time waiting for road construction season after season. Hence, it is essential to examine and understand the essential cracking temperature, for example, in cold region, of the asphalt cement and concrete so as to prevent failures.

However, laboratory tests that assess rutting use the maximum pavement design temperature, while tests that examine fatigue potential use the average pavement design temperature. Nevertheless, thermal cracking tests use the minimum pavement design temperature plus 10^0C. The minimum pavement design temperature is increased by 10^0C to decrease the testing time. These results are corrected to the minimum temperature using the time-temperature shift factor [70].

Currently, rutting is an important kind of damage of asphalt pavement at home and abroad, particularly the question of initial rutting of the asphalt pavement. Rutting creates a remarkable financial loss to country roads and highways and it is a disadvantage to the community that needs

close attention. Presently, the successive steps are to enhance high-temperature stability performance of asphalt mixtures, the primary methods regulate the aggregate grading of asphalt mixtures, use modified asphalt or compound modification asphalt (uniquely altered asphalt, Specially Modified Asphalt (SMA)), building up constructional management and quality control of asphalt pavement. Despite the fact that all of the approaches have additional development in high-temperature stability performance of asphalt mixtures to some extent, it does not resolve the current problems. Methods that search for an affordable and efficient strengthening method for solving asphalt pavement rutting in a subtropical region throughout the summertime is essential [70].

Asphaltene is notorious for clogging the oil wells and related facilities. The phenomenon of clogging has been observed in lighter crude oils as compared to the heavy oils. Although the Asphaltene are considered harmful to oil reservoirs they are used to construct roads, as waterproofing materials and inhibitors against corrosion [61].

The contents of asphaltene are crucial in order to determine the appropriate method that could be used for the processing and refining of crude oil. The elemental analysis of Asphaltene depicts that their carbon to hydrogen ratio approximately is 1:1.2 Out of the large number of methods available for gauging the molecular weight and size of the Asphaltene, only two methods are found to be reliable when it comes to the consistency in the finding, and these methods are called spectroscopy and molecular diffusion, which is comprised of different spectroscopy and diffusion technique. Different types of spectroscopy and diffusion methods suggest that molecular weight of the asphaltene lies somewhat between 750 g/mol to the 1,000 g/mol [61].

Nalco energy services is a method which is developed to thwart the formation damage by the Asphaltene, and this method has been quite successful in the inhibition of asphaltene deposition at the oil reservoirs and wells located in different parts of the world [61].

In Venezuela, 9,300 m lengthy pipeline was clogged, and all the apparent methods failed to clear the pipeline, but later on a 2-in. coiled tubing was entered from five different entry points that cleaned the plugged pipes and subsidized the potential loss of $1 million for the company. Moreover, despite many drawbacks of asphaltene, it is quite important to comprehend the oil reservoir's past circumstances and connectivity [61].

Through these experimental studies, it seems that high viscosity asphalt has the character of high viscosity, low penetration, high softening point and little ductility. The mixture has attributes of high intensity, high modulus, perfect high-temperature performance, water stability, anti-fatigue property and mechanical property. It is more best suited to asphalt middle layer and subsurface at high summer temperature and heavy axial load, which can mostly examine the high-temperature performance, water stability and fatigue life of asphalt pavement. Since they bring greater social and financial benefit, the application possibility of high viscosity asphalt is beneficial [70].

2.3 Precipitation of Asphaltene

The findings have also revealed that Asphaltene is more likely to precipitate if the gas is added to oil reservoir in a swift manner. It is a matter of the fact that the maximum amount of asphaltene in oil reservoir is predetermined, if asphaltene accumulates at the juncture of oil-water connection, then it has the potential to render the asphaltene quite unstable. These findings attest the

phenomenon that asphaltene has the propensity to deposit at the juncture of oil and water contact. [43].

There are specific conditions that render the precipitation of asphaltene during the oil production. Asphaltene could be defined as hydrocarbons which don't dissolve in straight chain aliphatic hydrocarbons, but they are easily soluble in aromatic hydrocarbons [61].

(Hussam et al., 2004) examined that asphaltene precipitation rate reliance on asphaltene content of the oil diminish as the heteroatoms content of both the crude oil and Asphaltene becomes higher. Nevertheless, asphaltene precipitation increase as the aromatic carbon fraction and the degree of branching of the asphaltene molecules increase [62].

However, asphaltene precipitation rate dependence on the amount of n-heptane (i.e., light paraffin hydrocarbon) added diminish as the tendency of the asphaltene molecules for aggregation increase [62].

(Groenzin et al., 1999) described that asphaltene molecular weights are identified to be, 800 g/mol [63]. Asphaltene study conducted at various length scales (such as nano scales) into a general picture involves creating structural relationships is the key part of Petroleomics [64].
Compositional variations of the fluid that contains Asphaltene specifically have an effect on their aggregation state. Furthermore, asphaltene molecules to correlate into small nano-aggregates that are transformed into larger clusters and finally precipitate. (Mullins, 2010) discovered a clear explanation of the relationship between molecular architecture and aggregation of asphaltene. In addition, the function of the resins, particularly on Asphaltene' stability, has always been

questionable [40]. Nevertheless, a more specific view is surfacing [65]. This is in relation to the author's knowledge in asphaltene research over the past several years. It concentrates on asphaltene separation, characterization, structure, and function of resins [65].

(Nikhil et al., 2001) revealed that Asphaltene of various attributes is discovered to precipitate at various pressure. Decreasing the pressure creates a few flocculants (flocs) and, created flocculants (flocs) are remaining the same. This feature reveals that Asphaltene is stable and should be resin deficient. Latter, flocculants (flocs) are most likely to have more resin and be tackier and thus having a negative impact on crude oil production. In addition, these authors discovered that field asphaltene precipitation is proven to be basically reversible with pressure over a certain time (minutes). It is even worse to identify that Asphaltene produced by pressure reduction on live crude oil really differ from those prepared by solvent precipitation from dead oils. Nevertheless, most authors use similar terminology, called asphaltene in each case [66].

Asphaltene precipitation in crude oils can take place not only by adding solvents such as heptane but also takes place at higher temperatures. Hence, self-precipitation of Asphaltene in crude oils with various compositions takes place at various temperatures [67]. This occurrence is only dependent on the composition compatibility; heavy crude oils with high asphaltene content may be more stable than light ones with low asphaltene content.

(Tharanivasan et al., 2009) identified a method to use and are called (conventional solution approach) to design asphaltene from the onset and quantity of asphaltene precipitation from their prepared specimen diluted with n-heptane. These authors' revealed that the composition of the samples could be identified using a mass average of the crude oil of saturates, aromatics, resins and Asphaltene (SARA) analysis [68]. The average aggregation number of the Asphaltene was a

molar average of the crude oil asphaltene aggregation numbers. Lastly, the molar mass distribution of the Asphaltene in the prepared specimen was organized by adding the weighted mole distributions from crude oil and attained a result showing the Asphaltene from the various crude oils and did not interact with each other for the limited timescale. To generalize the method created, the results need to be tested over longer timescales, the data support models that presume no such interaction [68].

Nevertheless, the models effectively estimate the amount of heptane needed to precipitate with Asphaltene in a range of blends and estimate it when blends are less stable than the constituent crude oils. However, the model was less successful at very high asphaltene dilutions, for instance, when toluene had been added to the crude oils before heptane addition. At these levels of dilutions, Asphaltene tends to dissociate, and the assumption that the average asphaltene aggregation number is constant doesn't work [68].

The research shows that there exists an inverse relationship between the pressures applied to extract oil and when the precipitation of asphaltene, is higher, the lower pressure will be the precipitated amount of asphaltene. In order to quantify the amount of precipitated asphaltene, a filtration technique has been proved to be the most effective one in this regard. The microscopic analysis of the particles of asphaltene helps to understand the different phases of asphaltene as the temperature and pressure changes, and the most suitable technique in this regard is the high-pressure microscope analysis developed by DowBR, (which is now Schlumberger). The precise evaluation of asphaltene precipitation highly depends on the quality of the sample [61].

A good background of understanding the conditions at which the Asphaltene precipitate and the level at which the precipitated Asphaltene can be redissolved is very essential. Even though there is substantial data obtainable in the literature on asphaltene precipitation, (Peramanu et al., 2001) research generally aimed at the measurement of the ratio of the solvent to bitumen at which Asphaltene start to precipitate. There is limited data available on the influence of the reversal of solvent addition and recovery. Also, these data assist in analyzing the validity of asphaltene precipitation models according to solution thermodynamics [69]. For example, the theory of thermodynamics forecasts that asphaltene precipitation is completely reversible while the colloidal theory forecasts irreversible precipitation.

2.4 Current Situation of Emerging Technologies for Upgrading Heavy Oils

Over the past years, several technologies have been established for residue oil and heavy crude upgrading. Processes that are grounded on hydrogen addition, carbon rejection or even a combination of both processes need to be upgraded more often. The change in the prices of crude oil and the increase in production of extra-heavy and heavy crude oils have rendered to the increase in the number of researchers that aim at upgrading the heavy materials. Emerging technologies are the new approaches to the aspects of crude oil. The technologies that have been established in the crude oil sector include processes that are grounded in hydrogen addition, rejection of carbon or an aggregation of both processes [71].

Carbon rejection has been used since 1913, and it is among the first processes of conversions used in the oil industry. The processes involved in these types of technologies include coking, thermal cracking, and visbreaking. A lot of technology has been developed to ease the processes, and the

last advancement was made in the last nine years. Hydrogen addition is done to reduce the ratio of carbon-hydrogen where hydrogen added is extracted from natural gas [71]. Their technologies are a group independence of the reactor in use such as slurry-bed, moving -bed and fixed-bed processes. Axens technology has got to a significant commercialization level as it utilizes its Hyvahl process. For the ebullating-bed processes, the LC-Fining process of the Chevron Lummus Global offers a final product that has around 25% of non-converted residue. The slurry reactor technologies utilize disposable catalysts that are intended at decreasing the catalyst inventory cost. The basic advantage of the combined technologies is based on the impurities reduction, low-value by-product elimination and the quality of products [71].

Some of the upgradings include the gasification, slurry phase reactor, delayed coking, and deasphalting. Emergence technologies have come up to curb the problems in the production of oil. Some of the problems in the oil industry include reservoirs getting scarce, inadequate processes to process the heavy and extra-heavy crude oils. The technologies include Hydrocracking technology (HCAT) processes, heavy to light (HTL), Genoil hydroconversion upgrader (GHU), Instituto Mexicano of petroleum (IMP), NexGen-Ultrasound processes, heavy residue hydroconversion (HRH), catalytic crude upgrading (CCU), Sonocracking, Sulphco Inc and Eni process.

The HCAT process was developed by the headwaters technology (HTIG) [71]. The technology is a catalytic heavy oil upgrading one as it converts low-quality feedstock into the synthetic crude oil. To achieve high conversion of oil, the procedure uses a catalyst that is molecule-sized, and it is chemically created within the reactor system by conditioning process. The technology reduces the formation of sediments as well as improving the conversion of heavy oil. Various feedstocks

have been tested using the HCAT technology to test its effectiveness, and it has been proven to meet its purposes [71].

HTL heavy oil upgrading was developed by Ivanhoe Energy. The technology is a heavy oil upgrading process that is used to convert crude oil that is heavy and viscous more valuable, transportable and lighter. It operates at a notable small scale. The plant can be located upstream or midstream. In the upstream location, it can be placed at the well-shed. It uses circulating transport bed in heating the heavy feedstock to convert them to lighter products. The main disadvantages of this technology include low capacity for extra-heavy oil processing, low sulfur reduction, large size equipment for recovery of heat, the high formation of products that are susceptible to polymerization [71]. The technology is currently in use in the Middle East, Latin America and Canada.

Genoil process technology is used to upgrade and increase the yields from refinery residues, bitumen, and heavy crude. Depending on the type of feedstock, the technology is known to make conversions ranging between 70%-90%. Genoil hydroconversion upgrader (GHU) converts heavy feed into gas oil, diesel, and naphtha as it is based on fixed-bed technology. The effectiveness of the technology was tested in 2007 where it showed a notable change in the quality of the upgraded oil [71]. The viscosity process was established by Ellycrack AS Company. The technology is used to upgrade heavy oil at the oil fled. The process is made technically feasible by exerting low pressure and low temperature. The advantages of this process include no advanced catalyst, low temperature, fine-grained minerals that are used as heat carriers, self-sustained with energy, sulfur and metal reduction. The current situation of the process is that the developers are preparing the

pilot plant for experimentation. The first testing program was done in 2007, and there were active results [71].

IMP-HDT process (IMP process is based upon the catalytic hydrotreatment/hydrocracking of the heavy oil) is designed to remove sulfur, metals, nitrogen and Asphaltene and an important conversion of the heavy sections of the feedstock to distillates that prove to be of more value. The technology is characterized by entrancing investments return due to a reduction in the costs of operation and relatively low investment. The characteristic of the IMP technology enhances the refining, conveyance, and handling of the heavy and extra-heavy crude oils [71]. The technology can be applied as a first step in the processing sector for heavy and extra-heavy crude oils and conversion of the heavy and extra-heavy crude oils to high-value crude oils. Currently, the technology has been tested, and it has shown satisfactory results where both the economic and technical advantages have been certified. Heavy residue hydroconversion (HRH) Process (Heavy Residue Hydroconversion) converts the heavy and extra-heavy crude oil to a more valued product. The process was created by Research Institute of Petroleum Industry. It can be used for two major functions that are wellhead and refining applications for hydroconversion. The process of the technology was investigated in demo scales and pilot plant. The technology is also used by the developers for other purposes such as process development package, transfer of technology and many other activities that are connected to engineering [71].

Catalytic crude upgrading (CCU) process curbs the problems brought about by the nontraditional crude production. Its function is based on the past principles of the fluid catalytic cracking (FCC). Due to its ability to produce a lot of coke, it produces electrical power and steam that are used by

the entire oil extraction and refining firm. It can be used in places where electricity and natural gas are a problem. It is suited to work in areas with heavy oil projects. It is generally used to improve the flow properties of the crude petroleum. Three companies have adapted to the use of the technology, and the results of its effectiveness are yet to be analyzed [71]. Eni Process also is known as The Eni Slurry Technology was created by the Eni Group companies. It is used to upgrade the oil products. Some of the functions of the process include nitrogen reduction, conradson carbon residue reduction, removal of metals and reduction of sulfur. The plant was to be in full operation by the end of 2012.

Heavy oil upgrade project (HOUP) Process puts its focus on two major areas that are a refining of heavy oil residues and converting heavy crude oils into the lighter synthetic crude oil. The process does not have to use hydrogen or a catalyst, and it is mainly based on the process of thermal cracking [71]. The technology is also found to require minimum infrastructure. The technology is yet to be tested so as to join the competitive technological industry. Uniflex Process is a slurry hydrocracking technology. The technology is cheaper as compared to other technologies performing the same function as it does not use expensive catalysts. The technology has already been implemented in countries such as Pakistan for lubricant production and maximization of diesel. It has been proved to be very effective in its functions [71].

Western research institute thermal enhancement (WRITE) Process is used for the process of upgrading. For partial upgrading, the process is very effective and cost saving as it does not require processes such as coking and diluents. The technology is used in the field of synthetic crude oil. Researchers concluded that the technology is effective for the upgrading of bitumen. Value

creation Technology is made of two steps that can either be used as a combination or individually. The technology is meant to produce low contaminants and residues as well as semi-sour crude oil that are light to medium. TRU process (TRU) is a technology used in the improvement of viscosity in oil sand bitumen and heavy oil. The process is used for the removal of metals, and its yields of premium synthetic crude oil are ultra-high [71]. The final product of the technology is usually low in sulfur. The technology has already started its licensing process where its use will be certified and allowed to kick-off in the oil industry.

The petrosonic process is a technology created by the Sonoro Energy Ltd. The technology is a multipurpose one as it is used for several functions. It is used in the reduction of metal and sulfur, increase the API, lower viscosity, upgrading of oil and recovering of solvents. The advantage of this process is that it provides enhanced transfer of mass and a unique cavitational and its use of sonic reactor technology. The selex-asp process also known as the selective asphaltene extraction is used in the removal of contaminants in the oil sand bitumen [71]. It helps in easing the refinery process of the crude oil. Its technical roots have been validated, and various laboratory tests have been conducted regarding the technology showing that its use is of major change in the extraction of oil in the oil industry. The technology was seen to remove sulfur and metals as well as Asphaltene [71].

The increased yields and qualities (IYQ) process is a technology used for the conversion of heavy crude oil that is bottomless and synthetic. The main advantage of the technology is that it greatly reduces short-circuiting as compared to other technologies in the same field. The demonstration of the effectiveness of this took place in 2015. There are many other technologies that have been

developed so far. Other technologies have been upgraded to meet the demands of the changing globalized world as well as the change in the oil industry [71].

EDIEMAC, HUOP, CPJ, WRITE, TRU, and Value creation technologies are used for the rejection of carbon. The Selex-Asp process is used in the extraction of oil while NEXEN Snocracking is used for an ultrasound. For hydrogen addition, processes such as Uniflex, HCAT, ENI (Energetico Nacionale Italiano), IMP, HRH, CCU, and Genoil are used. The processes used in the hydrogen addition can be utilized for the full upgrade of crude oil. The processes used for rejecting carbon have lower oil quality although their cost of production is a bit cheap than those used for hydrogen addition or other purposes [71]. The hydrogen addition processes have been highly tested as compared to other processes, and a large number of the emerging technologies which have undergone through lab testing for verification. Other technologies are yet to be tested in the laboratory while other technologies are waiting for their laboratory test results to be released. Some of the emerging technologies are already in use in the oil industry.

The need for the development of the emerging technologies is to convert the heavy and extra-heavy oils into valuable products through cost minimization. Removal of impurities in the oil has also been part of the project as experts in the oil industry try to digitize the sector. Most of the processes are in the process of being tested or implemented making it hard to testify which technology is more effective than the other. The traditional technology only aimed at hydrogen addition and rejection of carbon in the oil. The oil industry experts are expected to make some considerations before implementing any of the technologies such as properties of the feedstock, the degree of the development of the technology and the oil's chemical properties [71].

Chapter 3

3. Experimental

3.1 Experimental Investigation of Asphalt Binder

The chemical properties of molecular size and structure of asphalt binder are quite important, and asphaltene is the material, which is left after the distillation of the petroleum and crude oil. Asphalt binder is used for the construction of the roads, runways, and pavement, and that is why it is always in high demand. For the chemical characterization of the asphalt binder, there are many techniques, one of which is X-ray diffraction, the short form of which is XRD [39].

Table 3.1 represents a summary of what has been done before in previous studies over the past ten years in investigation experiment of asphaltene in the area of the science of asphaltene.

Table 3.1: Issues in asphaltene science that have been resolved over the past 15 years [27].

Scientific issue	Range of reported values (as of ~1998)	Values (as of 2010)	Width of distribution (as of 2010)
Asphaltene molecular weight	Less than 1000 Da to 1000000000 Da	750 Da	400-1000 FWHM
Number of PAHs in an asphaltene molecule	1 to 20	1 dominates	Small mass fraction with 0,2,3, etc., ring systems
Number of fused rings per PAH in asphaltene	2 to 20	7	4-10
Number of PAH stacks in Asphaltene nanoaggregate	Unknown	1	---
Aggregation number of nanoaggregates	10-100	<10	4-10
Critical nanoaggregate concentration of asphaltenes	50 mg liter^{-1} to 5g liter^{-1}	100 mg liter^{-1}	50-150 mg liter^{-1}
Concentration of cluster formation	Unknown	~3g liter^{-1}	2-5 g liter^{-1}
Size of cluster	Unknown	6mm for small clusters	Probably larger cluster also depending on temperature, concentration
Role of resins in asphaltene nanoaggregate	None to necessary	~15% of crude oil nanoaggregates are resins; resins are not surfactants	Depends on definitions
Relation of nanoaggregates to cluster	Unknown	Clusters consist of nanoaggregates	---
Relation of nanoaggregates in toluene to those in crude oil	Unknown	Very similar in size and composition	---

It is established that the unit of the structure of the asphaltic substances is a structure of aromatic that consist of condensed benzene rings which have a heterocyclic rings inclusion and it forms a flat sheet with a substituent side, i.e., alkyl chain and naphthene rings that are formed pings; around the edges [72]. The individual structural sheet interaction units result in the formation of particles by which the sheets of aromatic hydrocarbons are condensed and are located parallel to one another out of a pile that is surrounded by rings that is either aliphatic or naphthenic.

In the X-ray asphaltene structural studies, the presence of particles that has an ordered arrangement of carbon aromatic atoms on the Asphaltene diffractograms as a peak in the area of 20° to 26°(Cu-Kα-radiation), this peak comes along with observed for graphite which goes with the reflection of (002) band starting from the parallel layers of the carbon atoms. However, there is a superimposed a noise that scatters from the disoriented carbon atoms and a scattering that comes from parallel order aliphatic on the peak that is Methane and alicyclic (non-aromatic character) grouping gamma band. There was a report from (Yen et al., 1961) that in the range of angle regions that are large at 20° to 43° and 20° to 78°, the diffract grams X-rays reveal the peaks of reflections respectively bands (100) and (110) from the two-dimension (2D) flat sheet of the saturated aromatic hydrocarbons.

In order to gain insight of different chemical phases of the asphalt binder, an analysis of the different forms of spectral lines was undertaken with the help of X-ray diffraction. For the experiment, asphalt binder was acquired from the raw oil, and for X-ray diffraction, equipment from Rigaku Dmax 2200V-PC was selected. Moreover, the software used to aid this research study was Version 6.1 Jade software. The set conditions for X-ray diffraction were Cu-K-α radiation, electricity calibrations of 40 kV and 40 mA operations, and scanning speed was

0.001° 2θ/s. For the sake of profiling of data obtained as a result of XRD, two mathematical models, i.e., Pearson VII, pseudo-Voigt and generalized Fermi function (GFF) were used [39].

The analysis of data revealed that asphaltene X-ray diffraction configurations are composed of four peaks. Moreover, mathematical models, i.e., Pearson VII and the pseudo-Voigt depicted that there were totally distinct peak shapes for XRD peak profile [39]. The results obtained with the help of Jade software demonstrated that there exists a significant level of association between the X-ray diffraction peak shapes obtained from mathematical models, i.e., Pearson VII and the pseudo-Voigt and that of GFF data from Mathematical models [39].

The crystalline parameters were computed, which were either low or high owing to the correctness of X-ray diffraction profile fitting. The background intensities of profile fittings were determined by applying three types of backgrounds, i.e., linear, parabolic and 3rd order polynomial, and the residual error of fit was calculated for each of the background intensity with the help of two mathematical functions [39]. The X-ray background intensities could be ranked in the order of their residual error of fit with the parabolic being the lowest, linear somewhere between the parabolic and polynomial and 3rd order polynomial being the highest in terms of X-ray background intensity. In order to gauge the extent of aromaticity and the distance between the layers of aromatic sheets, three exponential and Lorentzian values were used for Pearson VII and pseudo-Voigt, respectively [39].

3.2 Setup Components

The knowledge that most people have regarding the internal structure of amorphous and the crystal solid is gotten from the study of X-ray diffraction. The crystalline structure of the Asphaltene is

known by XRD. If any diffraction is to take place in a crystal where atoms are arranged in planes, the wavelength of the incident radiation has to be in the same order with the distance of the atom's space, which is between crystallographic planes. The planes have a large atomic number that gives rise to a strong X-rays reaction incident.

According to (Trejo et al., 2007), the XRD gives the macro-structural information as well as the crystallite parameter of the molecules that are associated with the asphaltene aggregates. XRD also gives a quality intensity curves. Parameter structure is also gotten from the position and shape of the peaks. The peak broadening that is observed in the patterns of the diffraction is determined by the quantity of amorphous material that is to be investigated in the pattern of the diffraction [73]. Different naphthenes, paraffin and aromatic in the XRD patterns always show that the gamma band could likely rise primarily from the side of the aliphatic chains or the aliphatic ordering ring; the band of graphene (002), that comes from the stacks in the molecules of aromatic and the corresponds bands of (100) to the closet as well as the second-closest neighbor in the ringed compounds [74]. The importance of the band of gamma is that it stands for the packing distance of the chain of aliphatic as well as the layer of condensed rings that is saturated [38]. The technique of the X-ray that is used in this work belongs to [2] and [74] that is used in Asphaltene studies. The crystallite parameter which includes the distance interlayer, the distance interchain, the aromatic cluster diameter, and the aromatic sheet diameter can be calculated from the X-ray pattern of the Canadian derived asphaltene samples.

In the X-ray asphaltene structural studies, the presence of particles that has an ordered arrangement of carbon aromatic atoms on the Asphaltene diffractograms as a peak in the area of 20° to 26°(

Cu-Kα radiation), this peak comes along with observed for graphite which goes with the reflection 0f (002) band starting from the parallel layers of the carbon atoms. However, there is a superimposed noise scatters from the disoriented carbon atoms and a scattering that comes from parallel order aliphatic on the peak that is Methane and alicyclic (non-aromatic character) grouping gamma band. There was a report from (Yen et al., 1961) in the range of angle regions that are large at 20° to 43° and 20° to 78°; the diffract grams X-rays reveal the peaks of reflections respectively bands (100) and (110) from the 2D dimension flat sheet of the saturated aromatic hydrocarbons [2].

The X-ray measures intensities over a range of 2θ=3° to 90°. A similar qualitative peak is exhibited by the curve. The literature studies as made it cleared that XRD pattern of asphaltene contains four main band characteristics, which include the gamma band, the band (002), the band (110) and band (100).

In order to gain insight of different chemical phases of the asphalt binder, an analysis of the different forms of spectral lines was undertaken with the help of X-ray diffraction. For the experiment, asphalt binder was acquired from the raw oil, and for X-ray diffraction, equipment named Rigaku D/max 2200V-PC was selected. Moreover, the software used to aid this research study was Version 6.1 Jade software. The set conditions for X-ray diffraction were Cu-K-α radiation, electricity calibrations of 40 KV and 40 mA operations, and scanning speed was 0.001° 2θ/s. For the sake of profiling of data obtained as a result of XRD, two mathematical models, i.e., Pearson VII, pseudo-Voigt and generalized Fermi function (GFF) were used.

The analysis of data revealed that asphaltene X-ray diffraction configurations are composed of four peaks. Moreover, mathematical models, i.e., Pearson VII and the pseudo-Voigt depicted that there were totally distinct peak shapes for XRD peak profile. The results obtained with the help of Jade software demonstrated that there exists a significant level of association between the X-ray diffraction peak shapes obtained from mathematical models, i.e., Pearson VII and the pseudo-Voigt and that of GFF data from Mathematical models.

The crystalline parameters were computed, which were either low or high owing to the correctness of X-ray diffraction profile fitting. The background intensities of profile fittings were determined by applying three types of backgrounds, i.e., linear, parabolic and 3rd order polynomial, and the residual error of fit was calculated for each of the background intensity with the help of two mathematical functions. The X-ray background intensities could be ranked in the order of their residual error of fit with the parabolic being the lowest, linear somewhere between the parabolic and polynomial and 3rd order polynomial being the highest in terms of X-ray background intensity. In order to gauge the extent of aromaticity and the distance between the layers of aromatic sheets, three exponential and Lorentzian values were used for Pearson VII and pseudo-Voight, respectively [39].

The pattern of the XRD in the Canadians asphaltene seen in present work has similar characteristics with those seen in the literature of [74] [38] [2]. As seen in the next chapter (4) XRD patterns of Canadian Asphaltene have similarities and have 3 peaks characteristics which provide at least three maxima which could be seen at 20° gamma approximately, 002 graphene at 25° and 44° 100 band is a weak indicator of a broad peak 110 which is position in the middle at

2θ=80° is seen. These broad features show that there is a dispersed ordering in the Asphaltene [75]. The distance median is indicated using the graphene band 002 maximum which is seen at an existing of around 25° of the 2θ axis than the line the sheet aromatic of Asphaltene that is calculated by a Bragg equation. The peak 002 is seen around 2θ=25°, showing an interlayer spacing nearly about 3.55 [75]. The peak 002 represents the space that exists between the condensed layers of the aromatic structure. As seen in the literature review, a single graphite crystal structure with an interlayer spacing of about 3.35 and an amorphous carbon which is an interlayer distance of about 3.55 [75] [73].

The value of d_M is associated with the thickness as well as the size of the aromatic sheets. The distance of the interlayer of the asphalt cures of the Canadian samples can be seen in the range of amorphous materials of small order. The average of the distance that is between the saturated structures is calculated in a close manner using the relationship:

$$d\gamma = \frac{5\,\lambda}{8sin\theta} \tag{3.1}$$

The value $d\gamma$ of is calculated, and the report is seen in the next chapter (4). The height average of the cluster of the asphaltene, L_c was determined using the Scherrer crystallite size equation, that demands the value of the total width in a half maximum (FWHM) of the band graphene:

$$L_c = 0 \cdot 9\omega\, cos\,\theta = \frac{0{\cdot}45}{B[1/2]} \tag{3.2}$$

The value for the L_a is reported in chapter 4. The aromatic sheets average number in a cluster stacked, M is determined using the L_c values and d_M through the equation,

$$M = \frac{L_c}{d_M} + 1 \tag{3.3}$$

The diameter of the average layer in the aromatic sheets, L_a can be determined using the Scherer crystallite formula size from the breadth B [1/2] of either (100) band or the (110) band.

$$L_a = \frac{1{\cdot}84\gamma}{\omega \cos\theta} = \frac{0{\cdot}92}{B[1/2]} \tag{3.4}$$

Looking at the XRD derived aromaticity, f_a that is determined by the gamma and peak area (002), the ratio of the carbon atoms that are seen in the aromatic ring even up to the total Asphaltene carbon atoms for aromaticity f_a

$$\boldsymbol{f_a} = \frac{\boldsymbol{A_{(002)}}}{(\boldsymbol{A_{(002)}} + \boldsymbol{A_\gamma})} \tag{3.5}$$

Where $A_{(002)}$is the area under the (002) peak, A_γ is the area under the gamma (γ) peak.

3.3 Sample Preparation

The sample of the asphalt binder is prepared in a thin film on the side of the glass holder by heating up to 150°C for close to 10 minutes in an oven that is dry and this followed by air cooling and removal from the atmosphere of the room.

3.3.1 Thin Film Method

There are different special factors that need to be considered when using the sample of XRD thin film. A high angular resolution is needed due to the fact that the peak from the semiconductor materials is very sharp as a result of the fact that the material has low defect densities. In addition, a number of monochromator crystals in multiple forms are used to give a very high collimated X-

ray beam to the measurement. Before the XRD, each of the samples was put on one glass side and annealed at 150° C for about 10 minutes so to create a thin film that as a thickness of about 1mm.

The diffraction of X-ray measurement is run on a Rigaku D/Max-2200v-PC through the use of monochromatic Cu-K-α radiation operation at 40kV and 40mA. The category of the scan used is about 5-110°2θ at a rate of $0.01°2\theta s^{-1}$ and a time of 5 s/step. The setup is made in such a way that it has a slit divergence of 0.5° and a receivable slit of 0.3mm. Samples were aged for one week and then analyzed at room temperature of 20°C. The width is at half maximum (FWHM), and the fit of the profile is obtained through the use of a person VII and pseud-Voigt which have a background that is fixed ranging over 5 to 35°2θ and 60 to 110°2θ. The pattern of the X-ray creation and analysis were performed through the use of a Jada version having 6.1 software incorporation package Pearson VII and pseudo-Voigt function. The data that has been collected was normalized, and it continued to a background that was common and compared the features using the four main peaks that were measured, i.e. gamma, $(002)_{graphene}$, (100) and (110). The diffraction of all X-ray samples was ready in the sample of the aluminum holder after testing a specimen dimension of 25 mm diameter and thickness of 1mm.

In Table (3.2), we can see the collected specimen from each specific location in some are not known; the samples show followed the PG standard that was set by CGSB.

3.3.2 Powder Method

The powder XRD is the most generally used diffraction X-ray technique for characterizing the materials. As suggested by the names, the form of the sample is mostly in a powder form that consists of fine grains of a one and only crystalline material that needs to be studied. The technique

is widely used for particle studying in suspensions liquid or solid polycrystalline or even the thin film materials. The powder term actually means that the domain of the crystalline is oriented randomly in the sample. Therefore, whenever the 2-D diffraction pattern is calculated, a concentric ring of a peak scattering that is corresponding to various spacing in the lattice of the crystal. The intensities, as well as the positions of each of the peaks, is used to show the structure underlying in the material such as the diffraction graphite lines which is likely to be different from the diamond despite the fact they are gotten from the carbon atoms. The identification of this face is actually very vital due to the properties of the materials, which are structural dependent (i.e. diamond and graphite).

Table 3.2: Pertinent asphalt binder properties [58].

Asphalt Binders	Source	Modification Type	Grades
T1	Western Canada	Timmins, Ontario	PG 64-34
T2	Unknown	RET+ PPA Oxidized	PG 64-34
T4	Unknown	SBS + acid-modified	PG 64-34
T7	Unknown	Acid-modified Lamont, Alberta	PG 64-34
L2	Montana/Bow River	Straight	150/200 B, PG 52-28
L5	Lloydminster	Oxidized	80/100 A, PG 64-28

Those who investigated had calculated the aromaticity and the crystallite parameter, which was seen in the powder of the asphaltene samples, which will produce a model of a cross-section that is collected by the data of the X-ray diffraction and this can be viewed from the cross-sectional asphaltene model. The portion of the aromatic of the molecules has the ability to form a stack in the influence of London dispersion forces, which is referred to as pi stacking. Aliphatic side Chains that resides within the model of asphaltene exceeds out of the aromatic central module portion of the asphaltene. The side chains could likely be the site's template for the crystallization [76]. Isolated the naturally occurring paraffin waxes out of the asphalt cement and investigated their X-ray spectra.

3.4 Spectral Lines Shapes Modelled Using Mathematical Functions

The separation of the band (002) and gamma band in the manner seen above so as to determine the aromaticity, f_a, as to do with three essential error sources and this study dealt with each a satisfactory and a very reasonable way. The first is the errors possibility, which arises out of a small angle scattering which has the ability to increase the density with angles that are increasing. Which assumes a γ band symmetrical; the possibility of attributing some of the intensity in a low band angle side to a small a very small angle scattering and excluding it out of the calculation of f was possible. The other factor is the fact that the intensity (002) band as a result of seven layered unit of about 2.4mm thickness is likely to exhibit a 1.17 intensity times of the band of a two-unit layer of 0.7-1.1 mm thickness approximately. In addition, as such a variation in the size of a distribution of the unit that is repeated from sample to sample would likely result in an error in the

f. The asphalt binders which is undergoing study have about the same L, and FWHM of the γ band which indicates a similar size distribution.

3.5 Pearson VII and Pseudo-Voigt

A lot of different tools were used for the diffraction more than decades ago that has to do with instrumentation and data analysis especially. Lots of computer programs offer a solution for the entire task and the quality of information that is obtained out of a powered sample diffraction scanning is very astonishing. Therefore, there is a probability that the broadening of the line analysis will actually be a part of the program routine output, as well as the line positions, intensities lattice parameters and much more [78]. The full pattern software analysis like some refinement program received includes a parameter that can be refined and which corresponds to the domain strain and size [78]. Unfortunately, the inspection of the broadening analysis is sometimes inaccurate as a result of models that are inadequate that are used in retrieved programs mostly. However, the method that is based on Voigt function, which is generally more applicable and probably more accurate than current models.

It is obvious that the Cauchy nor Gauss functions have the ability to model diffraction broadening line. It was seen that a model that was based using a Voigt function have the ability to be more accurate and realistic. In addition, divergent approaches such as the Warren-Averbach analysis and integral-breadth methods are very close [79]. Some common occurrence in Warren-Averbach analysis specifically the effect of the "hook", the functional dependence of the square of the mean strains on averaging ratio and distance of volume that is weighted to the surface size domain from the Voigt double model [79]. There is the possibility of limitation of the Voigt-based model that

is both of conceptual and practical nature. When there are not better functions of choice in the future, the Voigt function is likely to still prove to be an approximation that is satisfactory in lots of cases.

The functional Voigt form is the basis for most of the quantitative analysis of the X-ray photoelectron spectroscopy (XPS) spectra. However, unfortunately, a form of analysis for the Gaussian convolution with a Lorentzian (G*L) is not accessible and as such practical system adopted approximately two of the true function of the Voigt [80]. Gaussian or Lorentzian Product Form is as follows:

$$GL(x.F.E.m) = \frac{exp(-4ln2(1-m)\frac{(x-E)^2}{F^2}}{(1+4m\frac{(x-E)^2}{F^2})} \quad (3.6)$$

Gaussian / Lorentzian sum form:

$$SGL(x.F.E.m) = (1-m)exp(-4ln2(1-m)\frac{(x-E)^2}{F^2} + \frac{m}{(1+4\frac{(x-E)^2}{F^2})} \quad (3.7)$$

3.5.1 Exponential Asymmetric Blend Based upon Voigt-Type Line-Shapes

When given any of the Gaussian or Lorentzian symmetric line-shapes above, a profile of asymmetric is gotten from a blend function such as:

$$Y(x) = GL(x) + (1 - GL(x) * T(x) \quad (3.8)$$

Where;

$$T(x.k.F.E) = \begin{cases} exp\left(-k\dfrac{(x-E)}{F}\right) & if x \leq E \\ 1 \qquad Otherwise \end{cases}$$

3.5.2 Line Shapes Analysis with the Use of Peak Search and Profile Fit

There was a peak searched of XRD spectra with the use of a parabolic filter (10, 000) raw data points, screened out kα-2 peaks, peak location summit, threshold sigma 3.0 intensity cut off 0.1 percent, range to find background 1.0, points to average background 7 about the range of the angle 5° - 110°. The FWHM and profile fits are obtained through the use of Pearson VII or pseudo-Voigt function (Lorentzian=0.3,0.5,and 0.7, Exponent= 0.5,1.0, and 1.5,with 3 background which is Linear, Parabolic, and 3rd Order backgrounds) over the range 5° to 35° 2θ and 60° to 110° 2θ on the spectra line XRD that is of interest. The XRD spectra also modeled in Mathematica by using a generalized Fermi Function (GFF).

3.6. Generalized Fermi Function (GFF)

The GFF (Eq.4.6) used in Mathematica software, and it is employed to fit raw data out of the XRD on the GFF. Some of the methods and codes that are followed during coloration as well specimens will be in Appendix.

Chapter 4

4. Results and Discussion

Four key peaks are present in the asphaltene binders of the XRD patterns (Gamma, *(002)*$_{graphene}$, (100), (110)) just as Yen model describes it. The data From Table 4.1 shows that there is a little difference between GFF values and Pearson VII and pseudo-Voigt values at crystallite parameters (L_a and L_c). These data mean that the profile fitting in GFF is not consistent as Pearson VII (P) and pseudo-Voigt (V) because XRD patterns are asymmetry, and there is no role for the background or difference values for the parameters (Pearson VII and pseudo-Voigt). Hence, the sensitivity of GFF to asymmetry is higher.

4 .1 XRD Patterns

The standard techniques methods stated in Jade, as well as other experimental software, were used to create the XRD patterns from the samples used in the 6-asphalt binder. It is seen from Figures 4.1 to 4.3 that these asphalt binders (T1, L2, T2, T4, T7, as well as L5), with a different value for Exponent and Lorentzian and different backgrounds as follows:

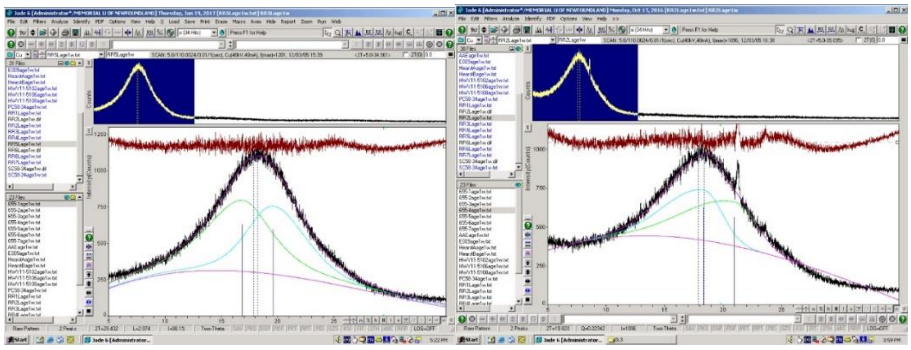

Figure 4.1: Specimen T1 & L2 of XRD (3rd Order Background, Lorentzian=0.7).

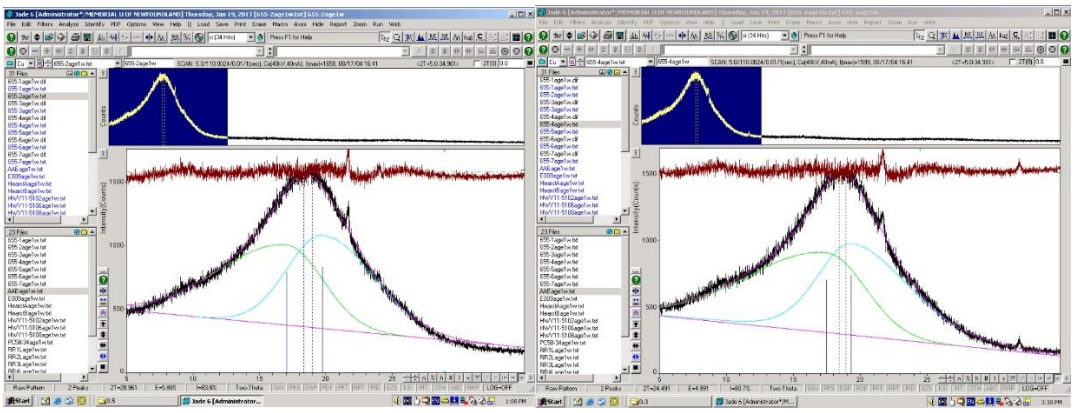

Figure 4.2: Specimen T2 & T4 of XRD (Linear Background, Lorentzian=0.5).

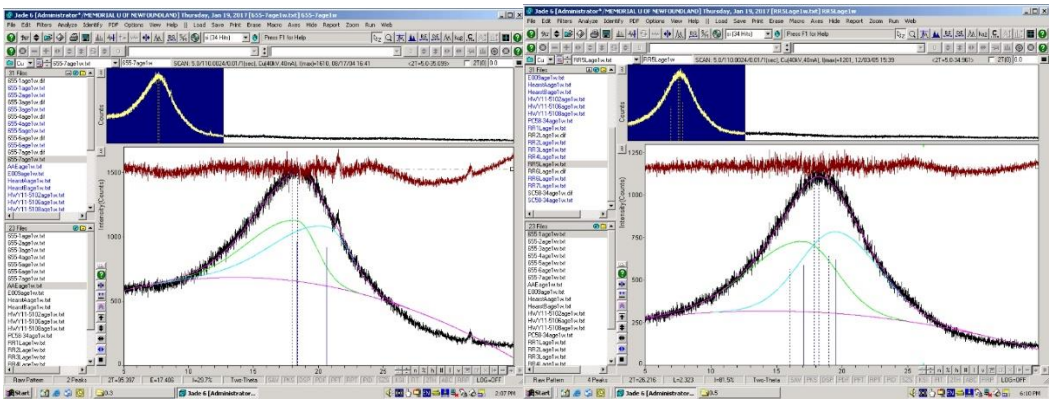

Figure 4.3: Specimen T7 & L5 of XRD (Parabolic Background, Lorentzian=0.3).

4.2 XRD Measurements and Calculations

A profile function that is either Pearson VII or pseudo-Voigt was used to fit the XRD data (see Figure 4.4). A true Voigt is a complexity of the Lorentzian and Gaussian components, but it is not easily implemented computationally, and a Pseudo-Voigt is a linear permutation of Lorentzian and Gaussian components. This leaves Pearson VII an exponential combination of Lorentzian and Gaussian components. Further explanation of the symmetry, shape, and application of Pearson VII and Pseud-Voigt will be given in the following section.

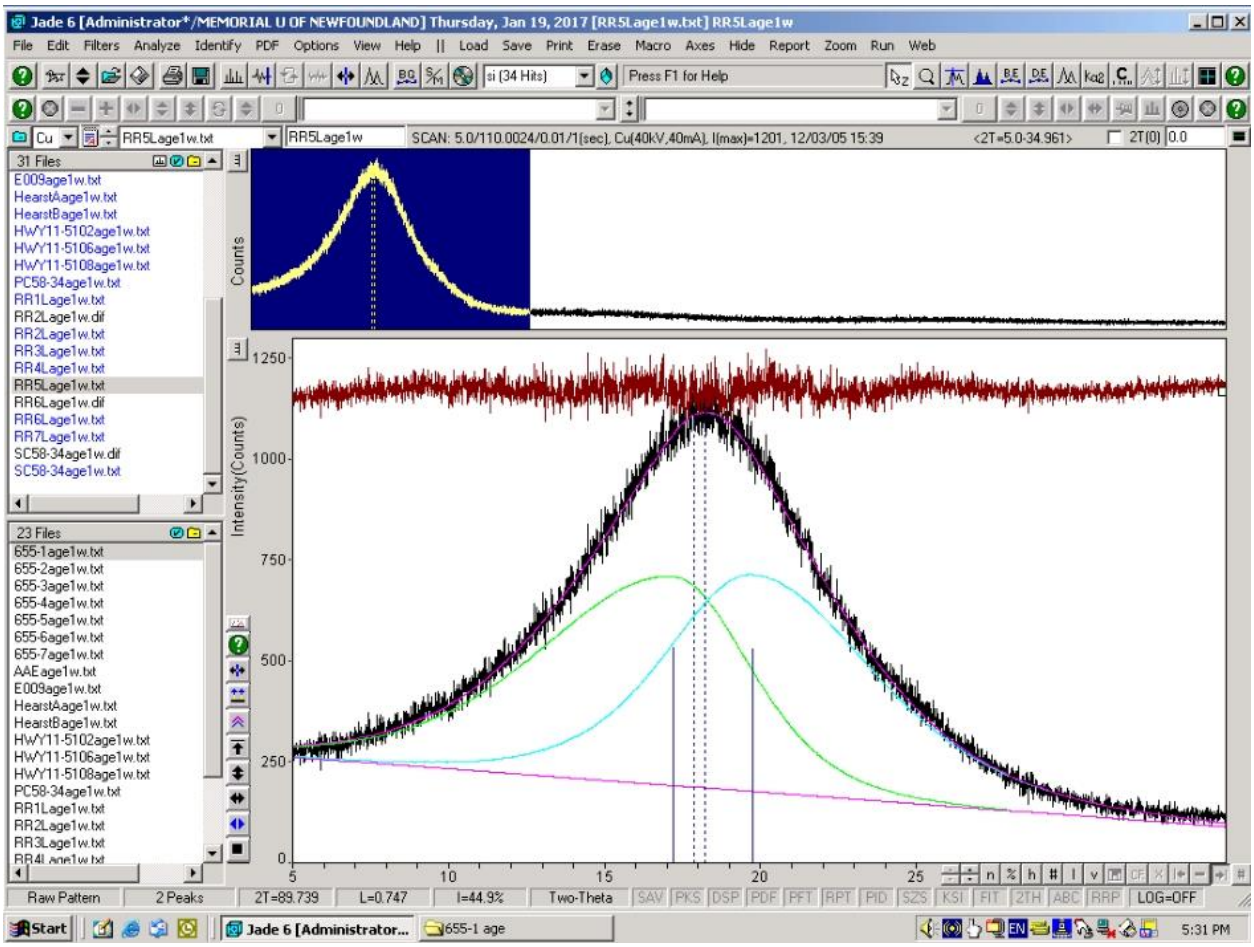

Figure 4.4: Profile fit of Asphalt Binder.

4.3 Peak Shape Functions

Taking a look at (Figures 4.1 to 4.3) we can see that the Y(i), (intensity), which is the point (i^{th}). ($1 \leq i \leq n$), *w*here *n* represents the total number of the points measured) of the diffraction pattern, generally is the summation of the $y_{k,}$ (contributions) from the *m* overlapped distinct Bragg peaks ($1 \leq k \leq m$) as well as the *b(i),* (background)

$$Y(i) = b(i) + \sum_{k=1}^{m} I_k \left[y_k(x_k) + 0.5 y_k(x_k + \Delta x_k) \right] \qquad (4.1)$$

Where:

Δx_k represents the difference between Bragg angles of K$\boldsymbol{\alpha}_1$ and K$\boldsymbol{\alpha}_2$ components in the XRD (γ) doublet, graphene(002) in asphalt binders, I_k represents the intensity of k^{th} Bragg reflection, and $X_k = 2\theta_i - 2\theta_k$. The Bragg intensity present in the equation above as a multiplier makes it possible for the introduction and analysis of the different normalized functions' behavior which is independent of the intensity of the peak. This means; taking of the definite integral in each case of a peak shape function that is calculated from the negative to the positive infinity to be unity. The four commonly used empirical peak shape functions (y) are shown below:

Lorentz:

$$y(x) = L(x) = \frac{C_L^{1/2}}{\pi H'}(1 + C_L x^2)^{-1} \tag{4.2}$$

Gauss:

$$y(x) = G(x) = \frac{C_G^{1/2}}{\sqrt{\pi} H}\exp(-C_G x^2) \tag{4.3}$$

Pearson-VII:

$$y(x) = PVII(x) = \frac{\Gamma(\beta)}{\Gamma\left(\beta - \frac{1}{2}\right)}\frac{C_P^{1/2}}{\sqrt{\pi} H}(1 + C_P x^2)^{-\beta} \tag{4.4}$$

Pseudo-Voigt (Linear combination of Gaussian and Lorentzian)

$$y(x) = PV(x) = \eta\frac{C_G^{1/2}}{\sqrt{\pi} H}\exp(-C_G x^2) + (1 - \eta)\frac{C_L^{1/2}}{\pi H'}(1 + C_L x^2)^{-1} \tag{4.5}$$

GFF:

$$h(s) = \frac{A}{\exp\big(-a(s-c)\big) + \exp(b(s-c))} \tag{4.6}$$

where A, a, b, c are parameters not known to be input and s = $\frac{2\sin\theta}{\lambda}$ while c and A define the position and the amplitude of the fit, a and b control the fit shape.

H and *H'*, represent the (FWHM) full widths at the half maximum.

$$X = \frac{(2\theta_i - 2\theta_k)}{\mathrm{H}_k} \tag{4.7}$$

is fundamentally the Bragg angle of the point i^{th} in the diffraction pattern having its origin in the k^{th} peak position divided by the FWHM of the peak.the Bragg angle of the point i^{th} of the diffraction pattern is $2\theta_i$, $2\theta_k$, is the ideal or calculated Bragg angle of the k^{th} Bragg reflection.

C_G= 4ln 2, also $\frac{\sqrt{\mathrm{C_G}}}{\sqrt{\pi}\mathrm{H}}$ is the Gauss function normalization factor such that,

$$\int_{-\infty}^{\infty} \frac{\sqrt{\mathrm{C_G}}}{\sqrt{\pi}\mathrm{H}} \exp(-C_G\ x^2)\, dx = 1 \tag{4.8}$$

C_L= 4, and$\frac{\sqrt{\mathrm{C_L}}}{\pi H'}$, is the Lorentz function normalization factor for the such that,

$$\int_{-\infty}^{\infty} \frac{\sqrt{\mathrm{C_L}}}{\pi H'} (1 + C_L\ x^2)^{-1}\, dx = 1 \tag{4.9}$$

C_P=4($2^{1/\beta} - 1$), and $[\frac{(\Gamma_\beta)}{\Gamma_{(\beta - 1/2)}}] \frac{\sqrt{\mathrm{C_P}}}{\sqrt{\pi}\mathrm{H}}$

is the Pearson-VII function normalization factor such that,

$$\int_{-\infty}^{\infty} \frac{\Gamma_{\beta}}{\Gamma_{(\beta-1/2)}} \frac{\sqrt{C_P}}{\sqrt{\pi}\mathrm{H}} (1 + C_P\ x^2)^{-\beta}\, dx = 1 \tag{4.10}$$

$$\mathrm{H}=\sqrt{(\mathrm{U}tan^2\theta\ +\ \mathrm{V}\tan\theta + \mathrm{W})} \tag{4.11}$$

is known as the Caglioti formula. It is the FWHM as a function of θ for Pseudo-Voigt, Pearson-VII functions, and Gauss, as well as *U*, *V* and *W* are free variables [77].

$$\mathrm{H}' = \frac{U}{cos\theta} + V\ tan\theta \tag{4.12}$$

represent the FWHM which is a function of θ for the Lorentz function, *U, as well as V,* are free variables.

$$\eta=\eta_o + \eta_1 2\theta + \eta_2 \theta^{\,2} \tag{4.13}$$

where, $0 \leq \eta \leq 1$, and η represent the Pseudo-Voigt function mixing parameter, which is the Gauss function small contribution into the linear mixture of Lorentz and Gauss functions, Γ , is the gamma function and η_o , η_1 and η_2 are free variables.

$$\beta = \beta_o + \frac{\beta_1}{2\theta} + \frac{\beta_2}{(2\theta)^2} \tag{4.14}$$

β represent the exponent which is a function of Bragg angle in Pearson-VII function, while β_2, β_1, and β_o, are free variables.

Lorentz (solid line) peak shape and Gauss (dashed-dotted line) functions and the FWHM are illustrated as thick horizontal arrows (see figure 4.5).

Gaussian and Lorentzian distributions are respectively represented by the two simplest peak shape functions of the Bragg peak intensity. The figure shows that there are no tails at the base of

the Gauss function but rather around maximum. The Lorentz function is sharp close to its maximum with the presence of long tails on each side close to its base. They are both centrosymmetric, i.e., L(x) = L (- x) and G(x) = G (- x). Simple Gaussian or Lorentzian distributions in the XRD especially in X-ray diffraction rarely gives a detailed description of the shapes of true Bragg peaks, that results from the convolution of multiple specimen and instrumental functions. The experimental peak shapes are usually cited somewhere in-between Lorentz and Gauss distributions, and they are better indicated as the collection of two functions. One of the ways is to convolute the Lorentz and Gauss functions in separate proportions. This convolution is a complex process requiring numerical integration.

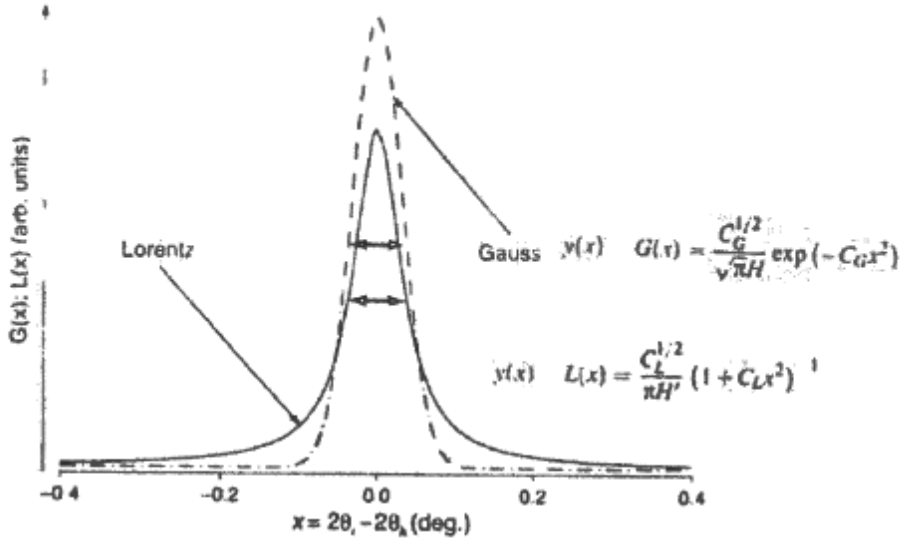

Figure 4.5: Gauss and Lorentz peak shape functions [58].

Whenever there are changes in the parameters of a peak shape function or several peak shape functions, Pseudo-Voigt, a simpler linear mixture of Lorentz and Gauss functions are employed

instead of a convolution. The Lorentzian and Gaussian compounds are mixed into η to 1-η ratio, so that the mixing parameter's value η, can vary from 0 Lorentz to 1 Gauss. Moreover, it is meaningless outside this given range. Pearson-VII (Eq.4.4) is the other peak shape function used. It has similarities with Lorentz distribution just that it has a varying exponent β, while that of the Lorentz function is constant (β= 1). The intensity distribution provided by Pearson-VII when the exponent, β= 1, is near the Pseudo-Voigt function, which is similar to the Lorentz distribution, so also, Pearson-VII equal is equal to Gaussian function when $\beta \cong 10$.

Therefore, when the range of the exponent is in $0.5 < \beta < 1$ or $\beta > 10$, there is a significant extension of the shape beyond Gauss or Lorentz functions respectively, but in practice, the β values are rarely noticed. The (x,) argument, present in all the above four empirical functions shows the location of the peak maximum, which is vividly seen when $x = 0$ and $2\theta_i = 2\theta_k$.

For Pearson VII and pseudo-Voigt functions:

-The modeling of the Peak shape is done with the Pearson VII or pseudo-Voigt functions.

-H, in the FWHM term, is a factor of the two functions.

-The FWHM is connected to crystallite microstrain and size.

-The Cagliotti Equation is used to model the FWHM (Eq.4.11).

-The most strongly associated parameter with strain widening is U.

-U and Ware used to calculate the Crystallite size.

-For anisotropic broadening, U can be divided into (hkl) dependent constituents.

Therefore, the peak FWHM in most cases at a fixed 2θ angle is denoted as,

$$FWHM = H = \sqrt{U\ tan^2\theta + V \tan\theta + W} \quad (4.15)$$

Another parameter that determines the argument value is the FWHM, H. H varies with about 2θ and it depends on the Bragg angle which is mostly shown by an empirical peak widening function that possesses three free parameters W, V and U (apart from Lorentzian, that is usually made up of two free variables)

4.4 Spectral Line Shapes Analysis

The profile fits of XRD (PVII and Pseudo-Voigt) and GFF simulation results. The remained results can be seen in the Appendix.

4.5 Comparing the Results of all Asphalt Samples

The observed X-ray diffraction patterns need fitting of the theoretical distributions that are very important to acquire information the spectral lines. Pseudo-Voigt and Pearson-VII fitting procedures are employed, and the 3 main bands γ, (002), and (100) cited at approximately 2θ = 20°, 25°, and 44° were employed as the first estimates. It is possible to observe the (004) band on the high 2θ side in some situation at 2θ at approximately 53°. Also, by estimating the intensity and peak width, the regression can be initiated. A major factor in X-ray diffraction patterns of asphaltene are backgrounds (T1& L2=3rd Order, T2&T4= Linear, T7& L5=Parabolic) as seen in this work. The baseline on the low 2θ side is not adequately well defined, so the X-ray diffraction pattern's high value end and fixed as a constant baseline. This brings us to a tangible assumption, stimulated deduction, or statistical impreciseness that could affect the result in the operator's benefit. The result in most cases like the aromaticity is not much influenced by the change in baseline. In order to enhance the regression coefficients, there were additions of refinement in all

cases. However, this influences the alteration of the position of peak and the width, resulting to somewhat a real but uncertain degree of operator preference involved which affects the outcomes.

Table 4.1: The aromaticity and crystallite parameters calculated with the use of Pearson VII, Pseudo-Voigt, and GFF.

			Fa			d_m			d_γ		
Samples	**Exp**	**Lor**	**P**	**V**	**GF**	**P**	**V**	**GF**	**P**	**V**	**GF**
T1	0.5	0.3	0.508	0.496	0.52	4.338	4.223	4.816	5.946	5.942	6.02
	1.0	0.5	0.526	0.420	0.52	4.467	4.486	4.816	6.456	5.845	6.02
	1.5	0.7	0.562	0.445	0.52	4.466	4.530	4.816	6.332	6.572	6.02
T2	0.5	0.3	0.403	0.367	0.43	4.140	3.772	4.689	6.039	5.800	5.862
	1.0	0.5	0.573	0.494	0.43	4.493	4.492	4.689	6.458	6.506	5.862
	1.5	0.7	0.565	0.503	0.43	4.448	4.452	4.689	6.461	6.505	5.862
T4	0.5	0.3	0.498	0.469	0.51	4.340	4.598	4.868	6.297	6.285	6.085
	1.0	0.5	0.519	0.488	0.51	4.360	4.594	4.868	6.302	6.338	6.085
	1.5	0.7	0.501	0.550	0.51	4.327	4.561	4.868	6.246	6.520	6.085
T7	0.5	0.3	0.593	0.528	0.53	4.352	4.302	4.79	6.306	6.045	5.987
	1.0	0.5	0.537	0.522	0.53	4.308	4.273	4.79	6.222	5.972	5.987
	1.5	0.7	0.518	0.517	0.53	4.281	4.300	4.79	6.194	5.934	5.987
L2	0.5	0.3	0.465	0.603	0.51	4.279	4.319	4.895	6.393	6.261	6.119
	1.0	0.5	0.522	0.517	0.51	4.285	4.237	4.895	6.422	6.045	6.119
	1.5	0.7	0.398	0.452	0.51	4.274	4.204	4.895	6.311	6.201	6.119
L5	0.5	0.3	0.472	0.516	0.52	4.516	4.549	4.868	6.648	6.510	6.085
	1.0	0.5	0.476	0.482	0.52	4.495	4.546	4.868	6.434	6.425	6.085
	1.5	0.7	0.477	0.491	0.52	4.505	4.491	4.868	6.520	6.357	6.085

			L_a			L_c			M_e		
Samples	**Exp**	**Lor**	**P**	**V**	**GF**	**P**	**V**	**GF**	**P**	**V**	**GF**
T1	0.5	0.3	7.841	7.226	5.732	3.835	3.534	2.803	1.883	1.836	1.582
	1.0	0.5	8.996	5.606	5.732	4.400	2.742	2.803	1.984	1.611	1.582
	1.5	0.7	8.180	7.475	5.732	4.001	3.656	2.803	1.895	1.807	1.582
T2	0.5	0.3	7.699	6.600	5.58	3.765	3.228	2.729	1.909	1.855	1.582
	1.0	0.5	6.720	5.688	5.58	3.286	2.782	2.729	1.731	1.619	1.582
	1.5	0.7	7.062	5.977	5.58	3.454	2.923	2.729	1.776	1.656	1.582
T4	0.5	0.3	7.912	5.072	5.795	3.870	2.480	2.834	1.891	1.539	1.582
	1.0	0.5	7.965	5.075	5.795	3.896	2.482	2.834	1.893	1.540	1.582
	1.5	0.7	8.021	5.271	5.795	3.923	2.578	2.834	1.906	1.565	1.582
T7	0.5	0.3	8.836	8.773	5.701	4.322	4.291	2.788	1.992	1.997	1.582
	1.0	0.5	8.789	7.846	5.701	4.299	3.838	2.788	1.997	1.898	1.582
	1.5	0.7	8.857	8.061	5.701	4.332	3.943	2.788	2.011	1.916	1.582
L2	0.5	0.3	10.151	10.351	5.827	4.965	5.063	2.85	2.160	2.172	1.582
	1.0	0.5	10.230	9.124	5.827	5.004	4.463	2.85	2.167	2.053	1.582
	1.5	0.7	12.680	12.775	5.827	6.202	6.249	2.85	2.451	2.486	1.582
L5	0.5	0.3	8.668	6.859	5.795	4.240	3.354	2.834	1.938	1.737	1.582
	1.0	0.5	7.473	6.673	5.795	3.655	3.264	2.834	1.813	1.717	1.582
	1.5	0.7	7.727	6.664	5.795	3.779	3.259	2.834	1.838	1.725	1.582

Table 4.1 shows the results from calculation of aromaticity (f_a) and crystallite parameters (the interlayer distance between the aromatic sheets d_M , the interchain layer distance $d_{\gamma,}$ the diameter of the aromatic sheets L_a , the height of the stock of aromatic sheets L_c , and the number of aromatic sheets M_e) for Pearson VII (P) varying exponent (0.5, 1.0, 1.5), pseudo-Voigt (V) varying Lorentzian (0.3, 0.5, 0.7), and Generalized Fermi (GF) Function in 6 samples. The XRD results modeled in Generalized Fermi Function **(**GFF) provided a smooth shape (figure 4.5).However, analysis of aromaticity and crystallite size parameters using the XRD data were sometimes mixed

due to asymmetry in the GFF data and differences in calculating background intensity. In general, the results in XRD and GFF modeling are approximate there is a little difference between GFF values and Pearson VII and pseudo-Voigt values in L_a values at all samples and in L_c values at T1, T4, T7, and L2.

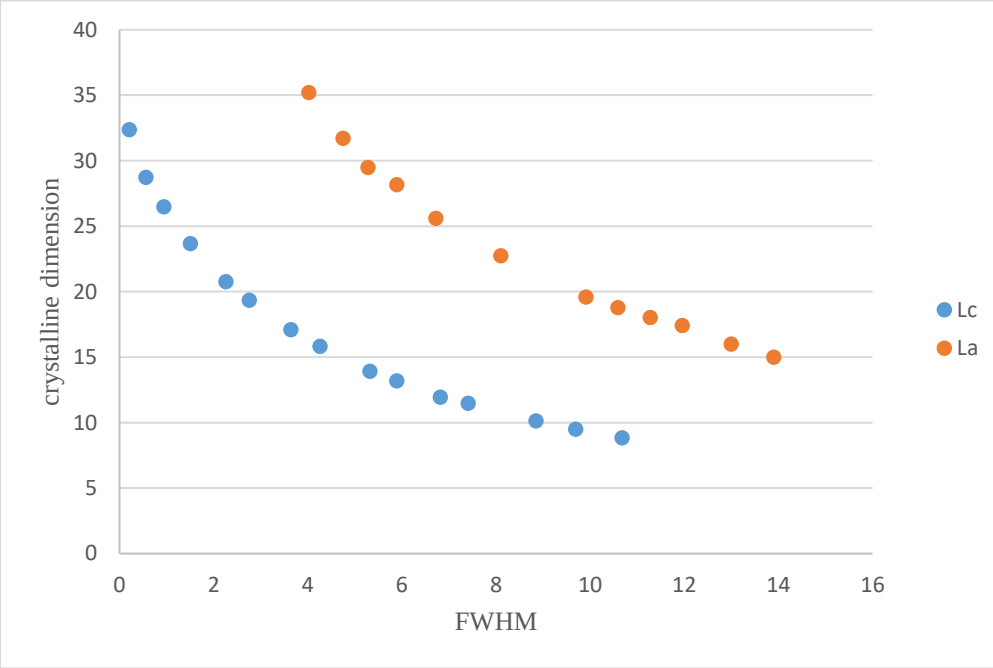

Figure 4.6: The Modified figure of relationship showing crystalline dimension (vertical) versus bandwidth (horizontal) [75].

L_c and L_a are the two key parameters needed to understand crystallite size. They are very sensitive parameters to FWHM, as seen in (Figure 4.6) above, showing a theoretical relationship between the two parameters (L_c and L_a) has been estimated. It is clearly seen that L_c is very sensitive to slight changes in γ, i.e. any change from 2θ = 5° to 6° will result in a decrease in the stack height from 3.0 to about 1.5nm.

As a result of the low sensitivity of the sheet diameter, it remains almost static at about 1.1 to 1.5nm, and it only gives a significant effect at the narrow (100) band. It is also seen that their differences in the basic results, even in terms of trends when they change in XRD from Pearson VII to Pseudo-Voigt.

There is a possibility to oversimplify the fitting procedure in that graphing normally by forming a non-symmetric (002) peaks which are usually formed from several contributions like noise present in the residue of the data.

4.6 Statistical Analysis of the XRD Results for Asphalt Samples.

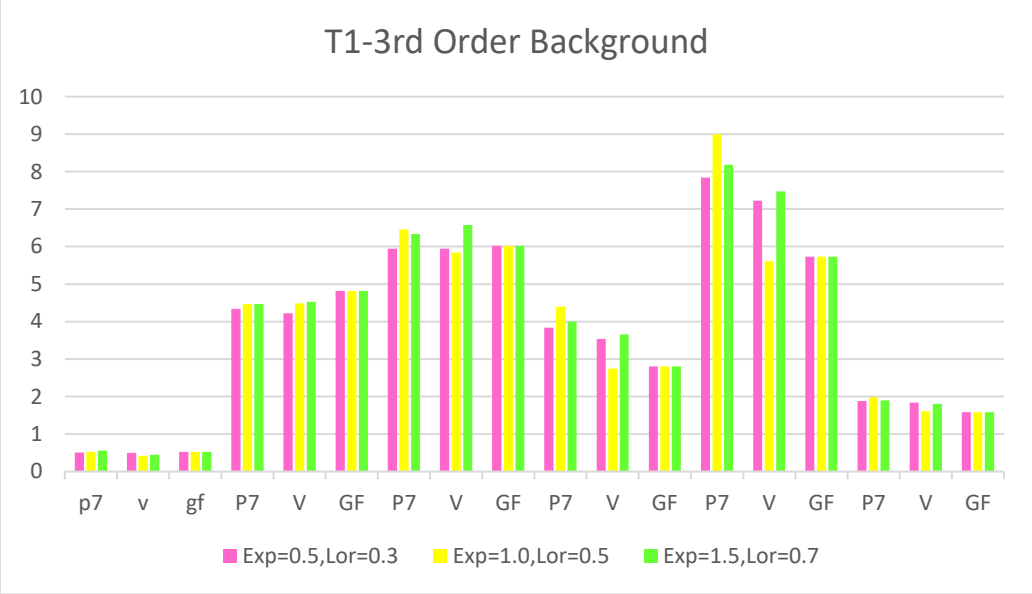

Figure 4.7: Aromaticity and Crystallite Parameters for Sample T1 Calculated Using Pearson VII, Pseudo-Voigt, and GFF with 3rd Background.

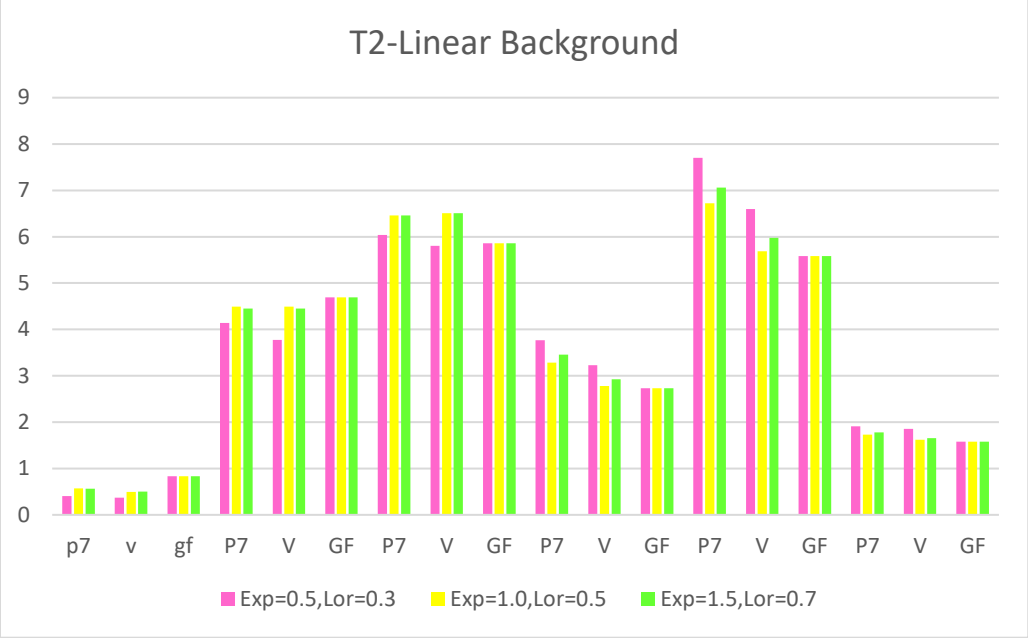

Figure 4.8: Aromaticity and Crystallite Parameters for Sample T2 Calculated Using Pearson VII, Pseudo-Voigt, and GFF with Linear Background.

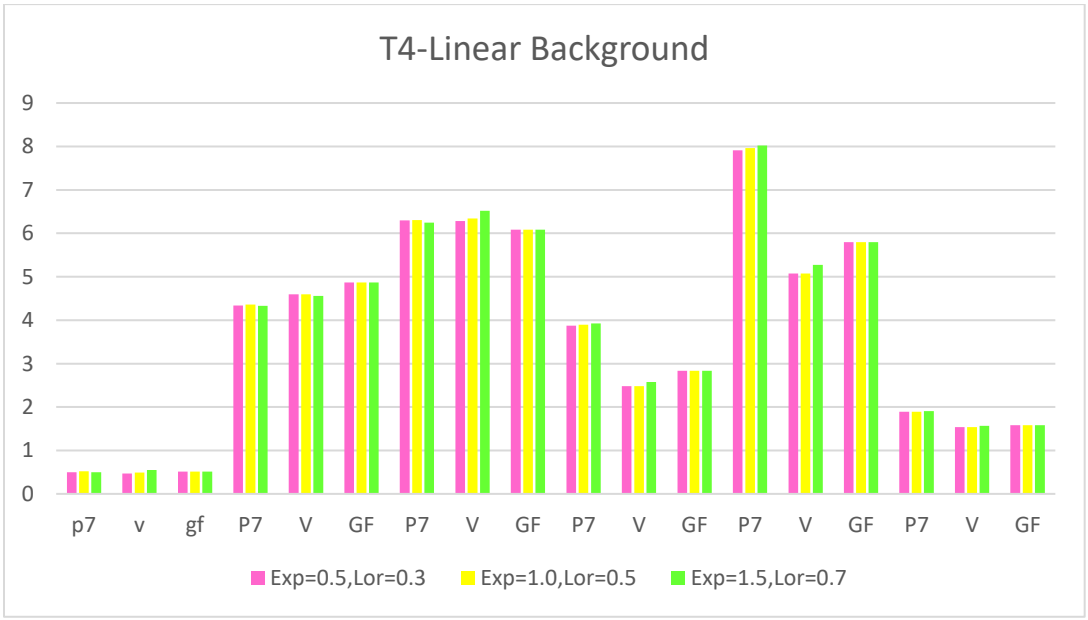

Figure 4.9: Aromaticity and Crystallite Parameters for Sample T4 Calculated Using Pearson VII, Pseudo-Voigt, and GFF with Linear Background.

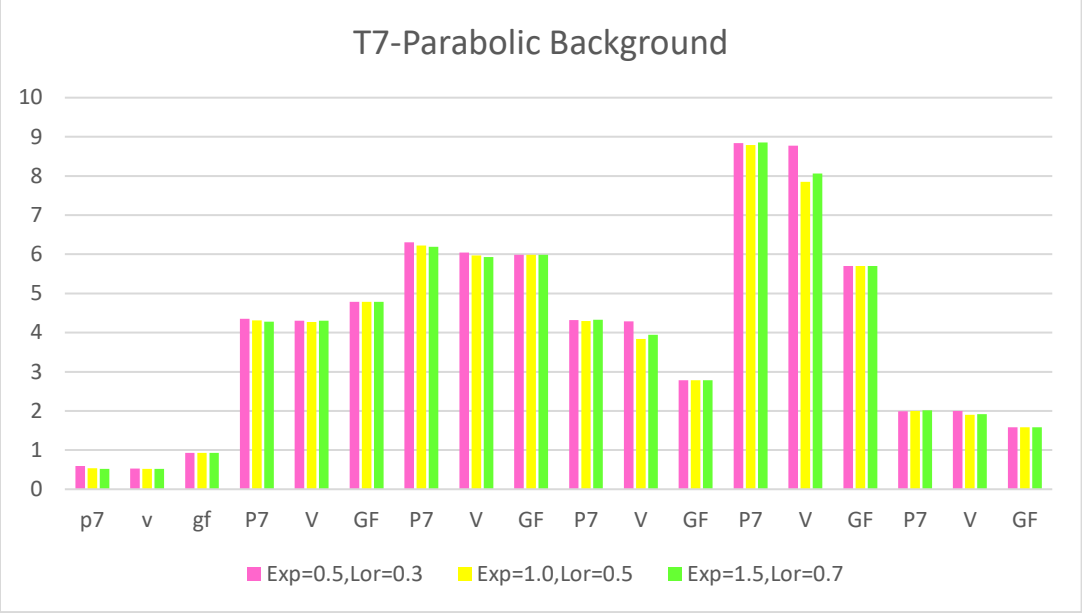

Figure 4.10: Aromaticity and Crystallite Parameters for Sample T7 Calculated Using Pearson VII, Pseudo-Voigt, and GFF with Parabolic Background.

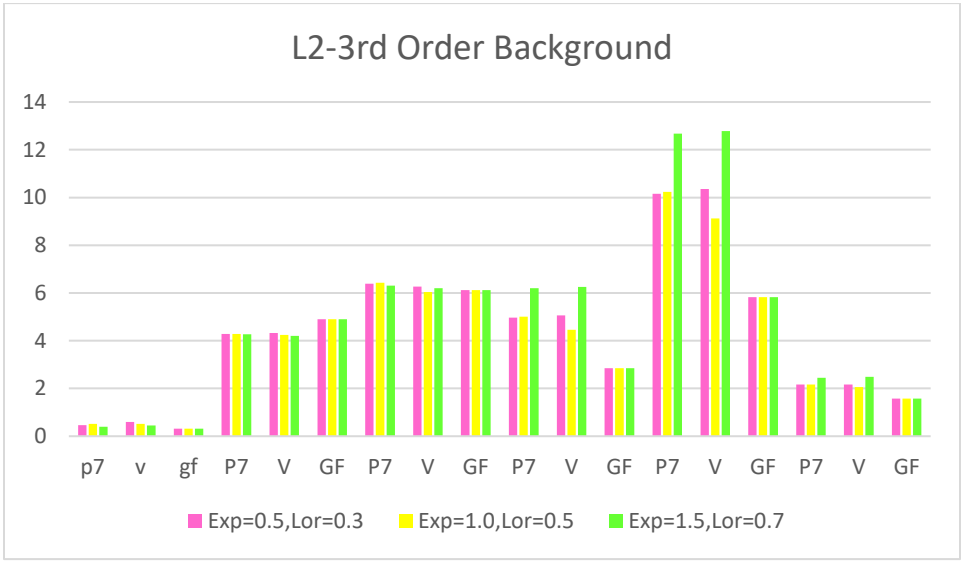

Figure 4.11: Aromaticity and Crystallite Parameters for Sample L2 Calculated Using Pearson VII, Pseudo-Voigt, and GFF with 3rd Background.

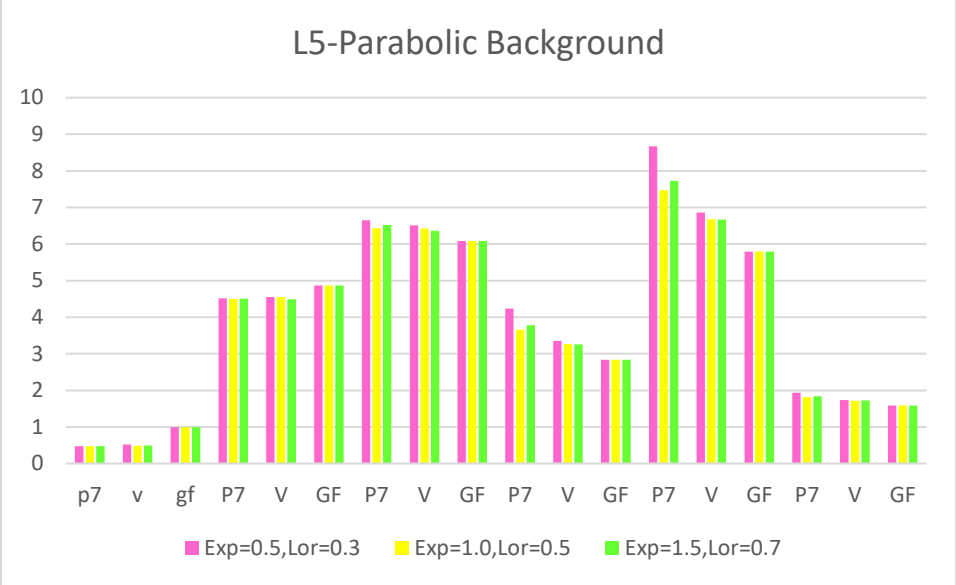

Figure 4.12: Aromaticity and Crystallite Parameters for Sample L5 Calculated Using Pearson VII, Pseudo-Voigt, and GFF with Parabolic Background.

Chapter 5

5. Conclusions

By using three major functions, which are Pearson VII, Pseudo-Voigt, and Generalized Fermi function (GFF) to compare XRD pattern profile fitting. Jada^{TM} software samples were used for Pearson VII, and Pseudo-Voigt to compare crystallite size and aromaticity with different values. In addition, Mathematica used to model the XRD data by using generalized Fermi function with varied results comparable to Pearson VII, Pseudo-Voigt functions.

For one week, the maturing procedure for every asphalt binder increased. With the passage of time, peaks were showing that crystallinity enhanced in tandem with asphalt binder aging. Moreover, even small modifications of profile angles resulted in shifts in atoms in the planes, thus indicating a direct association between Pseudo-Voigt and Pearson VII functions, as well as GFF.

The discoveries of this present investigation highlight the expanding capacity of XRD to precisely depict the properties (which are auxiliary and compositional in nature) in binders of asphalt. The facts discovered are all vital for getting a handle on how pavements and asphalt binders age in a true setting. Whilst labs testing of XRD can without much of a stretch supplement the structural designing outcomes from research works, they cannot really anticipate any problem that may emerge concerning the durability of pavements made from asphalt and how well they will perform. For that reason, extra research is needed to be done in this field, first to locate the potential issues and after that to determine them utilizing every accessible instrument close by.

Bibliography

1. *EAPA: European Asphalt Pavement Association. (n.d.). Retrieved from http://www.eapa.org/.*

2. *Yen, T.F.; Erdman, G.J.; Pollack, S.S. Investigation of the Structure of Petroleum Asphaltene by X-ray Diffraction. Analytical Chemistry.* ***1961****, 33, 1587-1594.*

3. *Speight, J. G. The Chemistry and Technology of Petroleum, 3rd edition, Marcel Dekker, Inc., New York,* ***1999****.*

4. *Moschopedis, S. E.; Fryer, J. F.; Speight, J. G. Investigation of Asphaltene Molecular Weights. Fuel* ***1976****, 55 (3), 227-223.*

5. *Ancheyta, J.; Centeno, G.; Trejo, F.; Marroqun, G.; Garca, J. A.; Tenorio, E.; Torres, A. Extraction and Characterization of Asphaltene from Different Crude oils and Solvents. Energy Fuels* ***2002****, 16 (5), 1121-1127.*

6. *Kharrat, A. M. Characterization of Canadian Heavy Oils Using Sequential Extraction Approach. Energy Fuels* ***2009****, 23 (2), 828-834.*

7. *Dettman, H.; Inman, A.; Salmon, S. Chemical Characterization of GPC Fractions of Athabasca Bitumen Asphaltene Isolated Before and After Thermal Treatment. Energy Fuels* ***2005****, 19 (4), 1399-1404.*

8. *Andersen, S. I.; Keul, A.; Stenby, E. Variation in Composition of Subfractions of Petroleum Asphaltene. Pet. Sci. Technol* ***1997****, 15 (7&8), 611-645.*

9. *Giusti, M. M.; Wrolstad, R. E. Characterization and Measurement of Anthocyanins by UV-Visible Spectroscopy. Current Protocols in Food Analytical Chemistry,* ***2001****.*

10. Nalwaya, V.; Tangtayakom, V.; Piumsomboon, P.; Fogler, S. Studies of Asphaltene Through Analysis of Polar Fractions. Ind. Eng. Chem. Res. ***1999****, 38 (3), 964-972.*

11. Yang, X.; Hamza, H.; Czarnecki, J. Investigation of Subfractions of Athabasca Asphaltene and Their Role in Emulsion Stability. Energy Fuels ***2004****, 18 (3), 770-777.*

12. Zhao, B.; Shaw, J. M. Composition and Size Distribution of Coherent Nanostructures in Athabasca Bitumen and Maya Crude Oil. Energy Fuels ***2007****, 21 (5), 2795-2804.*

13. Schuler, B.; Meyer, G.; Peña, D.; Mullins, O.; Gross, L. Unraveling the Molecular Structures of Asphaltene by Atomic Force Microscopy. Journal of the American Chemical Society ***2015****, 137(31), 9870-6.*

14. Yasar, M.; Akmaz, S.; Gurkaynak, M. Investigation of the Molecular Structure of Turkish Asphaltene. Petroleum Science and Technology ***2009****, 27(10), 1044-1061.*

15. Liu, Y.; Li, Z. Structural Characterisation of Asphaltene during Residue Hydrotreatment with Light Cycle Oil as an Additive. Journal of Chemistry ***2015****, 8.*

16. *El-Sayed, K.; El-Feky, A. A.; Ba, M. Asphaltene Using X-ray Diffraction and Raman Spectroscopy. Research Article ING of Egyptian Asphaltene Using X-ray Diffraction Raman Spectroscopy Feky, AA; 1Mohamed Bakr Mohamed, 2.*

17. Schuler, B.; Fatayer, S.; Meyer, G.; Rogel, E.; Moir, M.; Zhang, Y.; Peña, D. Heavy Oil-Based Mixtures of Different Origins and Treatments Studied by AFM. Energy Fuels ***2017****.*

18. Pujadó, D.; Jones, D.; Pujadó, P.; SpringerLink. Handbook of Petroleum Processing. Dordrecht: Springer, ***2006****.*

19. Parkash, S.; ProQuest; Books24x7, Inc. Refining Processes Handbook. Amsterdam; Boston: Gulf Professional Pub, ***2003****.*

20. SIC 2952.Asphalt Felts and Coatings. (n.d.). Retrieved from http://www.referenceforbusiness.com/industries/Petroleum-Refining-Related/Asphalt-Felts-Coatings.html.

21. Home Energy Saver. (n.d). Retrieved from http://hes.lbl.gov/consumer/.

*22. Dixon, C. R.; Gurley, K. R.; Masters, F. J.; Prevatt, D. O. Lessons Learned: Asphalt Shingle Testing Reveals Reasons for Shingle Blow-off. March **2014**. Retrieved from http://www.professionalroofing.net/Articles/Lessons-learned--03-01-2014/2418.*

*23. Sery, S. S. The Complete Guide to Roofing Materials. February 18, **2016**. Retrieved from http://www.jandjconstructionmt.com/the-complete-guide-to-roofing-materials/.*

*24. Romer, D. Wind Uplift Resistance of Asphalt Shingles. **2012**.*

*25. Allen, E.; Iano, J. Fundamentals of Building Construction: Materials and Methods (Sixth Edition.). New York; Toronto: Wiley, October **2013**.*

*26. Croom; Sutton; Zhao; Matta; Ghorbani. Modeling of Asphalt Roof Shingle-Sealant Structures for Prediction of Local Delamination under High Wind Loads. Engineering Structures **2015**, 96, 100-110.*

*27. Mullins, Oliver C. The Asphaltene. Annual Review of Analytical Chemistry **2011**, 4, 393-418.*

*28. Max von Laue; Eckert, M. The Discovery of X-ray Diffraction in 1912. Annalen der Physik, **2012**, 524(5).*

*29. Barbara Dutrow; Christine Clark. X-ray Powder Diffraction. Geochemical Instrumentation and Analysis. Carlton University, **2016**.*

*30. Gupta, Y.; Turneaure; Perkins; Zimmerman; Arganbright; Shen; Chow. Real-Time, High-Resolution X-ray Diffraction Measurements on Shocked Crystals at a Synchrotron Facility. Review of Scientific Instruments, 83(12), Review of Scientific Instruments, December **2012**, Vol.83 (12).*

31. Structure Factor. (n.d.). Retrieved from http://reference.iucr.org/dictionary/Structure_factor.

*32. Roessle, M. Basics of X-ray Scattering - EMBL Hamburg. **2009**. Retrieved from https://www.embl-hamburg.de/biosaxs/courses/embo2012/slides/x-ray-scattering-basics-roessle.pdf*

33. Grady, Brian P. Small-Angle X-ray Scattering. Polymer Characterization - Research Group - Small-Angle X-ray Scattering. Oklahoma University, n.d.

*34. McAlister, B.; Grady, B. Simulation of Small-Angle X-ray Scattering from Single-Particle Systems. Journal of Applied Crystallography **1998**, 31(4), 594-599.*

*35. McAlister, B.; Grady, B.; Kahovec, J. The use of Monte-Carlo Simulations to Calculate Small-Angle Scattering Patterns. Macromolecular Symposia. **2002**, 190(1), 117-130.*

*36. Slowik, J.; Son, S.; Dixit, G.; Jurek, Z.; Santra, R. Incoherent X-ray Scattering in Single-Molecule Imaging. New Journal of Physics **2014**, 16(7), 15.*

*37. Tsybulya, S.; Yatsenko, D. X-ray Diffraction Analysis of Ultradisperse Systems: The Debye Formula. Journal of Structural Chemistry **2012**, 53(S1), 150-165.*

*38. Siddiqui, M.N.; Ali, M.F.; Shirokoff, J. Use of X-ray Technique in Assessing. The Aging Patterns of Asphalt Fractions. Fuel **2002**, 81, 51-58.*

39. Seddig, H.; Shirokoff, J.; Lewis, J. C. A Study of Asphalt Binders by Computer Modeling X-ray Diffraction Spectral Line Shapes. IEEE Canadian Conference on Electrical and Computer Engineering (CCECE) ***2016****.*

40. Mullins, O.C. The Modified Yen Model, Energy Fuels ***2010****, 24, 2179-2207.*

41. Zuo, J. Y.; Chen, Y.; Pan, S.; Wang, K.; Mullins, O. C. Investigation of Density Inversion Induced by Gas Charges into Oil Reservoirs Using Diffusion Equations. Energy ***2016****, 100, 199-216.*

42. Mullins, O. C.; Sabbah, H.; Eyssautier, J.; Pomerantz, A. E.; Barré, L.; Andrews, A. B.; Lepkowicz, R. Advances in Asphaltene Science and the Yen–Mullins Model. Energy Fuels ***2012****, 26(7), 3986-4003.*

43. Zuo, J.; Pan, S.; Wang, K.; Mullins, O.; Dumont, H.; Chen, L.; Canas, J. Analysis of Asphaltene Instability Using Diffusive and Thermodynamic Models during Gas Charges into Oil Reservoirs. Energy & Fuels ***2017****, 31(4), 3717-3728.*

44. Bell. Summary Report on Aging of Asphalt Aggregate Systems, Transportation Research Board, ***1989****.*

45. Shirokoff, J.; Illiuta, S.; Hesp, S.A.M. Reversible Aging in Asphalt Binders. Energy Fuels ***2007****, 21, 1112-1121.*

46. Dow. Proceedings of the ASTM 6th Annual Meeting, Delaware, ***1903****, 3,349-373.*

47. Brown. Proceedings of the Association of Asphalt Paving Technologists, ***1958,*** *27,171-176.*

48. Philip, R.H.; John E.P.; George F.A.B. Oxidation of Roading Asphalts, Znd. Eng. Chem. Res. ***1994****, 33, 2801-2809.*

49. *Yapp, M.T.; Durrani, A.Z.; Finn, F.N. HP-GPC and Asphalt Characterization Literature Review, Report SHRP-A-503, Strategic Highway Research Program, National Research Council, Washington, D.C.,* ***1991****.*

50. Ensley, E. K.; Petersen, J. C.; Robertson, R. E. Asphalt—Aggregate Bonding Energy Measurements by Microcalorimetric Methods. Thermochimica Acta, ***1984,*** *77(1-3), 95-107.*

51. Yu, J .Y.; Feng, P.C; Zang, H.L.; Wu, S.P. Effect of Organa-Montmorillonite on Aging Properties of Asphalt, Construction and Building Materials, Article in press, ***2009****.*

52. Shenoy, A. Prediction of High-Temperature Rheological Properties of Aged Asphalts from the Flow Data of the Original Unaged Samples, Construction and Building Materials, ***2002****, 16,509-517.*

53. Lee, S.; Amirkhanian, S.N.; Park, N.; Kim, K.W. Characterization of Warm Mix Asphalt Binders Containing Artificially Long-Term Aged Binders, Construction Building Materials, **2009**, 23, 2371-2379.

54. Mills-Beale, J.; You, Z.; Fini, E.; Zada, B.; Lee, C.; Yap, Y. Aging Influence on Rheology Properties of Petroleum-Based Asphalt Modified with Biobinder. Journal of Materials in Civil Engineering ***2014****, 26(2), 358-366.*

55. Fini, E.; Kalberer, E.; Shahbazi, A.; Basti, M.; You, Z.; Ozer, H.; Aurangzeb, Q. Chemical Characterization of Biobinder from Swine Manure: Sustainable Modifier for Asphalt Binder. Journal of Materials in Civil Engineering ***2011****, 23(11), 1506-1513.*

56. Fini, E.; Al-Qadi, I.; You, Z.; Zada, B.; Mills-Beale, J. Partial Replacement of Asphalt Binder with Bio-Binder: Characterisation and Modification. International Journal of Pavement Engineering ***2012****, 13(6), 515-522.*

*57. Narve, A.; Harald, K.; Einar, E.J.; Johan, S. Asphaltene Aggregation from Crude Oils and Model Systems Studied by High-Pressure NIR Spectroscopy. Energy Fuels **2002**, 16, 1287-1295.*

*58. Gebresellasie, K. (**2012**). Investigation of asphalt binders by X-ray diffraction using Pearson-vii, pseudo-Voigt, and generalized Fermi functions. MSc Thesis, Memorial University of Newfoundland.*

*59. Kim, Y.R. Modeling of Asphalt Concrete, MH/ ASCE Press, First Edition, **2008**.*

*60. Sjöblom, J.; Simon, S.; Xu, Z. Model Molecules Mimicking Asphaltene. Advances in Colloid and Interface Science, **2015**, 218, 1-16.*

*61. Akbarzadeh, K.; Hammami, A.; Kharrat, A.; Zhang, D.; Allenson, S.; Creek, J.; Mullins, O. C. Asphaltene—Problematic but Rich in Potential. Oilfield Review, **2007**, 19(2), 22-43.*

*62. Hussam, H.L.; Raphael, O.I. Interrelationships Between Asphaltene Precipitation Inhibitor Effectiveness, Asphaltene Characteristics, and Precipitation Behavior during n-Heptane (Light Paraffin Hydrocarbon)-Induced Asphaltene Precipitation, Energy Fuels **2004**, 18, 1038-1048.*

*63. Groenzin, H.; Mullins, O.C. Asphaltene Molecular Size and Structure, Journal of Physical Chemistry A **1999**, 103, 11237-11245.*

*64. Mullins, O.C.; Sheu, E.Y.; Hammami, A.; Marshall A.G. Asphaltene, Heavy Oils and Petroleomics, Springer, NY, USA, **2007**.*

*65. Goual, L.; Sedghi, M.; Zeng, H.; Mostowfi, F.; McFarlane, R.; Mullins, O.C. On the Formation and Properties of Asphaltene Nanoaggregates and Clusters by DCConductivity and Centrifugation. Fuel **2011**, 90, 2480-2490.*

*66. Nikhil, B.J.; Mullins, O.C.; Jamaluddin, A.; Creek, J.; McFadden, J. Asphaltene Precipitation from Live Crude Oil. Energy Fuels **2001**, 15, 979-986.*

*67. Bayat, M.; Sattarin, M.; Teymouri, M. Prediction of Asphaltene Self-Precipitation in Dead Crude Oil. Energy Fuels **2008**, 22, 583-586.*

*68. Tharanivasan, A.K.; Svrcek, W.Y.; Yarranton, H.W. Measurement, and Modeling of Asphaltene Precipitation from Crude Oil Blends. Energy Fuels **2009**, 23, 3971-3980.*

*69. Peramanu, S.; Singh, C.; Agrawala, M.; Yarranton, H.W. Investigation on the Reversibility of Asphaltene Precipitation. Energy Fuels **2001**, 15, 910-917.*

*70. McGennis, R.B.; Anderson R.M.; Kennedy T.W.; Solaimanian, M. Background of Superpave Asphalt Mixture Design and Analysis, **1994**, Publication No. FHWA-SA-95-003.*

*71. Castaneda, L. C.; Munoz, J. A.; Ancheyta, J. Current Situation of Emerging Technologies for Upgrading of Heavy Oils. Catalysis Today, **2014**, 220, 248-273.*

*72. Sergienko, S.R. High-Molecular-Weight Compounds of Crude Petroleum, Khimiya, Moscow, **1964**.*

*73. Trejo, F.; Ancheyta, J.; Morgan, T.J.; Herod, A.A.; Kandiyoti, R. Characterization of Asphaltene from Hydrotreated Products by SEC, LDMS, LAMDI, NMR, and XRD. Energy Fuels **2007**, 21, 2121-2128.*

*74. Sadeghi, M.A.; Chilingarian, G.V.; Yen, T.F. American Chemical Society Syrup. Ser. **1986**, g, 99 (Chern. Abstr. 104: 151905R).*

*75. Andersen, S.I.; Jensen, J.O.; Speight, J.G. X-ray Diffraction of Subfractions of Petroleum Asphaltene. Energy Fuels **2005**, 19, 2371-2377.*

*76. Lu X.; Redelius P. Composition and Structural Characterization of Waxes Isolated from Bitumen. Energy Fuels **2006**, 20, 653-66.*

*77. Pecharsky, V.K.; Zavalij, P.Y. Foundamentals of Powder Diffraction and Structural Characterization of Materials, Springer, **2005**.*

*78. Ungár, T.; Borbély. The effect of dislocation contrast on x-ray line broadening: A new approach to line profile analysis. Applied Physics Letters **1996**, 69(21), 3173-3175.*

*79. Van Berkum, J.; Vermeulen, A.; Delhez, R.; De Keijser, T.; Mittemeijer, E. Applicabilities of the Warren–Averbach analysis and an alternative analysis for separation of size and strain broadening. Journal of Applied Crystallography **1994**, 27(3), 345-357.*

*80. Hesse, R.; Streubel, P.; Szargan. R. Product or sum: Comparative tests of Voigt, and product or sum of Gaussian and Lorentzian functions in the fitting of synthetic Voigt-based X-ray photoelectron spectra. Surface and Interface Analysis. **2007**, 39(5), 381-391.*

*81. Jahangir, R.; Little, D.; Bhasin, A. Evolution of asphalt binder microstructure due to tensile loading determined using AFM and image analysis techniques. The International Journal of Pavement Engineering **2015**, 16(4), 1-13.*

*82. Siddiqui, M. N.; Ali, M. F.; Shirokoff, J. Energy Fuels **2002**, 81, 51-58.*

6. Appendices

6.1 Procedure for Profile Fitting a Diffraction Pattern

1. Open the diffraction pattern (Jade software)
2. Overlay the PDF reference
3. Zoom in on first peak(s) to analyze
4. Open the profile fitting dialogue to configure options
5. Choose the background and put Exponent and Lorentzian values
6. Refine the profile fit for the first peak(s)
7. Review the quality of profile fit
8. Move to next peak(s) and profile fit
9. Continue until entire pattern is fit
10. Repeat steps from 1 to 9 with different background and Exponent and Lorentzian values

6.2 More Simulations using XRD

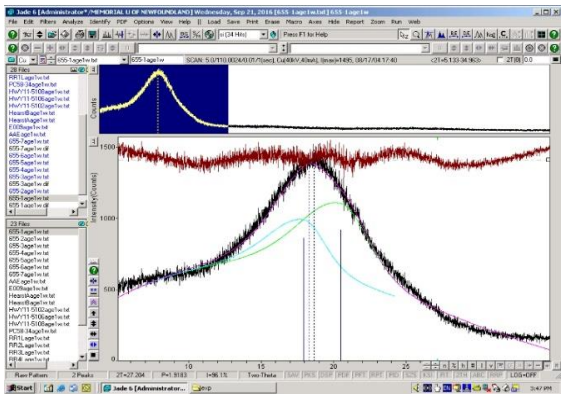

Figure 6.1: Specimen T1 (Exp=0.5, 3rd Order Background) on XRD.

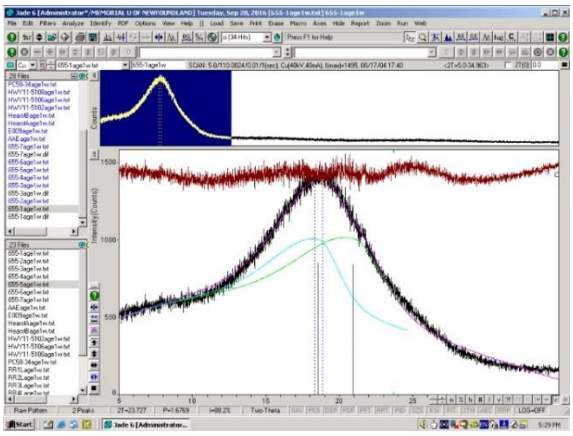

Figure 6.2: Specimen T1 (Exp=1.0, 3rd Order Background) on XRD.

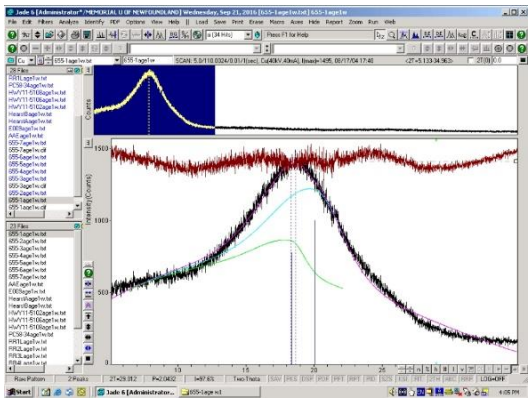

Figure 6.3: Specimen T1 (Exp=1.5, 3rd Order Background) on XRD.

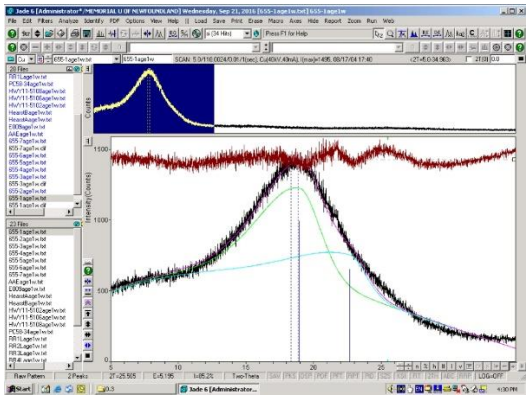

Figure 6.4: Specimen T1 (Lor=0.3, 3rd Order Background) on XRD.

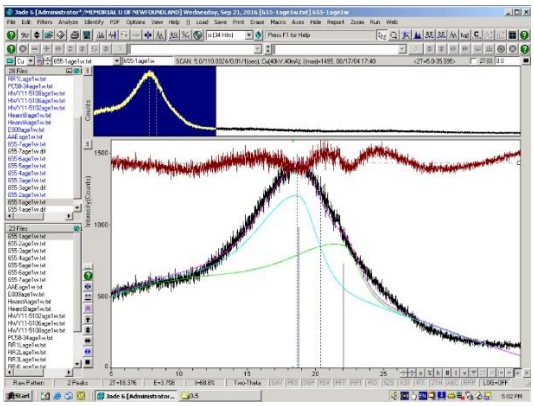

Figure 6.5: Specimen T1 (Lor=0.5, 3rd Order Background) on XRD.

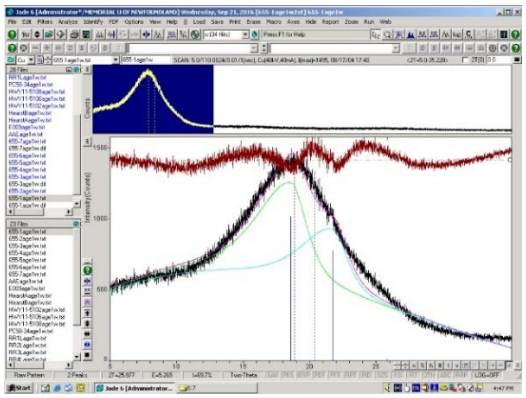

Figure 6.6: Specimen T1 (Lor=0.7, 3rd Order Background) on XRD.

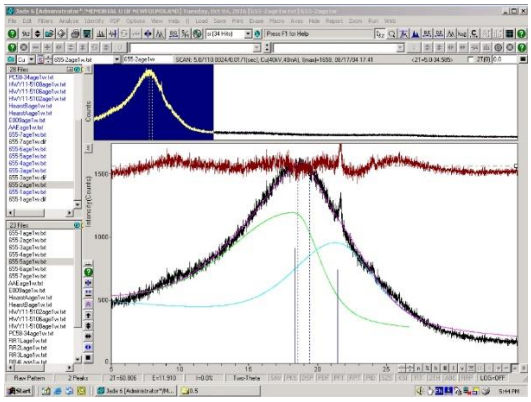

Figure 6.7: Specimen T2 (Exp=0.5, Linear Background) on XRD.

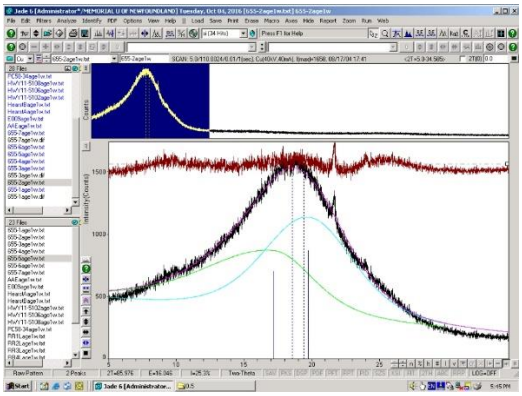

Figure 6.8: Specimen T2 (Exp=1.0, Linear Background) on XRD.

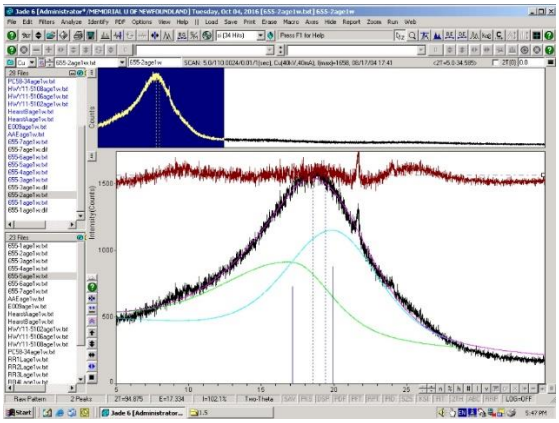

Figure 6.9: Specimen T2 (Exp=1.5, Linear Background) on XRD.

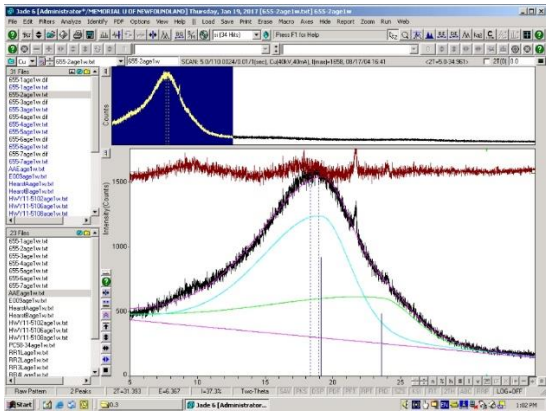

Figure 6.10: Specimen T2 (Lor=0.3, Linear Background) on XRD.

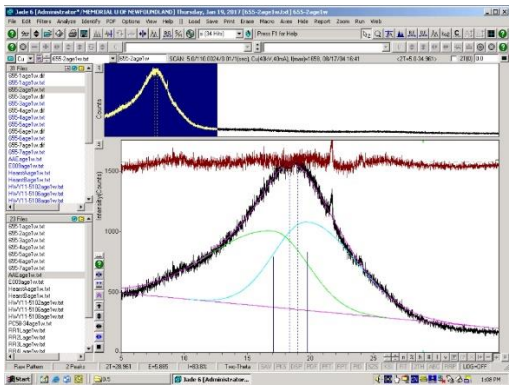

Figure 6.11: Specimen T2 (Lor=0.5, Linear Background) on XRD.

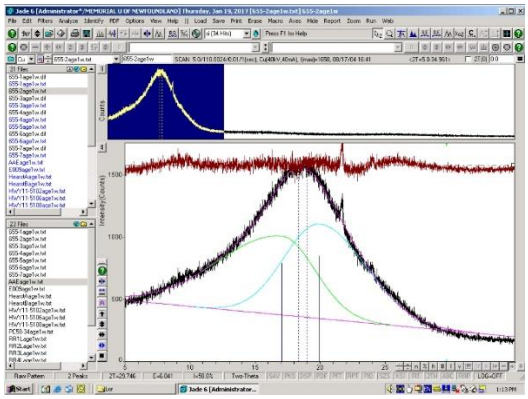

Figure 6.12: Specimen T2 (Lor=0.7, Linear Background) on XRD.

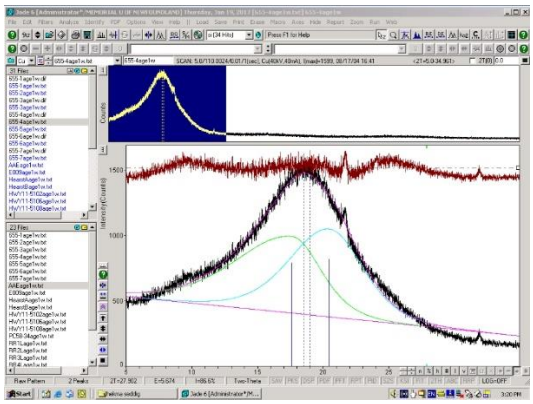

Figure 6.13: Specimen T4 (Exp=0.5, Linear Background) on XRD.

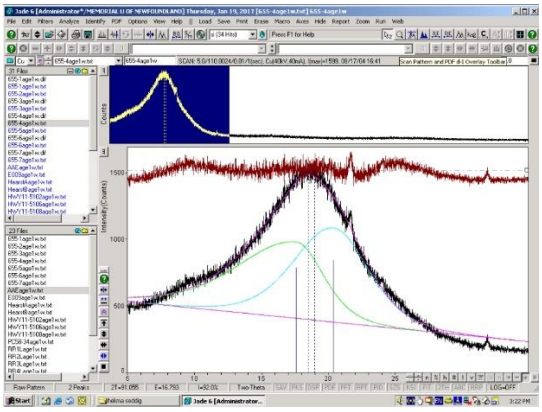

Figure 6.14: Specimen T4 (Exp=1.0, Linear Background) on XRD.

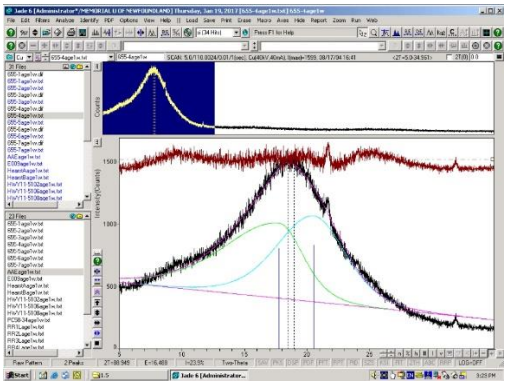

Figure 6.15: Specimen T4 (Exp=1.5, Linear Background) on XRD.

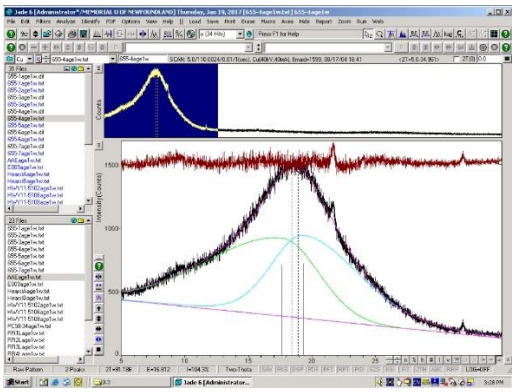

Figure 6.16: Specimen T4 (Lor=0.3, Linear Background) on XRD.

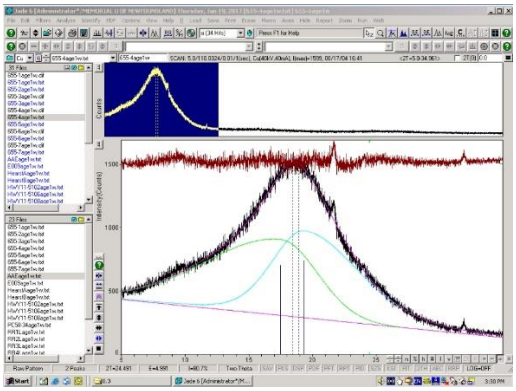

Figure 6.17: Specimen T4 (Lor=0.5, Linear Background) on XRD.

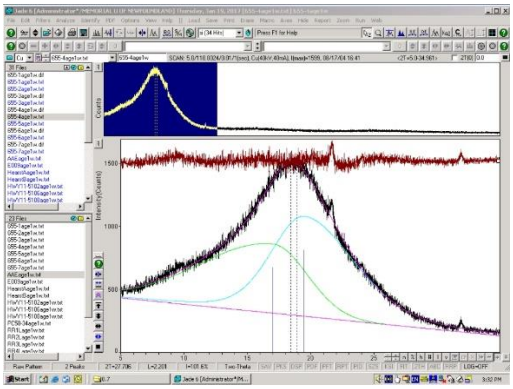

Figure 6.18: Specimen T4 (Lor=0.7, Linear Background) on XRD.

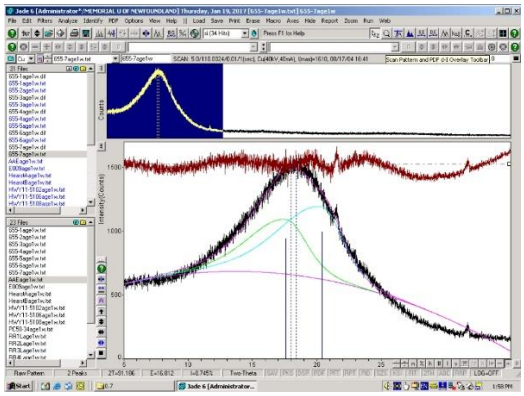

Figure 6.19: Specimen T7 (Exp=0.5, Parabolic Background) on XRD.

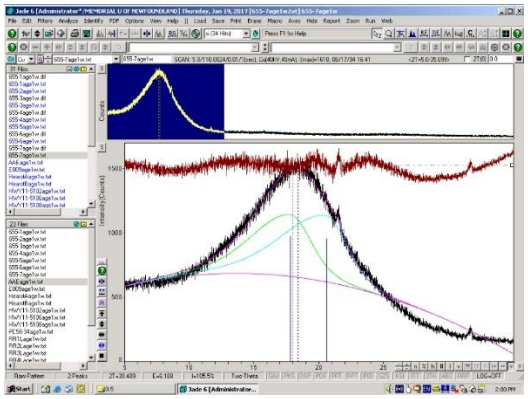

Figure 6.20: Specimen T7 (Exp=1.0, Parabolic Background) on XRD.

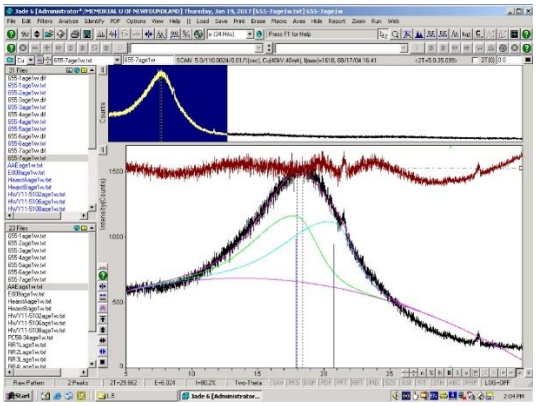

Figure 6.21: Specimen T7 (Exp=1.5, Parabolic Background) on XRD.

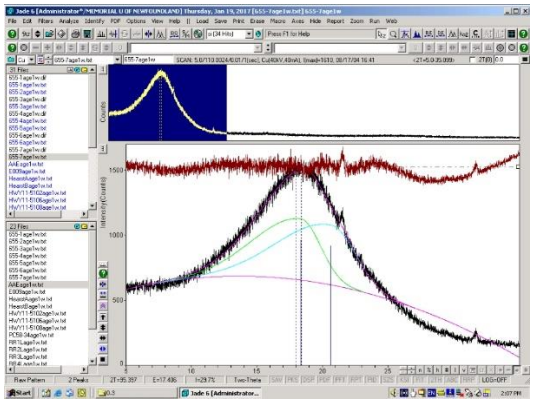

Figure 6.22: Specimen T7 (Lor=0.3, Parabolic Background) on XRD.

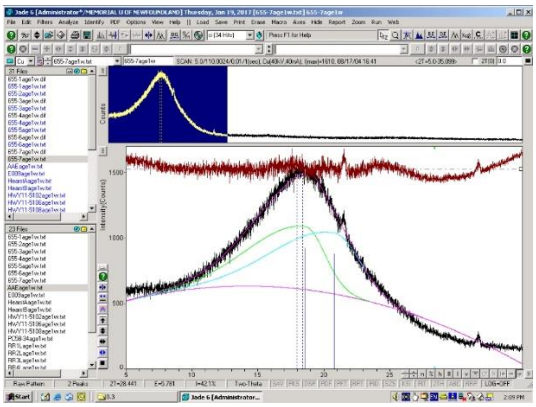

Figure 6.23: Specimen T7 (Lor=0.5, Parabolic Background) on XRD.

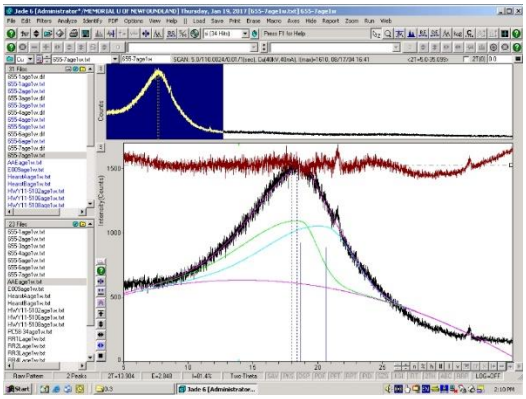

Figure 6.24: Specimen T7 (Lor=0.7, Parabolic Background) on XRD.

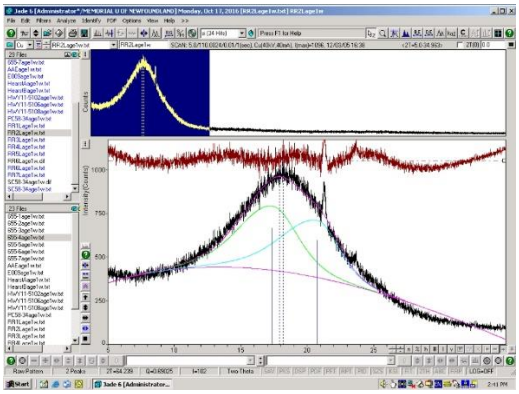

Figure 6.25: Specimen L2 (Exp=0.5, 3rd Order Background) on XRD.

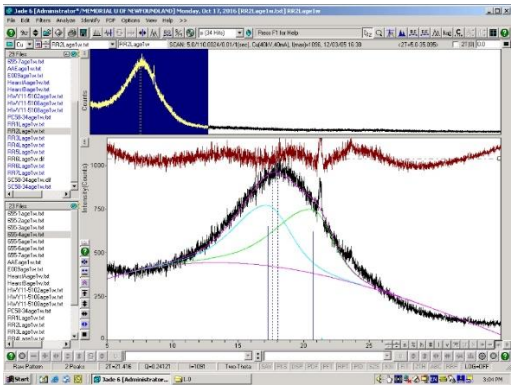

Figure 6.26: Specimen L2 (Exp=1.0, 3rd Order Background) on XRD.

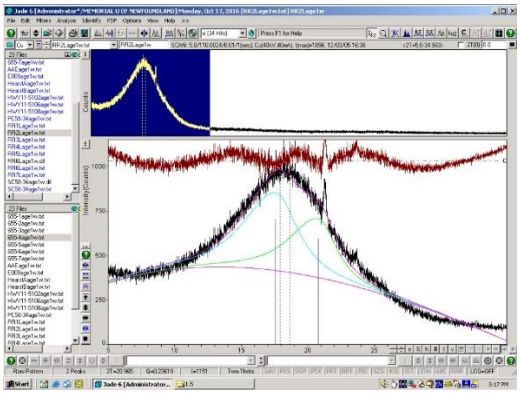

Figure 6.27: Specimen L2 (Exp=1.5, 3rd Order Background) on XRD.

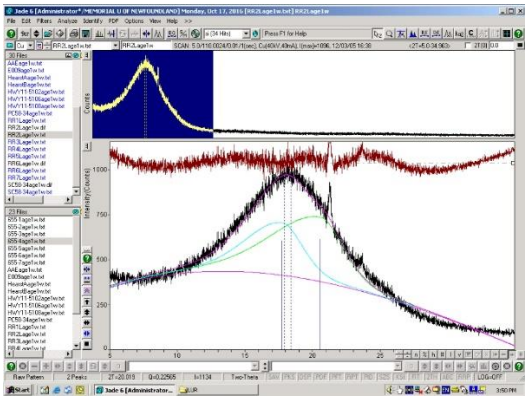

Figure 6.28: Specimen L2 (Lor=0.3, 3rd Order Background) on XRD.

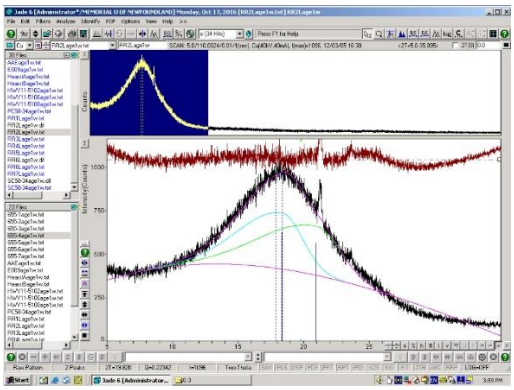

Figure 6.29: Specimen L2 (Lor=0.5, 3rd Order Background) on XRD.

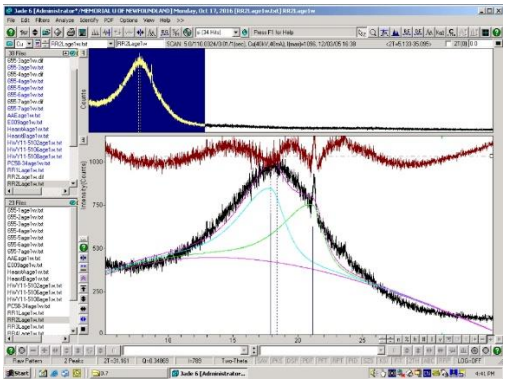

Figure 6.30: Specimen L2 (Lor=0.7, 3rd Order Background) on XRD.

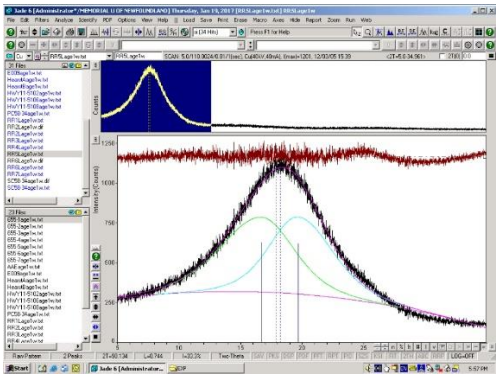

Figure 6.31: Specimen L5 (Exp=0.5, Parabolic Background) on XRD.

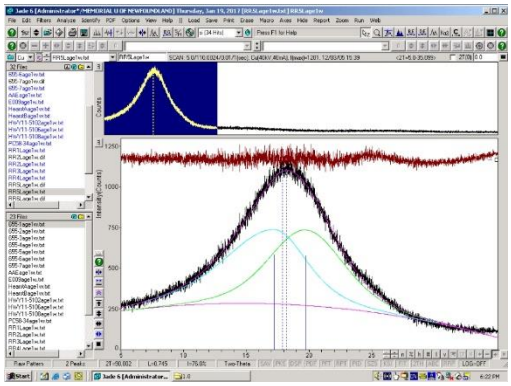

Figure 6.32: Specimen L5 (Exp=1.0, Parabolic Background) on XRD.

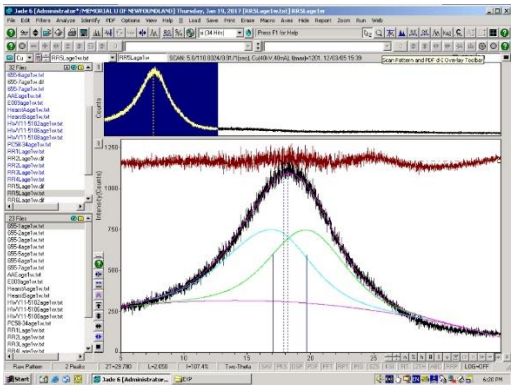

Figure 6.33: Specimen L5 (Exp=1.5, Parabolic Background) on XRD.

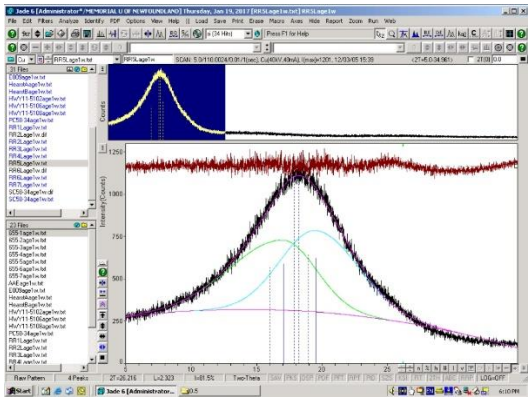

Figure 6.34: Specimen L5 (Lor=0.3, Parabolic Background) on XRD.

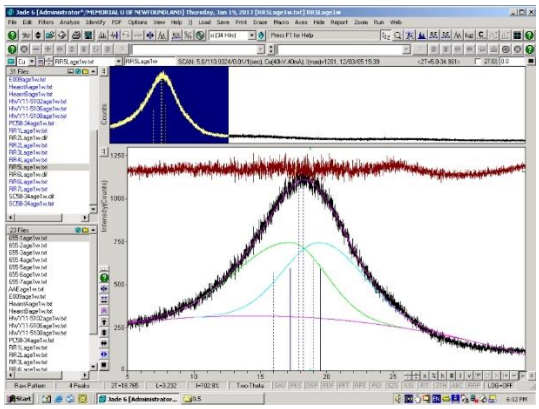

Figure 6.35: Specimen L5 (Lor=0.5, Parabolic Background) on XRD.

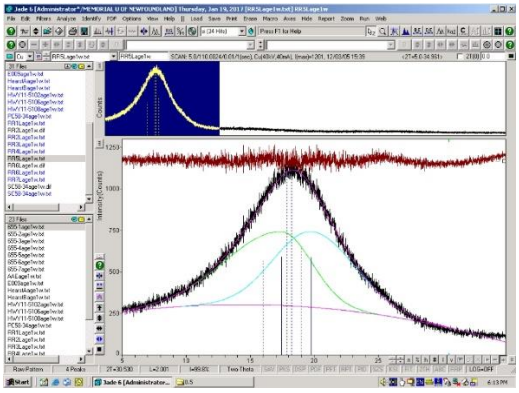

Figure 6.36: Specimen L5 (Lor=0.7, Parabolic Background) on XRD.

6.3 More Simulations Using Mathematica for Fitting the Samples with GFF

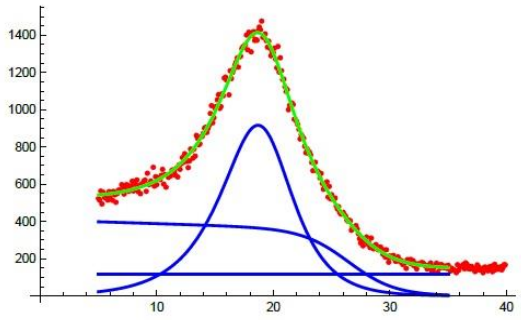

Figure 6.37: Specimen T1 on GFF.

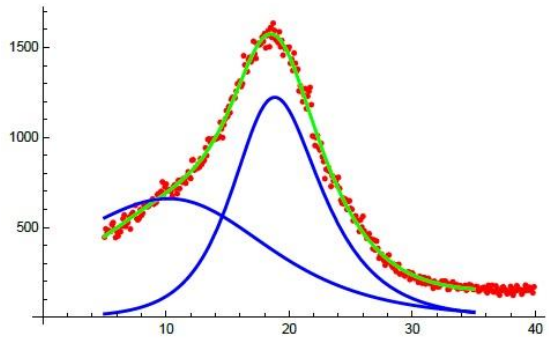

Figure 6.38: Specimen T2 on GFF.

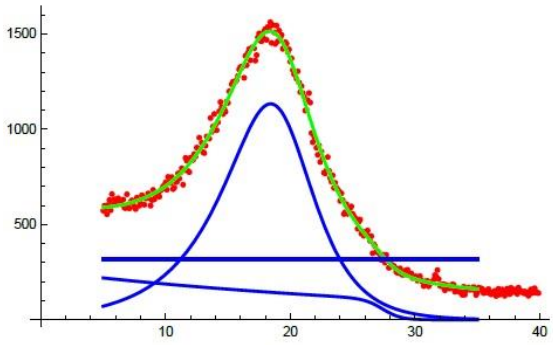

Figure 6.39: Specimen T7 on GFF.

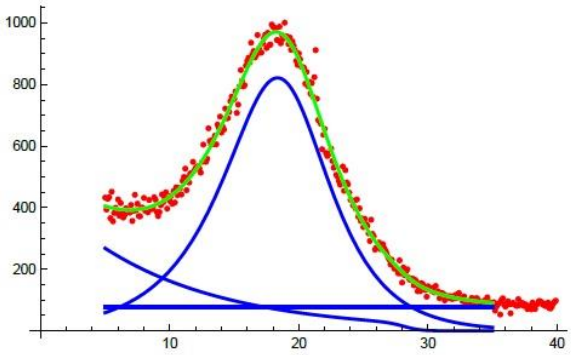

Figure 6.40: Specimen L2 on GFF.

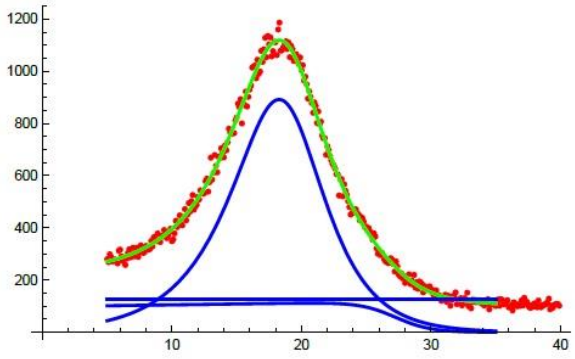

Figure 6.41: Specimen L5 on GFF.

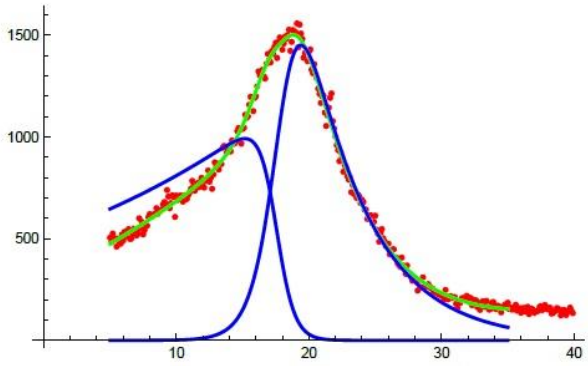

Figure 6.42: Specimen T4 on GFF.